ON INFRARED EXCESSES ASSOCIATED WITH Li-RICH K GIANTS

LUISA M. REBULL[1], JOLEEN K. CARLBERG[2,7], JOHN C. GIBBS[3], J. ELIN DEEB[4], ESTEFANIA LARSEN[5],
DAVID V. BLACK[6], SHAILYN ALTEPETER[5], ETHAN BUCKSBEE[5], SARAH CASHEN[3], MATTHEW CLARKE[5],
ASHWIN DATTA[3], EMILY HODGSON[3], AND MEGAN LINCE[3]

[1] Spitzer Science Center (SSC) and Infrared Science Archive (IRSA), Infrared Processing and Analysis Center (IPAC),
1200 E. California Blvd., California Institute of Technology, Pasadena, CA 91125, USA; rebull@ipac.caltech.edu
[2] NASA Goddard Space Flight Center, Code 667, Greenbelt, MD 20771, USA
[3] Glencoe High School, 2700 NW Glencoe Rd., Hillsboro, OR 97124, USA
[4] Bear Creek High School, 9800 W. Dartmouth Pl., Lakewood, CO 80227, USA
[5] Millard South High School, 14905 Q St., Omaha, NE 68137, USA
[6] Walden School of Liberal Arts, 4230 N. University Ave., Provo, UT 84604, USA

ABSTRACT

Infrared (IR) excesses around K-type red giants (RGs) have previously been discovered using *Infrared Astronomy Satellite* (*IRAS*) data, and past studies have suggested a link between RGs with overabundant Li and IR excesses, implying the ejection of circumstellar shells or disks. We revisit the question of IR excesses around RGs using higher spatial resolution IR data, primarily from the *Wide-field Infrared Survey Explorer*. Our goal was to elucidate the link between three unusual RG properties: fast rotation, enriched Li, and IR excess. Our sample of RGs includes those with previous IR detections, a sample with well-defined rotation and Li abundance measurements with no previous IR measurements, and a large sample of RGs asserted to be Li-rich in the literature; we have 316 targets thought to be K giants, about 40% of which we take to be Li-rich. In 24 cases with previous detections of IR excess at low spatial resolution, we believe that source confusion is playing a role, in that either (a) the source that is bright in the optical is not responsible for the IR flux, or (b) there is more than one source responsible for the IR flux as measured in *IRAS*. We looked for IR excesses in the remaining sources, identifying 28 that have significant IR excesses by ∼20 μm (with possible excesses for 2 additional sources). There appears to be an intriguing correlation in that the largest IR excesses are all in Li-rich K giants, though very few Li-rich K giants have IR excesses (large or small). These largest IR excesses also tend to be found in the fastest rotators. There is no correlation of IR excess with the carbon isotopic ratio, $^{12}C/^{13}C$. IR excesses by 20 μm, though relatively rare, are at least twice as common among our sample of Li-rich K giants. If dust shell production is a common by-product of Li enrichment mechanisms, these observations suggest that the IR excess stage is very short-lived, which is supported by theoretical calculations. Conversely, the Li-enrichment mechanism may only occasionally produce dust, and an additional parameter (e.g., rotation) may control whether or not a shell is ejected.

Key words: infrared: stars – stars: evolution – stars: late-type

Supporting material: machine-readable and VO table

1. INTRODUCTION

As stars evolve from the main-sequence (MS) to the red giant branch (RGB), they exhibit several characteristic changes. As the outer layers expand and cool, the star's rotation rate slows, the convection zone deepens and a series of shell-burning and core-burning phases begin to take place. A number of RGB K-type giants, however, exhibit uncharacteristically rapid rotation rates that also seem to be correlated with high lithium abundances, A(Li) (e.g., Carlberg et al. 2012, hereafter C12). These higher rotation rates and A(Li) are inconsistent with those predicted by standard stellar evolutionary models. It has also been suggested that many of these high-Li RGB stars have infrared (IR) excesses suggestive of a circumstellar shell or disk (de la Reza et al. 1996, 1997; Drake et al. 2002, and references therein). Various hypotheses have been proposed to explain the combination of high Li, rapid rotation rates, and IR excesses, including the accretion of nearby giant planets equivalent to a few Jupiter masses (e.g., Siess & Livio 1999) or a newly triggered nuclear fusion stage that could eject a dusty shell (e.g., de la Reza et al. 2015 and references therein).

The de la Reza et al. (1997; dlR97) study (and related studies) used data from the *Infrared Astronomy Satellite* (*IRAS*; Neugebauer et al. 1984), which surveyed at 12, 25, 60, and 100 μm. The spatial resolution, however, was relatively low, up to a few arcminutes. Despite the relatively low spatial resolution, many stars with IR excesses were identified (e.g., Gillett 1986; Paresce & Burrows 1987). In some regions with high source density, identifying the optical counterpart to the IR source can be difficult, but in many cases, the counterparts are easily identifiable. dlR97, as well as other studies, used these *IRAS* data to look for K giants with IR excesses.

Data are now available from the much higher spatial resolution (6″–12″) and much more sensitive *Wide-field Infrared Survey Explorer* (*WISE*; Wright et al. 2010). *WISE* surveyed the whole sky at 3.4, 4.6, 12, and 22 μm. While *WISE* does not detect wavelengths longer than *IRAS* channel 2 (25 μm), it is much higher spatial resolution, and can provide insight into how to interpret the *IRAS* data at 60 and 100 μm.

Some investigations subsequent to dlR97 have begun to question the connection between IR excesses and lithium abundance in red giants (RGs). Fekel & Watson (1998) found 6 giants with larger than typical lithium abundances out of 39 giants with IR excess (as determined from *IRAS*), which they point out is a similar fraction of stars with enhanced Li as found

in normal field giants. Jasniewicz et al. (1999) finds 8 Li-rich stars out of 29 stars with IR excesses (also as determined via *IRAS*), finding no correlation between Li abundance and IR excess. Lebzelter et al. (2012) report on 3 Li-rich giants (out of more than 400 studied), none of which have IR excesses suggestive of mass loss. The IR excesses in their paper were identified based on *WISE* data, but were limited to 12 μm and shorter because few of their targets were detected at 22 μm. However, they also looked for evidence of gas mass loss in their spectra, and found none. Kumar et al. (2015) report on a search for IR excesses in 2000 K giants. None of their far-IR excess sources are lithium-rich, and of their 40 Li-rich sources, they identify seven as having IR excess of any sort. These authors combined *IRAS* and *WISE* data to look for IR excesses.

In the present paper, we have also combined *IRAS* and *WISE* data, as well as data from several other IR surveys as discussed below. Large IR excesses are easily identified in the spectral energy distributions (SEDs), and we used tools developed in the context of the study of young stars to look for small but significant excesses. We started with the dlR97 *IRAS*-selected targets; these *IRAS*-selected targets are all quite bright in the IR. We added to this the sample from C12, who assembled a set of K giants consisting of rapid and slow rotators in which the relationship between $v \sin i$, lithium abundances, and carbon isotope ratios ($^{12}C/^{13}C$) could be explored with an intention of exploring evidence for planetary accretion. The C12 sample was assembled without regard to IR excess, so these objects are on average much fainter in the IR than the dlR97 sample. Finally, many Li-rich K giants (and candidates) have been reported in the literature, many of which are not in the dlR97 or C12 samples. We have included such Li-rich K giants in our sample. We looked for IR excesses among all of these targets, performing visual inspection of multi-wavelength images and assembling broadband SEDs for our targets.

We now assemble the list of targets (Section 2), and search various archives for images and photometry for these targets (Section 3). Then we drop some stars from our sample, some by necessity due to missing data, and some because they are likely subject to source confusion (Section 4). From the remaining sample, we can identify sources likely to have an IR excess (Section 5). Then we discuss some properties of the sample as a whole (Section 6). We find few stars with IR excesses, so our ability to find correlations with abundances is somewhat limited, but we discuss this in Section 7 before summarizing in Section 8.

2. ASSEMBLING THE TARGET LIST

There are 82 targets published in dlR97. They obtained spectra of the targets on their list, and reported the targets as Li-rich if the Li line at $\lambda6708$ had an intensity comparable to or higher than the Ca I line at $\lambda6718$. If the Li abundance was actually known, they took those with abundances larger than $\log \epsilon(\mathrm{Li}) = 1.2$ dex as Li-rich. Many of the targets have HD numbers, and thus finding coordinates for an optical counterpart is straightforward. However, many of their targets have only *IRAS* names, and so they took spectra of objects they believed to be counterparts of the sources listed; see discussion below. The target position we used for these sources is that reported in the *IRAS* catalogs.

There are 86 K giants reported in C12. Comparing this to the targets from dlR97, there is only one source in common between them, HD 31993. C12 reports lithium abundances,

$v \sin i$, and $^{12}C/^{13}C$ ratios, among other things, for their targets. Not all of these targets are Li-rich.

There is wide-ranging literature reporting on Li-rich K giants (and candidates). We compiled 149 additional targets that have been identified either consistently or at one time as confirmed or possible Li-rich K giants, but not included in either the dlR97 or the C12 samples. They include targets from Adamów et al. (2014), Anthony-Twarog et al. (2013), Carney et al. (1998), J. K. Carlberg et al. (2015, in preparation), Castilho et al. (2000), Drake et al. (2002), Fekel & Watson (1998), Hill & Pasquini (1999), Jasniewicz et al. (1999), Kirby et al. (2012), Kraft et al. (1999), Kumar et al. (2011) and references therein, Liu et al. (2014), Luck & Heiter (2007), Martell & Shetrone (2013), Monaco et al. (2014), Pilachowski et al. (2003), Ruchti et al. (2011), Silva Aguirre et al. (2014), Smith et al. (1999), and Torres et al. (2000). Kumar et al. (2015) appeared as we were finishing our analysis, and it has similar goals as the present paper. It uses as a starting point the list of 2000 low-mass K giants from Kumar et al. (2011), so all of the Li-rich sources from that sample are already in our sample. All of the literature sources are identified simply as "literature sources" in Table 1; the Appendix identifies the paper of origin for any given target.

Our complete list of 316 targets appears in Table 1. We obtained R.A., decl. positions for these targets, most of which are quite bright in the optical, primarily from SIMBAD, though literature was consulted for fainter sources as required. The positions we used are in Table 1, which also includes all the bandmerged brightness measurements discussed below. In the Appendix, Table 6 collects a few special notes about any special circumstances attached to that star, e.g., information about typos in previously published tables, or necessary tweaks to the positions. There are copious notes in the main text about targets called out as special (e.g., those with IR excesses).

3. ARCHIVAL DATA

In this section, we discuss the catalogs we searched for detections of our sources; they are summarized in Table 2, along with the fraction of the sample having matches in each of these catalogs. Table 1 includes all the crossmatched sources (names and reported brightnesses) discussed below.

3.1. Overall Approach to Archival Data

All of the large-area catalogs described here were merged by position with a catalog-dependent search radius to the position we obtained for our targets as described above. Typically, the closest source by position was taken to be the match, and often the best match was within 1″. However, each source was investigated in the images from the Palomar Observatory Digital Sky Survey, the Sloan Digital Sky Survey (SDSS), 2MASS, and *WISE*. Nebulosity, source confusion, or extended sources were all noted. SEDs were constructed (using zero points if necessary as provided in the corresponding survey documentation) as an additional check on the source matching—obvious discontinuities in the SED suggested problems with source matching, and a better match was sought (but not always found). If a source other than the closest source by position was determined to be a better match, then the match was forced to be the better match, even if it was >1″ away. We primarily used the Infrared Science Archive (IRSA) tool FinderChart[8] for this process, along with

---

Table 1
Contents of Online Catalog

Format	Units	Label	Explanations
A26	⋯	name	name of source
F11.6	deg.	R.A.	R.A. of source (J2000)
F11.6	deg.	Decl.	decl. of source (J2000)
A6	⋯	dlR97	flag to indicate source is part of the dlR97 sample
A4	⋯	C12	flag to indicate star is part of the C12 sample
A5	⋯	lit	flag to indicate star is selected from the literature as a Li-rich giant (but not C12 or dlR97)
A4	⋯	LirichLit	value of "yes" means source is identified in the literature as a Li-rich giant
A4	⋯	LirichHere	value of "yes" means source is selected here as a Li-rich giant
F7.2	⋯	ALiNLTE	A(Li) under the assumption of NLTE from the literature
A2	⋯	ALiLTEl	limit flag for A(Li) under the assumption of LTE from the literature
F7.2	⋯	ALiLTE	A(Li) under the assumption of LTE from the literature
A2	⋯	Cratiol	limit flag on ^{12}C/^{13}C ratio
F5.1	⋯	Cratio	^{12}C/^{13}C ratio
F5.1	km s^{-1}	vsini	projected rotational velocity $v \sin i$ in km s^{-1} from the literature
I5	K	Teff	Effective temperature from the literature
F5.1	⋯	logg	log g from the literature
F6.2	mag	Umag	Vega-based magnitude in U band
F6.2	mag	Umerr	Vega-based magnitude error in U band; taken to be 20% unless specified
F6.2	mag	Bmag	Vega-based magnitude in B band
F6.2	mag	Bmerr	Vega-based magnitude error in B band; taken to be 20% unless specified
F6.2	mag	Vmag	Vega-based magnitude in V band
F6.2	mag	Vmerr	Vega-based magnitude error in V band; taken to be 20% unless specified
F6.2	mag	Rmag	Vega-based magnitude in R band
F6.2	mag	Rmerr	Vega-based magnitude error in R band; taken to be 20% unless specified
F6.2	mag	umag	AB SDSS magnitude in u band
F6.2	mag	umerr	AB SDSS magnitude error in u band
F6.2	mag	gmag	AB SDSS magnitude in g band
F6.2	mag	gmerr	AB SDSS magnitude error in g band
F6.2	mag	rmag	AB SDSS magnitude in r band
F6.2	mag	rmerr	AB SDSS magnitude error in r band
F6.2	mag	imag	AB SDSS magnitude in i band
F6.2	mag	imerr	AB SDSS magnitude error in i band
F6.2	mag	zmag	AB SDSS magnitude in z band
F6.2	mag	zmerr	AB SDSS magnitude error in z band
A22	⋯	2Mname	Name from 2MASS or 2MASX catalog
A2	⋯	Jlim	limit flag for 2MASS J band
F6.2	mag	Jmag	Vega-based magnitude in 2MASS J band
F6.2	mag	Jmerr	Vega-based magnitude error in 2MASS J band
A2	⋯	Jqual	2MASS data quality flag for J (A = best)
A2	⋯	Hlim	limit flag for 2MASS H band
F6.2	mag	Hmag	Vega-based magnitude in 2MASS H band
F6.2	mag	Hmerr	Vega-based magnitude error in 2MASS H band
A2	⋯	Hqual	2MASS data quality flag for H (A = best)
A2	⋯	Klim	limit flag for 2MASS K_s band
F6.2	mag	Kmag	Vega-based magnitude in 2MASS K_s band
F6.2	mag	Kmerr	Vega-based magnitude error in 2MASS K_s band
A2	⋯	Kqual	2MASS data quality flag for K_s (A = best)
A18	⋯	DENISname	Name from DENIS catalog
F6.2	mag	Imag	Vega-based DENIS magnitude in I band
F6.2	mag	Imerr	Vega-based DENIS magnitude error in I band
F6.2	mag	Jmag	Vega-based DENIS magnitude in J band
F6.2	mag	Jmerr	Vega-based DENIS magnitude error in J band
F6.2	mag	Kmag	Vega-based DENIS magnitude in K band
F6.2	mag	Kmerr	Vega-based DENIS magnitude error in K band
A26	⋯	WISEname	Name from WISE (AllWISE) catalog or reject catalog
A2	⋯	W1lim	limit flag for WISE-1 ([3.4])
F6.2	mag	W1mag	Vega-based magnitude in WISE-1 ([3.4])
F6.2	mag	W1merr	Vega-based magnitude error in WISE-1 ([3.4]); value of −9 for those measures that are limits
A2	mag	W1qual	WISE-1 ([3.4]) data quality flag (A = best)
A2	⋯	W2lim	limit flag for WISE-2 ([4.6])
F6.2	mag	W2mag	Vega-based magnitude in WISE-2 ([4.6])
F6.2	mag	W2merr	Vega-based magnitude error in WISE-2 ([4.6]); value of −9 for those measures that are limits
A2	mag	W2qual	WISE-2 ([4.6]) data quality flag (A = best)

Table 1
(Continued)

Format	Units	Label	Explanations
A2	⋯	W3lim	limit flag for WISE-3 ([12])
F6.2	mag	W3mag	Vega-based magnitude in WISE-3 ([12])
F6.2	mag	W3merr	Vega-based magnitude error in WISE-3 ([12]); value of −9 for those measures that are limits
A2	mag	W3qual	WISE-3 ([12]) data quality flag (A = best)
A2	⋯	W4lim	limit flag for WISE-4 ([22])
F6.2	mag	W4mag	Vega-based magnitude in WISE-4 ([22])
F6.2	mag	W4merr	Vega-based magnitude error in WISE-4 ([22]); value of −9 for those measures that are limits
A2	mag	W4qual	WISE-4 ([22]) data quality flag (A = best)
A27	⋯	SEIPname	Name from SEIP source list
F6.2	mag	I1mag	Vega-based magnitude in IRAC-1 ([3.6])
F6.2	mag	I1merr	Vega-based magnitude error in IRAC-1 ([3.6])
F6.2	mag	I2mag	Vega-based magnitude in IRAC-2 ([4.5])
F6.2	mag	I2merr	Vega-based magnitude error in IRAC-2 ([4.5])
F6.2	mag	I3mag	Vega-based magnitude in IRAC-3 ([5.8])
F6.2	mag	I3merr	Vega-based magnitude error in IRAC-3 ([5.8])
F6.2	mag	I4mag	Vega-based magnitude in IRAC-4 ([8])
F6.2	mag	I4merr	Vega-based magnitude error in IRAC-4 ([8])
F6.2	mag	M1mag	Vega-based magnitude in MIPS-1 ([24])
F6.2	mag	M1merr	Vega-based magnitude error in MIPS-1 ([24])
A14	⋯	IRASPSCname	Name from IRAS Point Source Catalog (PSC)
F6.2	mag	IRAS1PSCmag	Vega-based magnitude in IRAS-1 ([12]) from PSC; errors taken to be 0.22 mag
F9.2	Jy	IRAS1PSCfd	flux density in Jy in IRAS-1 from PSC
A2	mag	IRAS1PSCqual	Data quality flag for IRAS-1 from PSC (3 = best, 1 = limit)
F6.2	mag	IRA21PSCmag	Vega-based magnitude in IRAS-2 ([25]) from PSC; errors taken to be 0.22 mag
F9.2	Jy	IRAS2PSCfd	flux density in Jy in IRAS-2 from PSC
A2	mag	IRAS2PSCqual	Data quality flag for IRAS-2 from PSC (3 = best, 1 = limit)
F6.2	mag	IRAS3PSCmag	Vega-based magnitude in IRAS-3 ([60]) from PSC; errors taken to be 0.22 mag
F9.2	Jy	IRAS3PSCfd	flux density in Jy in IRAS-3 from PSC
A2	mag	IRAS3PSCqual	Data quality flag for IRAS-3 from PSC (3 = best, 1 = limit)
F6.2	mag	IRAS4PSCmag	Vega-based magnitude in IRAS-4 ([100]) from PSC; errors taken to be 0.22 mag
F9.2	Jy	IRAS4PSCfd	flux density in Jy in IRAS-4 from PSC
A2	mag	IRAS4PSCqual	Data quality flag for IRAS-4 from PSC (3 = best, 1 = limit)
A14	⋯	IRASFSCname	Name from IRAS Faint Source Catalog (FSC)
F6.2	mag	IRAS1FSCmag	Vega-based magnitude in IRAS-1 ([12]) from FSC; errors taken to be 0.22 mag
F9.2	Jy	IRAS1FSCfd	flux density in Jy in IRAS-1 from FSC
A2	mag	IRAS1FSCqual	Data quality flag for IRAS-1 from FSC (3 = best, 1 = limit)
F6.2	mag	IRA21FSCmag	Vega-based magnitude in IRAS-2 ([25]) from FSC; errors taken to be 0.22 mag
F9.2	Jy	IRAS2FSCfd	flux density in Jy in IRAS-2 from FSC
A2	mag	IRAS2FSCqual	Data quality flag for IRAS-2 from FSC (3 = best, 1 = limit)
F6.2	mag	IRAS3FSCmag	Vega-based magnitude in IRAS-3 ([60]) from FSC; errors taken to be 0.22 mag
F9.2	Jy	IRAS3FSCfd	flux density in Jy in IRAS-3 from FSC
A2	mag	IRAS3FSCqual	Data quality flag for IRAS-3 from FSC (3 = best, 1 = limit)
F6.2	mag	IRAS4FSCmag	Vega-based magnitude in IRAS-4 ([100]) from FSC; errors taken to be 0.22 mag
F9.2	Jy	IRAS4FSCfd	flux density in Jy in IRAS-4 from FSC
A2	mag	IRAS4FSCqual	Data quality flag for IRAS-4 from FSC (3 = best, 1 = limit)
A28	⋯	AKARIIRCname	Name from AKARI IRC catalog, v1
F9.2	Jy	AKARI9fd	flux density in Jy in 9 microns from AKARI IRC
F9.2	Jy	AKARI9fderr	error in flux density in Jy in 9 microns from AKARI IRC
F9.2	Jy	AKARI18fd	flux density in Jy in 18 microns from AKARI IRC
F9.2	Jy	AKARI18fderr	error in flux density in Jy in 18 microns from AKARI IRC
A28	⋯	AKARIFISname	Name from AKARI FIS catalog, v1
F9.2	Jy	AKARI65fd	flux density in Jy in 65 microns from AKARI FIS
F9.2	Jy	AKARI65fderr	error in flux density in Jy in 65 microns from AKARI FIS
F9.2	Jy	AKARI90fd	flux density in Jy in 90 microns from AKARI FIS
F9.2	Jy	AKARI90fderr	error in flux density in Jy in 90 microns from AKARI FIS
F9.2	Jy	AKARI140fd	flux density in Jy in 140 microns from AKARI FIS
F9.2	Jy	AKARI140fderr	error in flux density in Jy in 140 microns from AKARI FIS
F9.2	Jy	AKARI160fd	flux density in Jy in 160 microns from AKARI FIS
F9.2	Jy	AKARI160fderr	error in flux density in Jy in 160 microns from AKARI FIS
A18	⋯	MSXname	Name from MSX catalog
F9.2	Jy	MsxAfd	flux density in Jy in MSX Band A (7.76 μm)
F9.2	Jy	MsxAfderr	error in flux density in Jy in MSX Band A (7.76 μm)—as reported, may be very large
F9.2	Jy	MsxB1fd	flux density in Jy in MSX Band B1 (4.29 μm)

Format	Units	Label	Explanations
F9.2	Jy	MsxB1fderr	error in flux density in Jy in *MSX* Band B1 (4.29 μm)—as reported, may be very large
F9.2	Jy	MsxB2fd	flux density in Jy in *MSX* Band B2 (4.35 μm)
F9.2	Jy	MsxB2fderr	error in flux density in Jy in *MSX* Band B2 (4.35 μm)—as reported, may be very large
F9.2	Jy	MsxCfd	flux density in Jy in *MSX* Band C (11.99 μm)
F9.2	Jy	MsxCfderr	error in flux density in Jy in *MSX* Band C (11.99 μm)—as reported, may be very large
F9.2	Jy	MsxDfd	flux density in Jy in *MSX* Band D (14.55 μm)
F9.2	Jy	MsxDfderr	error in flux density in Jy in *MSX* Band D (14.55 μm)—as reported, may be very large
F9.2	Jy	MsxEfd	flux density in Jy in *MSX* Band E (20.68 μm)
F9.2	Jy	MsxEfderr	error in flux density in Jy in *MSX* Band E (20.68 μm)—as reported, may be very large

(This table is available in its entirety in machine-readable and Virtual Observatory (VO) forms.)

the one-to-one catalog matching feature in the IRSA catalog search tool. Significant issues with images and SEDs will be discussed in the next section (Section 4).

3.2. Primary Catalogs

The 2MASS (Skrutskie et al. 2006) obtained data over the whole sky at JHK_s bands. We found matches to most of our sources well within $1''$—a histogram of distances peaks strongly below $0''.2$. However, $\sim$10% of the targets (largely those still having original coordinates from *IRAS*) required larger (by-eye) matches, up to $15''$ away. Many of our targets are quite bright and are therefore saturated in the 2MASS catalog. For most of these, we can obtain at least estimates of K_s from the Naval Observatory Merged Astrometric Dataset (NOMAD; Zacharias et al. 2005), though empirically we have found that the errors as reported there are likely significantly underestimated, perhaps representing statistical errors only (not including systematics). For one source, the JHK_s brightnesses had to be retrieved from the extended source catalog (rather than the point source catalog; PSC). For many of our bright targets, the formal photometric quality as reported in 2MASS may be poor, but the points are in good agreement with the rest of the SED assembled here. We thus retained 2MASS measurements even if the photometric quality was deemed poor by the 2MASS pipeline. (About 60% of the sources with 2MASS counterparts have K_s photometric quality "A"; $\sim$35% have nominal photometric quality "D" or worse.) Limits reported in the catalog were retained as limits here.

2MASS provides the coordinate system to which other catalogs including *WISE* are anchored, so, given the very close positional matches for 2MASS, we expected (and found) comparable high-quality matches with those other catalogs.

IRAS surveyed the sky in 1983 in four bands, 12, 25, 60, and 100 μm. As the first all-sky infrared survey, it is relatively low spatial resolution and relatively shallow. The PSC (Beichman et al. 1988) reports on sources smaller than $0'.5$–$2'$ in the inscan direction (where the native survey pixels are rectangular). The typical FWHM of sources in the *IRAS* Sky Survey Atlas (ISSA) data products (which is what appears in FinderChart) is $3'.4$–$4'.7$.[9] The *IRAS* Faint Source Catalog (FSC; Moshir et al. 1992) is a reprocessing of the *IRAS* data that obtains, among other things, better positional accuracy and reaches fainter flux densities. We searched both the *IRAS* PSC and FSC for counterparts to our sources. Since the dlR97 sources were selected based on *IRAS* properties, all of them have detections

in the PSC, and 36 are also detected in the FSC. Nearly half (103/235) of our remaining sources have *IRAS* detections in either the PSC or FSC in any band, though only about a third of the C12 sources have an *IRAS* detection (in any band). Overall, 181 have sources in either the PSC or FSC, and 99 have counterparts in both the PSC and FSC.

The *IRAS* data (where available) for our targets appear in Table 1. We used the non-color corrected flux density at the various bands as reported in the catalogs, and used the Vega zero points as reported in the online *IRAS* documentation[10] to convert the flux densities to magnitudes, namely 28.3, 6.73, 1.19, and 0.43 Jy for the four bands, respectively. No errors are reported, so we took a flat 20% flux density uncertainty, which is 0.22 mag. We merged catalogs without regard to flux quality, though the quality is noted in our catalog. Nearly all of the detected sources are the highest quality (qual = 3) in both the PSC and FSC at 12 μm, but >80% of these sources are the *lowest* quality in the PSC and FSC at 100 μm (qual = 1). The lowest quality measurements are, according to the documentation, meant to be limits. In some cases, even the nominal limits are in good agreement with detections from other instruments. We retained the measurements and the flux quality flags in our database.

WISE surveyed the whole sky at 3.4, 4.6, 12, and 22 μm; all of the available *WISE* data taken between 2010 January and 2011 February were incorporated into the AllWISE catalog (Cutri et al. 2014), which we used for this work. In three cases, brightnesses for a target had to be retrieved from the AllWISE catalog of rejects. Since the dlR97 sources were selected based on the relatively shallow *IRAS* data, many were saturated in at least one *WISE* band; many fewer of the C12 sources were saturated. Of the *WISE* detections, only those with data quality flags "A," "B," or "C" were retained, but most detections were "A" or "B"; the fraction of detections with data quality flag "C" is 10%, 5%, 1%, and 3% for the four *WISE* channels, respectively. For many of our very bright targets, the formal photometric quality as reported in *WISE* may be poor, but the points are in good agreement with the rest of the SED; limits from the catalog were retained in our database.

Given the relatively low spatial resolution of *IRAS* compared to 2MASS or *WISE*, we did not necessarily expect to find very close positional matches to sources with solely *IRAS* positions. However, many sources whose coordinates were the original *IRAS* positions found very close matches in 2MASS and/or *WISE*, demonstrating the high quality of those original *IRAS* positions. The places where *IRAS* did not match well were

---

[9] http://irsa.ipac.caltech.edu/IRASdocs/issa.exp.sup/ch1/C.html

[10] http://irsa.ipac.caltech.edu/IRASdocs/exp.sup/ch6/C2a.html

Table 2
Overview of Photometric Studies and Data Included

Dataset	Band(s) Used	Search Radius[a] ($''$)	Fraction with Match	Notes
2MASS	JHK_s (1.2–2.2 μm)	1[b]	304/316 = 96%	primary catalog; many saturated
WISE	3.4, 4.5, 12, 22 μm	1	311/316 = 98%	primary catalog; many saturated in part. ($\sim$20% of sample required $>1''$ counterpart match)
IRAS	12, 25, 60, 100 μm	<20	PSC: 159/316 = 50%; FSC: 121/316 = 38%	data used for original de la Reza studies
AKARI	9, 18, 65, 90, 140, 160 μm	1	IRC: 221/316 = 70%; FIS: 36/316 = 11%	supplementary data ($\sim$20% of IRC sources that had matches required $>1''$ counterpart match, most of the FIS required $>1''$.)
MSX	4.3, 4.4, 7.8, 12.0, 14.6, 20.6 μm	20	54/316 = 17%	supplementary data
SEIP	3.6, 4.5, 5.8, 8, 24 μm	1	39/316 = 12%	very low fractional coverage
DENIS	0.82, 1.25, 2.15 μm	1	83/316 = 26%	provides deeper K_s than 2MASS; only 58 have K_s, and none of those are lacking in 2MASS K_s
SDSS	$ugriz$ (0.29–0.91 μm)	2	94/316 = 30%	supplementary data
NOMAD, C12	$UBVR$ (0.36–0.7 μm)	1	277/316 = 88%	literature data from NOMAD or C12

Notes.

[a] Characteristic distance to source match; some sources with poor positions required a much larger search radius.

[b] Most sources found a match within $1''$ (histogram of distances peaks strongly below $0\rlap{.}''2$), but $\sim$10% required larger (by-eye) matches.

largely those where source confusion pulled the photocenter position off from the brightest source in *WISE*; see additional discussion on source confusion issues below.

All of the abundances and associated information (T_{eff}, log g) were most often taken from the papers reporting the star as Li-rich—see the Appendix table for the specific literature reference. We allowed A(Li) from the non-local thermodynamic-equilibrium (NLTE) estimates to take precedence over LTE estimates, but in some cases, only LTE abundances were available. In a few cases, only Li equivalent widths were available in the literature, in which case we did not even attempt to estimate an A(Li), and thus the sources are effectively dropped from analysis requiring A(Li). In ~20 cases, McDonald et al. (2012) provided a T_{eff} estimate when no other was available from the literature. For the 14 stars with super-solar metallicities in C12, we provide corrected NLTE abundances here.

3.3. Secondary Catalogs

The *AKARI* mission (Murakami et al. 2007) surveyed the sky in 2006–2007, in wavelengths between 1.8 and 180 μm using two instruments, the Infrared Camera (IRC) and the Far-Infrared Surveyor (FIS). We searched the IRC catalog for counterparts at 9 and 18 μm, and the FIS catalog for counterparts at 65, 90, 140, and 160 μm. A large fraction (~70%) of our sources have a counterpart in at least one IRC band; relatively few (~11%) of our sources have a counterpart in at least one FIS band. The *AKARI* data cover the whole sky, and can provide valuable data to help populate the SEDs of our targets. For the majority of targets where we have *AKARI* counterparts, the *AKARI* data are consistent with *WISE* and/or *IRAS* measurements. We did not sort the *AKARI* matches by photometric quality; because our sources are bright, even those with low photometric quality flags matched the existing SED quite well. For the FIS sources where the photometric quality is the lowest, no errors are given, so we adopted a conservative uncertainty of 50% for those sources.

The *Midcourse Space Experiment* (*MSX*; Egan et al. 2003) surveyed the Galactic Plane in 1996–1997 at several bands between 8 and 21 μm—Band A = 7.76 μm, $B1$ = 4.29 μm, $B2$ = 4.35 μm, C = 11.99 μm, D = 14.55 μm, and E = 20.68 μm. The spatial resolution of these images range from 20″ to 72″. Relatively few (just 54) of our targets have *MSX* counterparts, in no small part because of sky coverage, but the lower sensitivity of the *MSX* instruments also plays a role. The errors we report in Table 1 are the errors reported in the *MSX* catalog, and as such may be very large.

The Deep Near Infrared Survey of the Southern Sky (DENIS) conducted a survey of the southern sky at *I*, *J*, and *K* bands. It is deeper than 2MASS. In several cases, because the search radius for a counterpart had to be large, it was clear upon construction of the SEDs that the nearest source by position was not the best match (often because a fainter source was closer to the given position than the real target), and so the match was rejected. In the end, only 58 of our targets have a K_s magnitude from DENIS, and none of those are lacking a 2MASS K_s. Therefore, the DENIS measurements do not play a role in identification of IR excesses, but were retained in those few cases to better define the SED.

The entire archive of photometric 3–24 μm cryogenic-era *Spitzer Space Telescope* (Werner et al. 2004) data has been reprocessed and images and source lists released as part of the Enhanced Imaging Products (SEIP). *Spitzer* is generally more sensitive (and has higher spatial resolution) than *WISE* or *AKARI*. However, the SEIP source list is limited to those with signal-to-noise ratios greater than 10. Because *Spitzer* is a pointed mission, the entire sky is not covered, and only 12% of our sources have counterparts in the SEIP source list. These measurements were retained in those few cases specifically because they are higher spatial resolution, and can provide valuable insight into the reliability of the flux densities provided by *IRAS*, *AKARI*, and *WISE*. We have found that the errors as reported in the SEIP are likely statistical and probably do not include a calibration uncertainty floor. We have added 4% errors in quadrature to the reported errors.

The SDSS (see, e.g., Ahn et al. 2014 and references therein) has surveyed a significant fraction of the sky at *ugriz* (optical) bands. These data, where available, help define the Wien side of our objects' SEDs; they do not aid in calculation of IR excesses, but they "guide the eye" to identify the photosphere. About 30% of our targets have SDSS counterparts in at least one band. Several more of our targets appear in SDSS images, but are far too bright for reliable photometry. We used images and photometry as retrieved via IRSA's FinderChart.

The Digitized Sky Survey (DSS) is a digitization of the photographic sky survey plates from the Palomar (the Palomar Observatory Sky Survey, POSS) and UK Schmidt telescopes. We used images from the DSS retrieved via IRSA's FinderChart to check on source confusion and multiplicity.

NOMAD reports broadband optical photometry for most of our targets; C12 reports optical photometry for their targets. Those values were included in our database, as for the SDSS optical data above, to define the short-wavelength side of the SED.

4. DROPPED SOURCES

In this section, we describe the set of targets that we have to drop from our dataset because they are not detected at sufficient bands (Sections 4.1, 4.2), or that are likely subject to source confusion where the *IRAS* detection is likely composed of more than one source, or where the bright source in POSS is not responsible for the IR flux (Section 4.3). The 24 sources we identify as subject to source confusion come from studies with sources first identified in the low spatial resolution *IRAS* data and followed up in the optical.

4.1. Sources with Very Sparse SEDs

There are 10 sources that do not appear in many of the catalogs we used here, such that they have very sparsely populated SEDs. These SEDs are sparse enough that they cannot be handled in the same way as the other sources in the set—they have no K_s or [22] measures, and sometimes no *WISE* data at all. These sources are listed in Table 3. All of these very sparse SED stars are from Kirby et al. (2012), and are in dwarf spheroidal galaxies. They are just too far away to be detected in enough bands in the surveys we used. Comments on these objects appear in Table 3. For each source, we inspected the SED and the photometry, looking for any evidence of IR excess at the available bands, and found none.

These 10 sparse SED sources are, of necessity, frequently dropped from subsequent figures and discussion here. We reiterate, however, that they are all from the "addtional literature" sample; none are from C12 or dlR97.

Table 3
Objects with Sparse SEDs

Name	Very Sparse SED?[a]	IR Excess?[b]	Notes
Scl 1004838	x	⋯	Distant object; not well-populated SED. No evidence for IR excess.
Scl 1004861	x	⋯	Distant object; not well-populated SED. No evidence for IR excess.
For 55609	⋯	⋯	No W3W4 but 3 IRAC bands; no evidence for excess.
For 60521	⋯	⋯	No W3W4 but 3 IRAC bands; no evidence for excess.
For 90067	⋯	x	No W3W4, but all 4 IRAC bands. Excess possible at 8 μm despite large error. Following the approach in Section 5.4 below, but customized to this star, $\chi_{K,[8]}$ is 3.1.
For 100650	x	⋯	Distant object; not well-populated SED. No evidence for IR excess.
G0300+00.29	⋯	⋯	No W4; no evidence for excess
SDSS J0304+3823	⋯	⋯	No W3W4; no evidence for excess
RAVEJ043154.1−063210	⋯	⋯	No W4; no evidence for excess
G0453+00.90	⋯	⋯	No W4; no evidence for excess
SDSS J0535+0514	⋯	⋯	No W4; no evidence for excess
Be 21 T50	⋯	⋯	No W4; no evidence for excess
SDSS J0632+2604	⋯	x	No W4; W3 suggests most likely has excess ([3.4]–[12] = 1.45).
Tr5 3416	⋯	⋯	No W4; colors suggest could have small excess at [12] ([3.4]–[12] = 0.41); following the approach in Section 5.4 below, but customized to this star, $\chi_{[3.4],[12]} = 1.97$, not significant.
SDSS J0654+4200	⋯	⋯	No W4; no evidence for excess
G0653+16.552	⋯	⋯	No W4; no evidence for excess
G0654+16.235	⋯	⋯	No W4; no evidence for excess
SDSS J0720+3036	⋯	⋯	No W3W4; no evidence for excess
SDSS J0808−0815	⋯	⋯	No W4; no evidence for excess
SDSS J0831+5402	⋯	⋯	No W3W4; no evidence for excess
SDSS J0936+2935	⋯	⋯	No W3W4; no evidence for excess
G0935−05.152	⋯	⋯	No W4; no evidence for excess
G0946+00.48	⋯	⋯	No W4; no evidence for excess
LeoI 71032	x	⋯	Distant object; not well-populated SED. No evidence for IR excess.
LeoI 60727	x	⋯	Distant object; not well-populated SED. No evidence for IR excess.
LeoI 32266	x	⋯	Distant object; not well-populated SED. No evidence for IR excess.
LeoI 21617	x	⋯	Distant object; not well-populated SED. No evidence for IR excess.
C1012254-203007	⋯	⋯	No W4; no evidence for excess
SDSS J1105+2850	⋯	⋯	No W3W4; no evidence for excess
LeoII C-7-174	x	⋯	Distant object; not well-populated SED. No evidence for IR excess.
LeoII C-3-146	x	⋯	Distant object; not well-populated SED. No evidence for IR excess.
G1127−11.60	⋯	⋯	No W4; no evidence for excess
M68-A96 = Cl* NGC 4590 HAR 1257	⋯	⋯	No W4, but all 4 IRAC bands. No evidence for excess.
SDSS J1310−0012	⋯	⋯	No W3W4; no evidence for excess
CVnI 195_195	⋯	⋯	No W3W4, but 3 IRAC bands. No evidence for excess.
CVnI 196_129	x	⋯	Distant object; not well-populated SED. No evidence for IR excess.
M3-IV101 = Cl* NGC 5272 SK 557	⋯	⋯	No W4, but all 4 IRAC bands. No evidence for excess.
SDSS J1432+0814	⋯	⋯	No W3W4; no evidence for excess
SDSS J1522+0655	⋯	⋯	No W3W4; no evidence for excess
SDSS J1607+0447	⋯	⋯	No W3W4; no evidence for excess
SDSS J1901+3808	⋯	⋯	No W4; no evidence for excess
SDSS J1909+3837	⋯	⋯	No W4; no evidence for excess
KIC 4937011	⋯	⋯	No W4, but all 4 IRAC bands. No evidence for excess.
SDSS J2019+6012	⋯	⋯	No W4; no evidence for excess
SDSS J2200+4559	⋯	⋯	No W4; no evidence for excess
SDSS J2206+4531	⋯	⋯	No W4; no evidence for excess

Notes.
[a] This column is populated if the SED is very sparse (Section 4.1).
[b] This column is populated if the object could have an IR excess by 8–12 μm (Section 4.2).

4.2. Sources with Relatively Sparse SEDs Beyond 10 μm

There are 36 sources that have relatively well-populated SEDs, but are missing detections past 10 or 20 μm. We cannot treat those sources in exactly the same way as the rest of the stars in the set, but at least we can constrain whether or not there is an IR excess, more so than for the stars in the previous section. These sources are listed in Table 3. There are two sources for which an IR excess cannot be ruled out given the available detections. The star known as "For 90067" could be consistent with an IR excess at 8 μm, given the available IRAC data, but the error on the [8] point is large. (Following the approach below in Section 5.4, but customized to this star, $\chi_{K,[8]}$ is 3.1.) SDSS J0632+2604 has a much more convincing excess, with [3.4]–[12] = 1.45.

These sources do not often appear in the subsequent figures and discussion, because they are, for example, missing [22], and thus cannot appear in a figure plotting [3.4]–[22]. However, the two possible excess sources here are sometimes included in the counts of sources with IR excesses, and where we do so, we note it explicitly. Nearly all of these sources (26/36) are objects we take to be Li-rich. Of these, SDSS J0632 +2604 has the largest IR excess and also the largest Li abundance, with $A(\mathrm{Li})_\mathrm{LTE} = 4.2$ dex.

None of these relatively sparse sources are from the dlR97 sample. Seven of them are from C12, and the remainder are from the "addtional literature" sample.

4.3. Source Confusion

As mentioned above, it is often the case that a bright source in *IRAS* is also a bright source in the optical, but sometimes this is not a good assumption. Now that 2MASS and *WISE* images are available, it is far easier than it was in the 1990s to identify sources over 3 orders of magnitude in wavelength (0.5–100 μm). In 24 of our targets, we believe that there are likely issues of source confusion. In these cases, at least one of the following things can be seen in the images: (a) the IR excess seen in the *IRAS* images is due to more than one *WISE* (or 2MASS) source, likely unresolved in the *IRAS* catalog; or (b) the nearest bright source in POSS, which is most likely the source for which an optical spectrum to measure lithium was obtained, is not responsible for most of the IR flux density detetected via *IRAS*.

For the first kind of source confusion, where the IR excess seen in *IRAS* is due to more than one *WISE* source, understanding the original *IRAS* resolution is important, because these issues of *IRAS* spatial resolution can be subtle. Figure 1 shows a *WISE* 12 μm image of one of our targets, IRAS06365+0223, with circles overlaid to represent the various possible *IRAS* resolutions. The image is $300'' = 5'$ on a side. The original *IRAS* PSC was derived from images that had pixels that were substantially rectangular, but included sources believed to be point sources with sizes less than $\sim 0\rlap.{'}5$–$2\rlap.{'}0$ *in the in-scan direction.*[11] The small green circle in Figure 1 is representative of this 12 μm $0\rlap.{'}5$ resolution, and the large blue circle is representative of this 100 μm $2'$ resolution. Note that these are shown in the figure as circles, whereas in reality, this resolution is only obtained in the in-scan direction, which is roughly along lines of ecliptic longitude; the resolution is considerably worse in the cross-scan direction. (For this target, lines of ecliptic longitude are locally about 5° east of north, but this angle varies over the sky.) The typical FWHM of sources in the ISSA data products (ISSA images are shown in FinderChart) is $3\rlap.{'}4$–$4\rlap.{'}7$[12], which is represented by the large red circle in Figure 1 at $3\rlap.{'}4$ (diameter). The multiple sources seen in this *WISE* image, for example, are likely convolved together for at least some of the *IRAS* measurements. This is an important factor in several of the *IRAS* sources we discuss in this section, meaning that the IR flux attributed to a single optical source may not be correct, and the IR excess previously measured for a given optical source may be significantly overestimated.

The second kind of source confusion, where the bright source in POSS is not responsible for the IR flux, is source
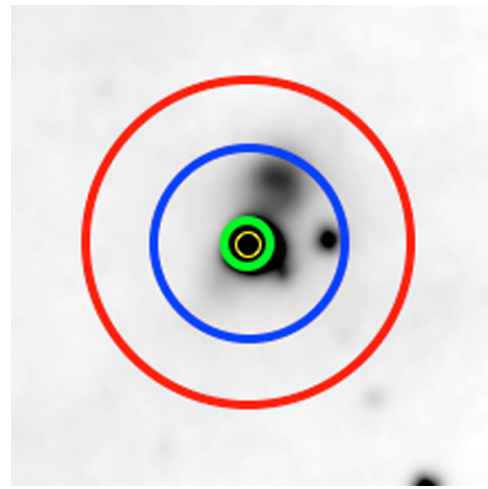

Figure 1. Image of IRAS06365+0223 in [12], reverse grayscale, $300''$ on a side as most of the subsequent image postage stamps are. The circles represent the range of *IRAS* spatial resolutions; see text for more discussion. The red circle is $3\rlap.{'}4$ in diameter, representative of the typical FWHM of shorter-wavelengths sources in the ISSA images. The blue circle and the green circle are 2 and $0\rlap.{'}5$ in diameter, and represent the in-scan direction resolution of the *IRAS* PSC. The small yellow circle here is $15''$ in diameter, representative of the "target" blue circle in subsequent $300''$ images. (It is yellow instead of blue just for enhanced visibility in this reverse grayscale image.)

confusion of a different nature. In many cases, it is a good assumption that the bright source in *IRAS* is also the bright source in POSS. However, in a significant number of cases, all the sources in the region are of comparable brightness in POSS, or the optically bright source is not the source of most of the IR light. Now that 2MASS and *WISE* are available, we can trace the source across wavelengths to securely identify the optical counterpart in the POSS images. In these cases, however, the spectrum obtained to assess lithium may very well have been of the bright POSS source, and not of the origin of the IR flux at all, especially in those cases where no optical counterpart can be found in the POSS images.

To demonstrate these issues of source confusion, we provide POSS, 2MASS, and *WISE* images for each of the 24 targets in Figures 2–7, specifically to allow readers to follow the same sources across wavelengths. (The FITS images can be interactively explored via IRSA's FinderChart.) For each of these figures, either a multi-color or single band image appears for each of POSS, 2MASS, and *WISE*, and the images are $300''$ on a side unless specified. For POSS, it is either DSS2 Blue/ Red/IR for the blue, green, and red bands, respectively, or it is a single-band DSS2 Red. For 2MASS, JHK_s corresponds to blue/green/red, respectively, and for *WISE*, [3.4], [4.5], and [12] correspond to blue/green/red unless specified. The source position is indicated with a small blue circle; white or black hash marks above and to the left help guide the eye to this position. A brief discussion of each of these sources appears in Table 4; a briefer still summary appears in the figure itself and the caption.

SEDs for these 24 sources appear in Figures 8 and 9. These SEDs correspond in most cases to the source position measured in *IRAS*, but may or may not be the origin of all of the *IRAS* flux density, or correspond to the optically bright source. Because we are matching sources largely by position to the sources in the catalogs, in several of the cases illustrated in Figures 2–7 where the true counterpart is is impossible to match, the counterparts across catalogs are not the same source, and the SED clearly

---
[11] http://irsa.ipac.caltech.edu/IRASdocs/exp.sup/ch5/A2.html
[12] http://irsa.ipac.caltech.edu/IRASdocs/issa.exp.sup/ch1/C.html

IRAS06365+0223
(WISE: b,g,r=[4.6],
[12],[22])
Small source
(resolved @JHK) is
source of IR emission

IRAS07419-2514
Multiple sources

IRAS09553-5621
Two sources

IRAS11044-6127
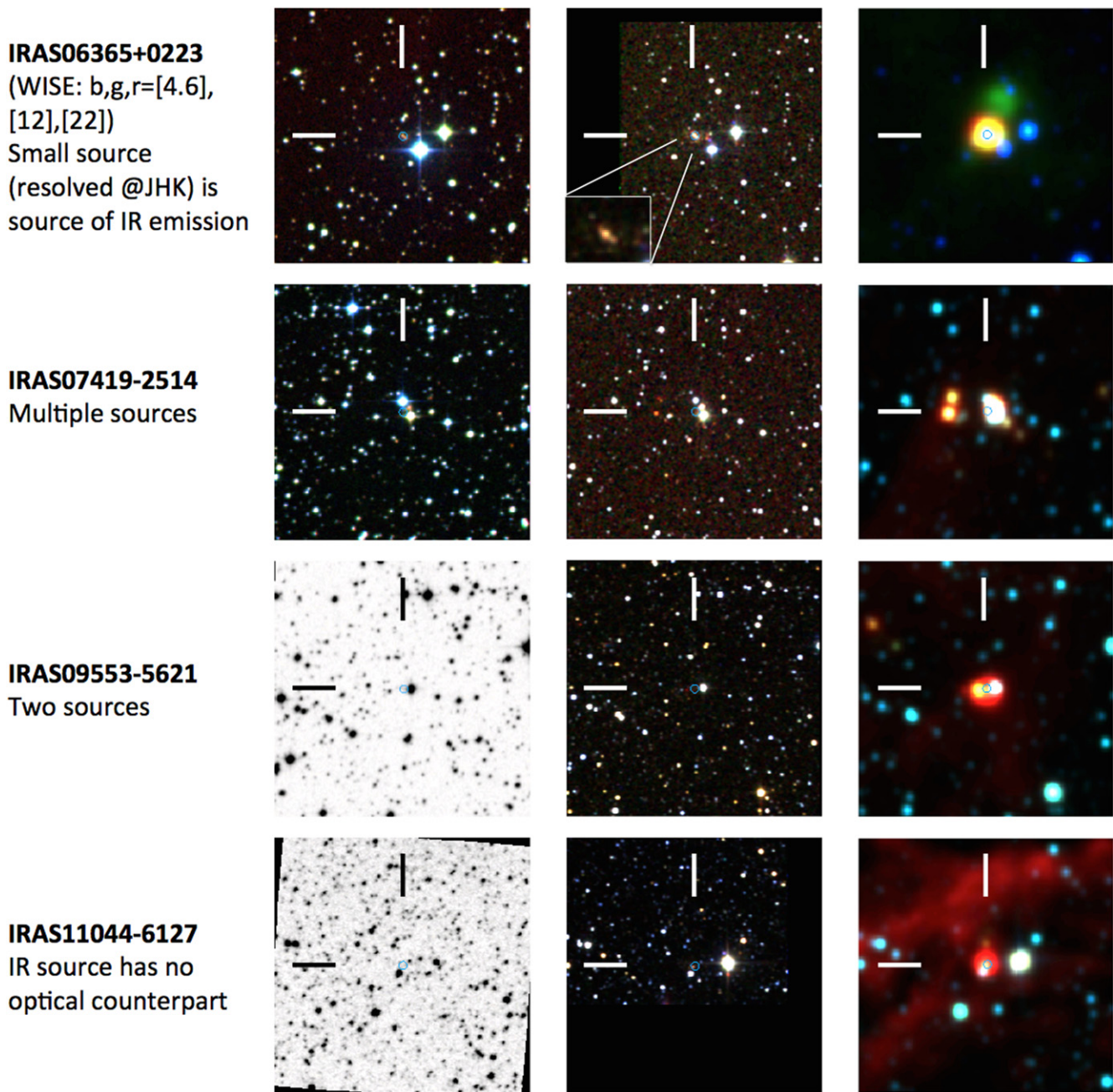IR source has no
optical counterpart

Figure 2. First image column: POSS 3-color (DSS2 Blue/Red/IR for $b/g/r$ planes), or it is a single-band reverse grayscale DSS2 Red. Second image column: 2MASS JHK_s color image. Third image column: *WISE* [3.4], [4.6], [12] for $b/g/r$, respectively, unless specified. Images are all $300''$ on a side unless specified. North-up. Small blue circle centered on position used for the target, and white/black hash marks above and to the left help guide the eye to this position. Four rows are: (1) IRAS06365+0223, where the 2MASS image has an additional inset with an enlargement of the source of the IR flux, and *WISE* has $b, g, r = $ [4.6], [12], [22]. The target position is correctly the source of most of the long-wavelength flux, but is not a match to either of the optically bright sources. (2) IRAS07419–2514. The target position is in among a small cluster of sources, and corresponds to the photocenter of the aggregate source seen by *IRAS*. (3) IRAS09553–5621. The target position is in between two sources bright at *WISE* bands, but only one source appears at K_s. That source that appears at K_s also appears in POSS images. The sources are not separable at [22], and are likely both contributing to the measured *IRAS* flux density. (4) IRAS11044–6127. There is no easily visible source at the target position in POSS; the bright source seen as white immediately to the west of the target is the brightest source in the field in the DSS-IR and 2MASS, but it is comparably bright to the other stars in DSS.

betrays this conglomeration of sources (see notes in Table 4). IRAS18334–0631(PDS 524) (Figure 9, 3rd row center) is the clearest example of this, where *AKARI* and *MSX* are seeing the same source, but it is a different source than the source that 2MASS, DENIS, and *WISE* identify, both of which are inconsistent with the flux densities measured in *IRAS*.

Eight of these sources have SEDs that do not resemble isolated stars. They rise steadily from 1 to 20 or even 100 μm and beyond. These would be SEDs consistent with extragalactic sources, or very heavily obscured stars of any age. These sources are noted in Table 4; IRAS16128–5109 is one of the best examples (Figure 8, 3rd row center). This source has measurements from 2MASS, *WISE*, *MSX*, *AKARI*, and *IRAS*, with the energy density at $\sim$20 μm being $\sim$5 orders of magnitude larger than the energy density at $\sim$1 μm. The *IRAS* data suggest a rollover in this SED near 60 μm. Most of these
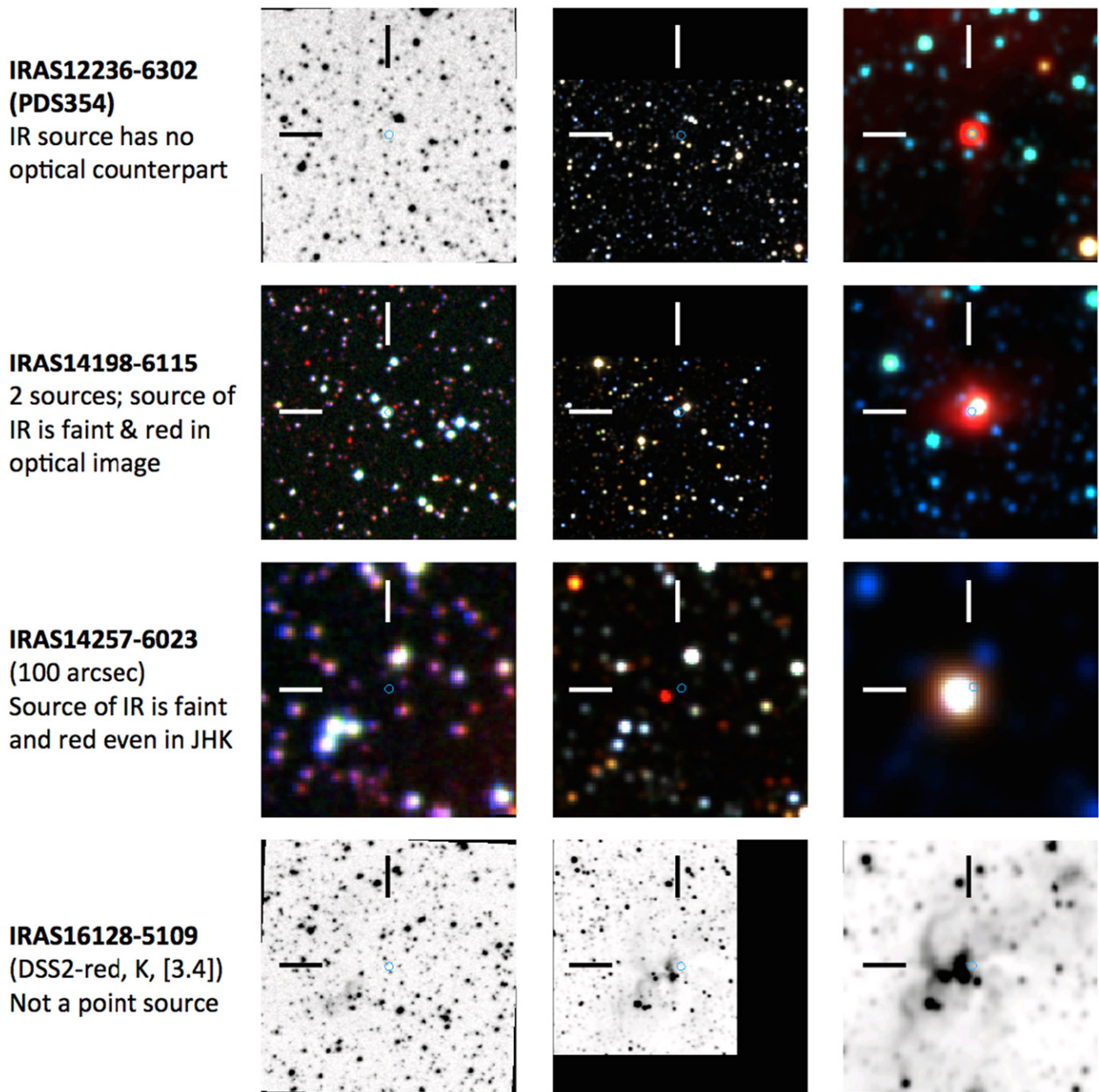
Figure 3. (Notation is as in Figure 2.) Four rows are: (1) IRAS12236–6302 (PDS 354). The blue arc immediately above the target in *WISE* can be seen to be three distinct sources in 2MASS and, combined, are the brightest thing in the POSS 300″ images. These sources are not responsible for most of the IR flux measured at the target position. (2) IRAS14198–6115. There are two sources here that are distinct in 2MASS and marginally resolved in [3.4], but are indistinguishable by [22]. (3) IRAS14257–6023. Images are 100″ on a side to better show the source that is very red in 2MASS and is dominating the measured flux by *WISE* bands. The brightest source in POSS is the source appearing as white in 2MASS to the north and slightly west of the target position, but it is not responsible for the IR flux. (4) IRAS16128–5109. This is not a point source in the IR, and is very bright (saturated in *WISE*) by [22]. Single bands are shown in the optical, NIR, and MIR to better show the nebulosity.

steep SEDs turn over at long wavelengths, but two of these eight sources have a peak in the SED at $\sim$22–25 μm, shorter than the others. These two sources, IRAS17582–2619 and IRAS19083+0119(PDS 562), could be of a different nature than the others.

One of these sources, IRAS17211–3458, is worthy of a few additional comments here because it is the most borderline of these source confusion cases. The images shown in Figure 5 (second row) show a small concave arc of sources in the optical near the target location; by H (middle panel), it is a convex arc

of sources, where only two sources (including our target) are bright in the POSS+2MASS images—they appear white in the 2MASS image in Figure 5. We identified source confusion here in part because these two sources are of comparable brightness at POSS, but also because *WISE* has trouble resolving the three close, IR-bright sources. *WISE* identifies some faint nebulosity here; in the *WISE* image in Figure 5, the surface brightness is barely visible. However, there are *Spitzer* data here too, which resolves complex striated nebulosity; see Figure 10. The *IRAS* target position is $\sim$2″ from the nearest 2MASS source, which is
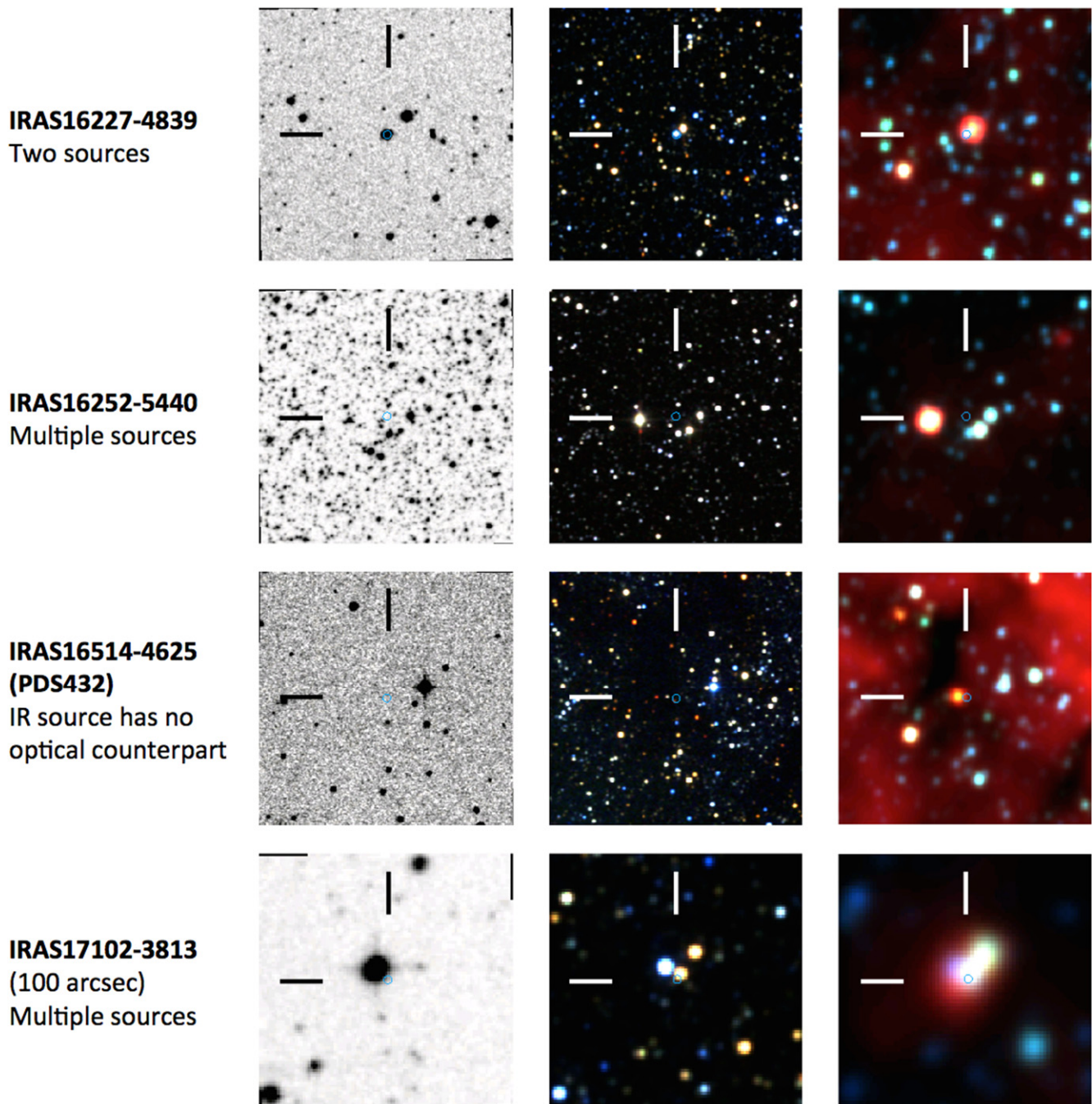
Figure 4. (Notation is as in Figure 2.) Four rows are: (1) IRAS16227–4839. There are two sources here that are resolved in 2MASS and marginally resolved at [3.4], but merged by [22], with the more northerly source dominating the IR flux. The more southerly source is brighter in POSS. (2) IRAS16252–5440. There is a cluster of sources that is responsible for the IR flux, with the target position at the photocenter. The field has no clearly dominant source in POSS. (3) IRAS16514–4625(PDS 432). A dark cloud is apparent in 2MASS and *WISE* . The brightest source in the optical is the center of the source seen in *WISE* as blue but not a point source because it aggregates three sources seen in 2MASS. The source that dominates by [22] is faint at [3.4]. (4) IRAS17102–3813. Images are $100''$ on a side to better show the trio of sources seen at JHK_s that become a smear dominated by the two sources to the southeast by [22]. The optically brightest source may contribute some but not all of the 22 μm flux density.

larger than typical uncertainties over the whole catalog. The *Spitzer* source corresponding to this object does not appear in the SEIP, perhaps because it either is or appears to be slightly resolved because of the high surface brightness nebulosity surrounding it. The SED (Figure 9, top center) is the source closest to the target position, where available. On the face of it, its shape would be consistent with a photosphere with large excess. That, plus the fact that there is a POSS source exactly at the location of the *IRAS* source (and is presumably the object

for which an optical spectrum to assess lithium was obtained), could conceivably place it in the set of objects with large excesses identified and discussed below. However, based on the images, bands longer than 12 μm (*WISE*, *MSX*, *AKARI*, *IRAS*) certainly are measuring net flux density from more than one point source, plus nebulosity near (in projection) to the source. This is also the point at which the SED starts to significantly diverge from the apparent photosphere. Because of this ambiguity, we have left it in the set of confused sources.
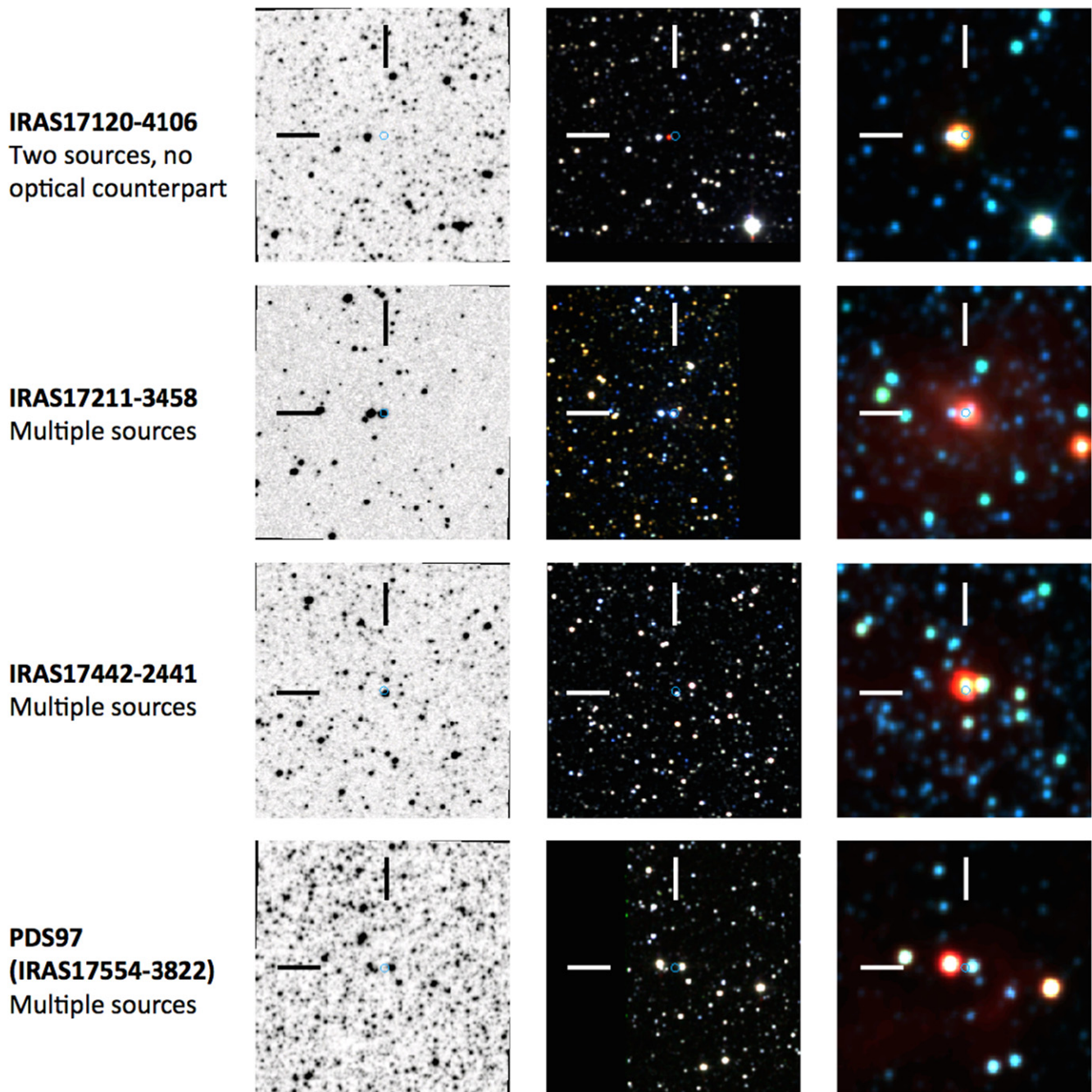
Figure 5. (Notation is as in Figure 2.) Four rows are: (1) IRAS17120−4106. Two sources are barely resolved at [3.4] that merge by [12] and [22]. There is no optical counterpart at the source position. (2) IRAS17211−3458. There are multiple sources that are barely resolved at [3.4], which merge at longer wavelengths. This is a complicated source; see the text. (3) IRAS17442−2441. Two sources at the source position are barely resolved at [3.4] that merge by [12] and [22] with each other and with other sources in the region. (4) PDS 97(IRAS17554−3822). Source position is in between two sources that are of comparable brightness at [3.4] (and, for that matter, POSS and 2MASS), with the easterly source dominating by [22].

It is not tagged as a Li-rich source in dlR97, so even if we were able to add it to the analysis we perform below, it is unlikely to have contributed significantly.

Because of the ambiguity about the sources and their counterparts, these 24 sources have to be dropped from our sample. IRAS07419−2514 was identified as a possible K giant in Torres et al. (2000), and PDS 97 (IRAS17554−3822) is from de la Reza et al. (1996). The remaining 22 sources compose ∼30% of the original dlR97 sample. We drop these sources from the bulk of our analysis, but show them in certain plots where relevant below.

5. SOURCES WITH IR EXCESSES BY ∼25 μm

5.1. Overview of Approach

Having omitted the objects for which we have substantial difficulty making matches across catalogs above, we have now a subset of objects for which we have established reliable multi-wavelength matches across catalogs. All of these objects have no or little ambiguity in the images to which we have access, e.g., they appear as clean point sources. We can now inspect the resultant assembled SEDs for evidence of an IR excess.
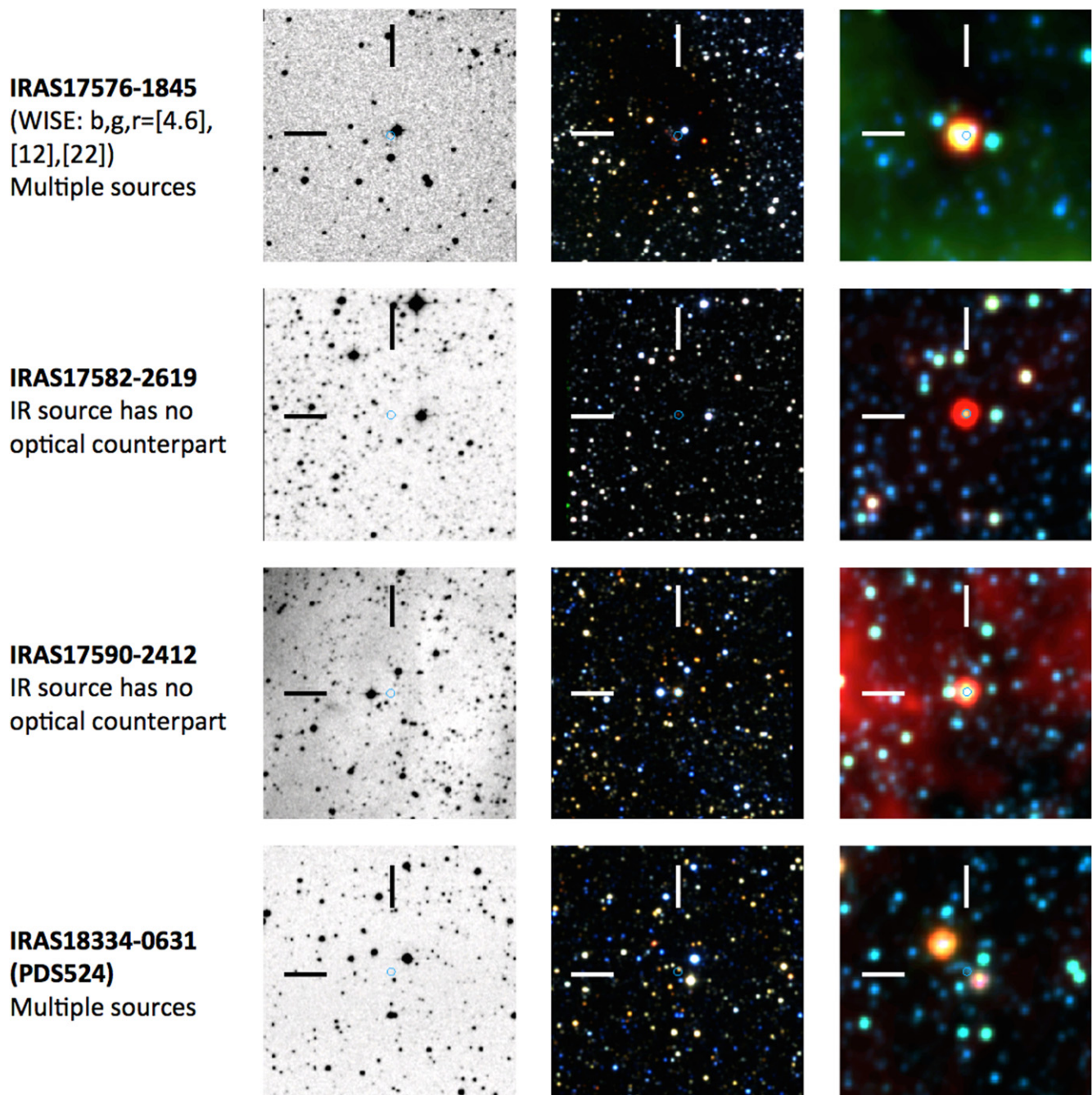
13

Figure 6. (Notation is as in Figure 2.) Four rows are: (1) IRAS17576–1845. The source dominating at [22] (and presumably *IRAS* bands) is smeary at [3.4]. The brightest source at POSS bands is not the source of the IR. (2) IRAS17582–2619. The brightest source in the IR has no optical counterpart, and is strongly dominated by the longest wavelengths. (3) IRAS17590–2412. The brightest source in the IR has no optical counterpart, and is strongly dominated by the longest wavelengths. Diffuse emission can also be seen. (4) IRAS18334–0631(PDS 524). There is no optical source at the target position; the target's *IRAS* flux has contributions from several sources in this viscinity, including the arc of blue in *WISE* precisely at the target position. The brightest POSS source is blue in *WISE*.

In assessing whether or not a star has an IR excess, one needs to compare a measure of brightness at relatively short wavelengths (expected to be dominated by the stellar photosphere) with that at relatively long wavelengths, where dust emission is likely to be present. We take a two-pronged approach to identifying excesses. There are some objects for which an IR excess is immediately apparent upon inspection of the SED; no detailed analysis is required. These objects are summarized in Section 5.2 and detailed in Section 5.3. There are other objects for which the IR excess is more subtle. For these latter objects, we employ an approach developed in the

context of finding small IR excesses around young stars, which is described in Section 5.4. Details of objects found to have these more subtle IR excesses can be found in Section 5.5. Table 5 summarizes the stars we identify as having either a large or small IR excess.

5.2. Overview: Sources with Very Large Excesses

There are 19 stars whose SEDs immediately reveal significant IR excesses at wavelengths $<20\,\mu$m, and maintain large excesses out to at least 25 μm. These sources
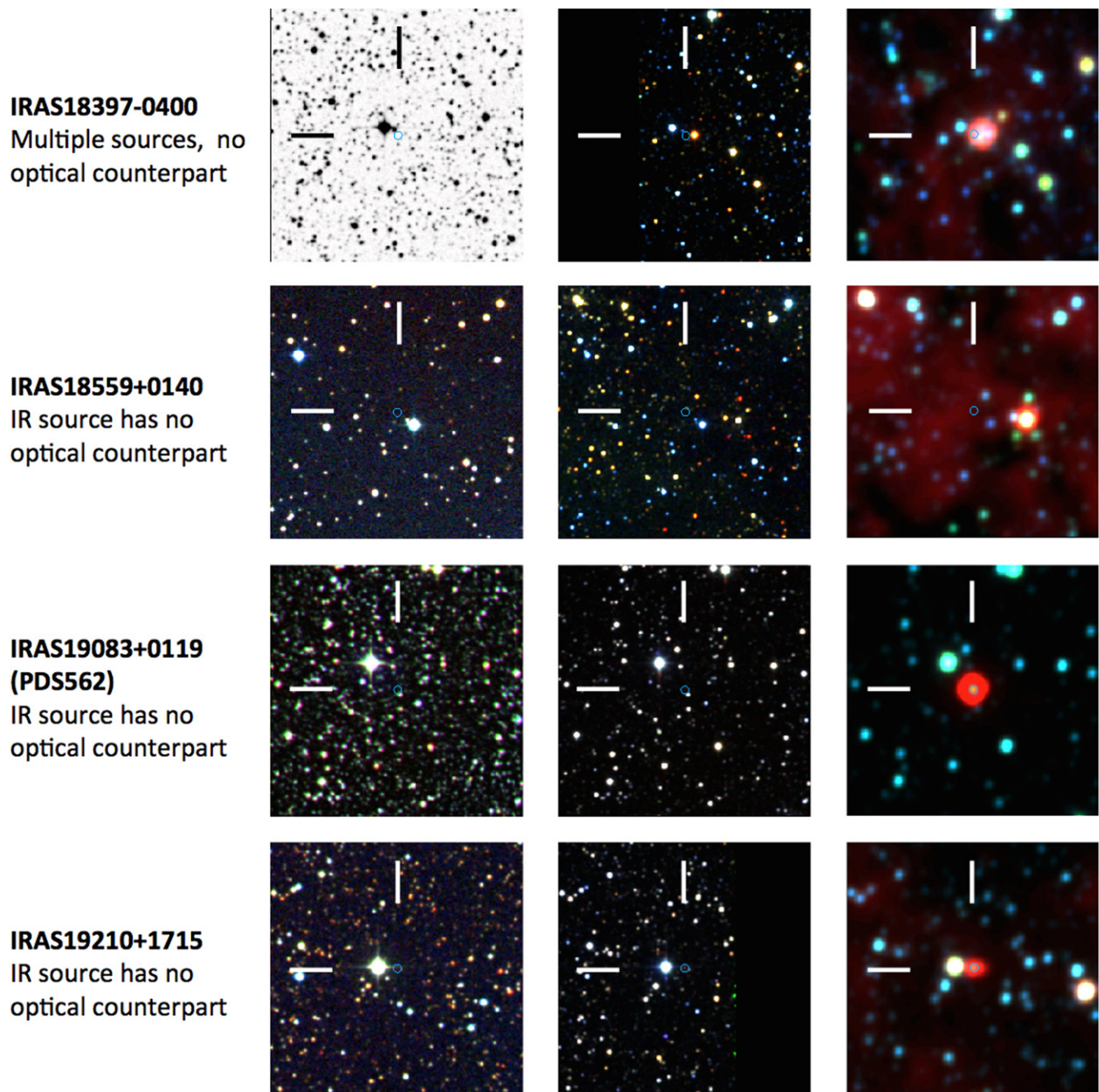
Figure 7. (Notation is as in Figure 2.) Four rows are: (1) IRAS18397–0400. The brightest source in the IR has no optical counterpart, and is dominated by the longest wavelengths. The brightest POSS source is blue in *WISE* . (2) IRAS18559+0140. There is no optical source at the target position; the bright POSS source to the southwest is not bright at all in the IR and is blue in the *WISE* data; the target's *IRAS* flux has contributions from several sources, most likely including the flux from the bright source to the upper left, pulling the photocenter off of the bright clump of sources to the right. (3) IRAS19083+0119(PDS 562). The brightest source in the IR has no optical counterpart, and is strongly dominated by the longest wavelengths. The brightest POSS source is blue in *WISE*. (4) IRAS19210+1715. There is no optical source at the target position; the bright POSS source to the east can be seen in the IR, but the target position matches the very red source to the west, which most likely dominates the *IRAS* flux.

often have detections in more surveys than just *WISE*; they often have data from *MSX*, *AKARI*, *IRAS*, and even *Spitzer*. Over the entire sample, including these sources with large excesses, the data from these various surveys are in reasonably good agreement, though some objects have more scatter than others. (The scatter could be due to complex backgrounds and variable beamsize across the surveys, or even intrinsic variability in the source.) If there is disagreement, however, it is typically *IRAS* that over-estimates the flux density from the object, which makes

sense since *IRAS* is the lowest spatial resolution of all the surveys used here.

The SEDs for these objects with unambiguous, large excesses appear in Figures 11 and 12. For stars without circumstellar dust (at least those warm enough to have the peak of their photospheric SED be at $<1 \mu$m), measurements in the IR ($\geqslant 2 \mu$m) should fall on a line consistent with a Rayleigh–Jeans (R-J) slope. To guide the eye, in Figures 11 and 12, we have added an R-J line extended from 2μm. All of the sources with very large excesses can be seen to deviate from this line.

Table 4
Objects that are Dropped from the Main Sample

Name	Src Conf?[a]	Steep SED?[b]	Notes
IRAS06365+0223	x	⋯	Target position on an optically faint source within a grouping of optically bright sources, and corresponds to a very red, resolved source seen as resolved in K_s (fluxes retrieved from 2MASS extended source catalog). This extended source is the origin of most of the long-wavelength flux. dlR97 source.
IRAS07419–2514	x	⋯	Target position in among a grouping of optically bright sources, with somewhat different sources bright in the IR. Position corresponds to the photocenter of the aggregate source seen by *IRAS*. Because target center does not correspond to an optically detected source, there are no short-wavelength measurements in the SED (so it appears to have a sparse SED). Source identified in Torres et al. (2000), and notes there say that *IRAS* flux may come from CO cloud WB 1046. *IRAS* flux probably attributable to ⩽ 5 IR-bright sources seen in *WISE*.
IRAS09553–5621	x (m?)	x	Target position in between two sources that are comparably bright at 4.6 μm. Only one source is apparent at optical through K_s, and by 22 μm, the sources have merged into one apparent source, likely responsible for the measured *IRAS* flux. SED assembled from closest source by position and thus may represent fluxes from different sources. Steep SED. *AKARI* consistent with *IRAS* at longest bands. dlR97 source.
IRAS11044–6127	x	x	High surface density of comparably bright sources in the optical; no easily visible source exactly at the target position in the optical. There is a faint source that starts to appear in 2MASS images, and a source to the west that becomes bright. The source exactly at the target position is still faint and blended with a source to the south at 3.4 μm. The target source is rising fast and dominates by 12 μm, dominating all the sources in the field by 22 μm (and therefore probably dominates the measured *IRAS* flux). Steep SED. dlR97 source.
IRAS12236–6302(PDS 354)	x	x	Another crowded field with comparably bright sources in POSS; there is an optically brighter source above and to the west of the target position that can be seen to be three distinct sources in 2MASS. In *WISE*, these sources are not resolved and form a blue arc immediately above the target. A source at the target location strongly dominates the field at 12 and 22 μm, and is presumably responsible for most of the *IRAS* flux (and, for that matter, that from *MSX* and *AKARI*). Steep SED. dlR97 source. Torres et al. (2000) mention that their optical spectrum of the source they took to be the counterpart of the IR emission has strong Hα emission and could be an H II region.
IRAS14198–6115	x (m?)	⋯	There are two sources here that are distinct in 2MASS and marginally resolved in [3.4] (though AllWISE catalog identifies only one), but are indistinguishable by [22]. There are several sources in this viscinity in the optical. SED assembled from closest source by position and thus likely represents fluxes from different sources. dlR97 source.
IRAS14257–6023	x (m?)	⋯	The brightest source in POSS is to the north and slightly west of the target position, but it is not responsible for the IR flux. There is a source to the southeast that is very red in 2MASS and is dominating the measured flux by *WISE* bands, and is likely responsible for the *IRAS* flux. SED assembled from closest source by position and thus may represent fluxes from different sources. dlR97 source.
IRAS16128–5109	x	x	This is not a point source in the IR, and is very bright (saturated) by [22]. It appears in SIMBAD as an H II region; the morphology of the image suggests a dense clump of sources from which emanate long streamers of extended emission. Steep SED. dlR97 source.
IRAS16227–4839	x	⋯	There are two sources that are resolved in 2MASS and marginally resolved at [3.4], but merged by [22], with the more northerly source dominating the IR flux. The more southerly source is brighter in POSS. Some extended emission visible in *WISE*. dlR97 source.
IRAS16252–5440	x	⋯	This is also PDS 146. In POSS, there is a high surface density of comparably bright sources. By 2MASS, an aggregate of at least 4 IR-bright sources is apparent. In *WISE*, it can be seen that the target position corresponds roughly to the photocenter of the aggregate of sources seen at [12]. The brightest source by [22] is to the east of the target position and is probably responsible for most of the *IRAS* flux. The SED we have assembled for this source corresponds to the source closest by position to the target position, and as such does not represent correctly the source of the longest wavelength flux. dlR97 source. Torres et al. (1995) lists this as "other" and "probably not young," and later implies it may be a normal MS star.
IRAS16514–4625(PDS 432)	x	x	A dark cloud is apparent near this source in *WISE* images. The brightest source in the optical is to the northwest of the target position, which is resolved into at least 3 sources in 2MASS. The source that dominates the IR by [22] (and probably also *IRAS*) is faint at [3.4]. Steep SED. dlR97 source. Torres et al. (2000) list it as a confirmed giant but the source that was measured may not be responsible for the IR flux.
IRAS17102–3813	x (m?)	⋯	A trio of sources seen at 2MASS become a smear dominated by the two sources to the southeast by [22]. The optically brightest source may contribute some but not all of the [22] (and *IRAS*) flux. SED assembled from closest source by position and thus may represent fluxes from different sources. dlR97 source.
IRAS17120–4106	x	⋯	Nothing is at the target position in POSS, though there is a source straight east of the target position. That easterly source persists through [3.4]. There is a faint source closer to the target position appearing by K_s. The two sources are barely resolved at [3.4], and merge by [12] and [22]. Given the [22] photocenter, some flux is likely attributable to each source, even in *WISE*. dlR97 source.
IRAS17211–3458	x (m?)	⋯	Two comparably bright sources are resolved in POSS, and in 2MASS. The two sources are barely resolved at [3.4] and merge by [12] and [22]. SED assembled from closest source by position, so may represent fluxes from different sources. dlR97 source. See text for additional discussion.

Table 4
(Continued)

Name	Src Conf?[a]	Steep SED?[b]	Notes
IRAS17442–2441	x (m?)	⋯	The DSS images are dense with sources of comparable brightness, though there is a source close to the target position. Similarly, in 2MASS, no source dominates, though there is a source close to the target location. There is a source at the target position and another comparably bright one to the west just resolved at [3.4]; they merge by [12] and [22]. SED assembled from closest source by position and thus may represent fluxes from different sources. dlR97 source.
PDS 97(IRAS17554–3822)	x (m?)	⋯	Target position in between two sources of comparable brightness at POSS and 2MASS. It is also between two comparably bright sources at [3.4] and [4.6]; by [12] the easterly source dominates, and by [22], all the flux is likely from the easterly source. Source from de la Reza et al. (1996). Gregorio-Hetem et al. (1992) list it as a high velocity giant with strong Li, and "incorrect identification in PSC" because KL Cra is 78″ to east, outside error ellipse. SIMBAD lists it as a T Tauri.
IRAS17576–1845	x	⋯	The multi-wavelength images suggest extinction in this field. The source position is reasonably close to a bright POSS source, but the target position can be seen to have several sources in 2MASS and *WISE* . The source dominating at [22] (and presumably *IRAS* bands) is "smeary" at [3.4]. dlR97 source. Coadella et al. (1995) list it as a candidate to be related to high-mass star forming regions with an ultracompact H II region, though it remained undetected in their survey.
IRAS17582–2619	x	x	The brightest source in the IR has no optical counterpart, and the IR is strongly dominated by the longest wavelengths. The optically brightest source is to the west of the target source, and has faded substantially by [12] and [22] μm. Steep SED to 20 μm, well-defined, with data from multiple surveys in good agreement with each other. Turnover from steep SED happens abruptly at ∼20 μm, shorter wavelengths than most of the other steep SEDs identified here (the other one like this is IRAS19083+0119(PDS 562)). dlR97source. SIMBAD lists this as an OH/IR star. Yoon et al. (2014) and references therein identify it as a post-AGB star (OH4.02-1.68). It appears in Ramos-Larios et al. (2012) and as a heavily obscured post-AGB star or PN candidate, and García-Lario et al. (1997) as a PN candidate. It appears in de la Reza et al. (2015) as an early AGB star.
IRAS17590–2412	x	⋯	The brightest source in the IR has no optical counterpart, and is strongly dominated by the longest wavelengths. Diffuse emission can also be seen in the field in various bands. dlR97 source. Messineo et al. (2004) identify a SiO emitter in this region but suggest that it may not be associated with the source from which an optical spectrum had been obtained by dlR97. They note that this *IRAS* source is the only mid-infrared source within their 86 GHz beam.
IRAS18334–0631(PDS 524)	x (m?)	⋯	There is no optical source at the target position; the target's *IRAS* flux likely has contributions from several sources in this viscinity, including a source resolved as an arc in *WISE* [3.4] and [4.6] precisely at the target position. The brightest POSS source is to the northwest of the target, and the brightest source by K_s is to the southwest. The brightest source by [22] is to the northeast. SED assembled from closest source by position and thus likely represents fluxes from different sources. dlR97 source.
IRAS18397–0400	x	⋯	The brightest source in the IR has no optical counterpart, and is dominated by the longest wavelengths. The brightest POSS source is to the northeast, though it is no longer the brightest source by 2MASS. The source responsible for most of the IR flux is slightly to the west of the target position, and is visible in 2MASS. *MSX* measurements have very large errors but are consistent with the rest of the SED. dlR97 source.
IRAS18559+0140	x (m?)	⋯	There is no optical source at the target position; a bright POSS source is to the southwest and is not bright at all in the IR. The target's *IRAS* flux has contributions from several sources, including a small clump to the east; the photocenter is pulled to the west, off of the bright clump of sources, and this offset of the *IRAS* position is the farthest off from the *WISE* source in the entire dataset. The assembled SED corresponds to the closest source by position and as such does not represent the brightest IR source here, and likely represents more than one source. dlR97 source.
IRAS19083+0119(PDS 562)	x	x	The brightest source in the IR has no optical counterpart, and is strongly dominated by the longest wavelengths. There is a faint source at the target position by K_s and it rises quickly through the *WISE* bands. Steep SED, with data from several surveys in good agreement with each other. Turnover from steep SED happens near ∼20 μm, shorter wavelengths than most of the other steep SEDs identified here (the other one like this is IRAS17582–2619). dlR97 source. SIMBAD lists it as a possible planetary nebula. Yoon et al. (2014) and references therein identify it as a post-AGB star.
IRAS19210+1715	x	x	There is no optical source at the target position; though there is a bright POSS source to the east, which can be seen in the IR. However, the target position matches a very red source, marginally visible in the 2MASS images, and rising quickly through the *WISE* bands, which most likely dominates the *IRAS* flux. There may be a contribution at [22] from a nearby source bright at [12]. Steep SED. dlR97 source.

Notes.
[a] This column is populated if the object is likely subject to source confusion of either of the sorts described in the text. "x (m?)" indicates that there may be multiple sources represented in the SED, e.g., the object shown in the SED at 2 μm may not be the same object as that shown at 22 μm.
[b] This column is populated if the object's SED rises steadily from 2 to at least 20 μm, as described in the text.

Out of these 19 stars with large IR excesses, 14 (73%) are from the dlR97 sample, five are from the literature sample, and none are from C12. However, four of the 19 may not be K giants —one of the dlR97 stars, IRAS17578–1700, is a carbon star, one of the stars from the literature sample, V385 Sct, is a very cool S-type star, and the other two may be too cool to be first ascent K giants. Some of these stars have detections indicating that the SEDs are rising beyond 90 μm, suggesting that sub-mm observations are needed to constrain the outer extent of the IR excess. Some of these objects have been identified in recent literature (e.g., Kumar et al. 2015) as having an IR excess, but for others, this is the first confirmation that the objects have an IR excess using data more recently obtained than *IRAS*.

5.3. Notes on Sources with Very Large Excesses

IRAS00483–7347. This is an extremely well-populated SED, with data from *WISE*, *MSX*, *AKARI*, *IRAS*, and even *Spitzer*. However, the SED is wide compared to other SEDs in this study. The SED suggests that K_s is not on the R-J side of the SED, perhaps because the star is significantly cooler than a K giant. A R-J line extended from 2 μm as shown, or even a R-J line extended from ∼5 μm, suggests a substantial IR excess around this star. Data from multiple sources are in good agreement with each other, and *AKARI* suggests that there is a significant long-wavelength component to the IR excess, with the SED rising again at the longest wavelengths. This source is identified in Castilho et al. (1998) as a Li-rich K giant, though no $T_{\rm eff}$ estimates are available in the literature. This star may be too cool to be a K giant, though it clearly has a large IR excess. Additional spectroscopy of this source would be helpful for a better understanding of the $T_{\rm eff}$ and where the excess starts.

HD 19745. The IR excess for this source starts to appear past 10 μm; *WISE* and *AKARI* are in good agreement. *IRAS* overestimated the IR flux density from this star, but it still has a clear excess. This source is known to be a Li-rich K giant (Reddy & Lambert 2005), and is incorrectly identified in SIMBAD as a T Tauri. Reddy & Lambert (2005) identify it as a red clump star. This star was identified in Kumar et al. (2015) as having an IR excess.

IRAS03520–3857. This object is a dlR97 source, and it had to be offset from the nominal *IRAS* position by 11″ to pick up the counterparts, which is very large in the context of the other positional shifts needed in the rest of our sample. However, the field is relatively clean (consisting of one bright source) and is not suggestive of source confusion. There is good agreement between *WISE*, *AKARI*, and *IRAS* for 10–20 μm. There is about an order of magnitude more energy density emerging at 10–20 μm than at 3–4 μm. However, compared to other sources here, there are few detections blueward of ∼2 μm, and it would be nice to see the SED turn over to define the Wien side of the SED. This object is identified in two papers as a possible galaxy based on *IRAS* colors (Saunders et al. 2000; Wang & Rowan-Robinson 2009) but is not identified as a confirmed galaxy in either paper. SIMBAD identifies it as a "peculiar star." This source has no $T_{\rm eff}$ in the literature.

IRASF04376–3238. This object's IR excess starts at least by 5 μm, if not actually at 3 μm. *WISE*, *AKARI*, and *IRAS* are in good agreement. However, compared to other sources here, there are few detections blueward of ∼2 μm, and it would be nice to see the SED turn over to define the Wien side of the SED. This object is identified as a K giant in Torres et al. (2000), but as a candidate T Tauri in Magnani et al. (1995). It

does have an SED consistent with SEDs found in young stars (see, e.g., Rebull et al. 2011). SIMBAD lists it as a "peculiar star." Spectroscopy would be useful to distinguish a young star with low gravity from an old star with low gravity, and assess its Li abundance. (An uncertain equivalent width for Li is given for it in Torres et al. 2000, but no abundance.) This source has no $T_{\rm eff}$ in the literature.

IRAS07227–1320(PDS 132). This star has a substantial IR excess that evidently starts abruptly between 4.6 and 7.8 μm. *AKARI*, *MSX*, *WISE*, and *IRAS* are consistent with each other. This object is part of the dlR97 sample, and Torres et al. (2000) list it as a confirmed giant. However, Torres et al. (1995) lists this as "other" and "probably not young" in their paper on young stars; it is implied to be a normal MS star. García-Lario et al. (1997) identify it as a possible PN (planetary nebula) based on its IR excess. It is identified as a post-AGB star and an M1 I giant in Suárez et al. (2006). Szczerba et al. (2007) identify it as "not a post-AGB (asymptotic giant branch) star," but Yoon et al. (2014) identify it as a post-AGB star of type M3 IV. This source has no $T_{\rm eff}$ in the literature. Additional data are needed to clarify the status of this object.

IRAS07456–4722(PDS 135). This star's IR excess is small at 3.4 and 4.6 μm, but becomes substantial by ∼10 μm. There is scatter but generalized agreement among *IRAS*, *AKARI*, and *WISE*. This object is part of the dlR97 sample. Torres et al. (2000) list it as a confirmed giant, though Torres et al. (1995) categorize it as a "Probable post-FU Ori star." SIMBAD lists it as a T Tauri, apparently on the basis of Torres et al. (1995). As with other sources here, it has an SED consistent with SEDs found in young stars (see, e.g., Rebull et al. 2011), and spectroscopy would be useful to distinguish a young star with low gravity from an old star with low gravity. This source has no $T_{\rm eff}$ in the literature.

IRAS07577–2806(PDS 260). There is good agreement between *WISE*, *AKARI*, *MSX*, and *IRAS* here, and there is more energy density near 20 μm (from dust) than near 1 μm (from the photosphere). *AKARI* provides detections out past 100 μm. The IR excess may start at 3.4 μm. This source is from the dlR97 set, and Torres et al. (2000) list it as a confirmed giant. SIMBAD identifies it as a post-AGB star, and reference García-Lario et al. (1997), but this object does not appear in the paper. Szczerba et al. (2007) retain it as a candidate AGB star. It does not have a $T_{\rm eff}$ in the literature.

HD 233517. This star's SED suggests an excess that starts past 5 μm. This is an original dlR97 source, and this star was identified in Kumar et al. (2015) as having an IR excess, as well as in Fekel & Watson (1998), Jasniewicz et al. (1999), and Drake et al. (2002), among others.

IRASF08359–1644. This SED suggests an IR excess that most likely starts at ∼10 μm. *WISE* and *IRAS* (and the single *AKARI* point) are in good agreement with each other. Torres et al. (2000) identify this source as a Li-rich K giant. No other information about this source is apparently available (including $T_{\rm eff}$); additional data would be useful.

HD 96195. This SED is more complicated than ones above. Reliable *WISE* points at the shortest two bands do not exist; *MSX* provides a link between K_s and [12]. *MSX*, *AKARI*, *WISE*, and *IRAS* are all in rough agreement between 10 and 20 μm, though there is some scatter (and large error bars in one case). Assuming that K_s is on the photosphere (and on the R-J side of the SED, that is, assuming that this source is hot enough), there is a significant IR excess by 10 μm: K_s−[12] = 1.14 mag. We
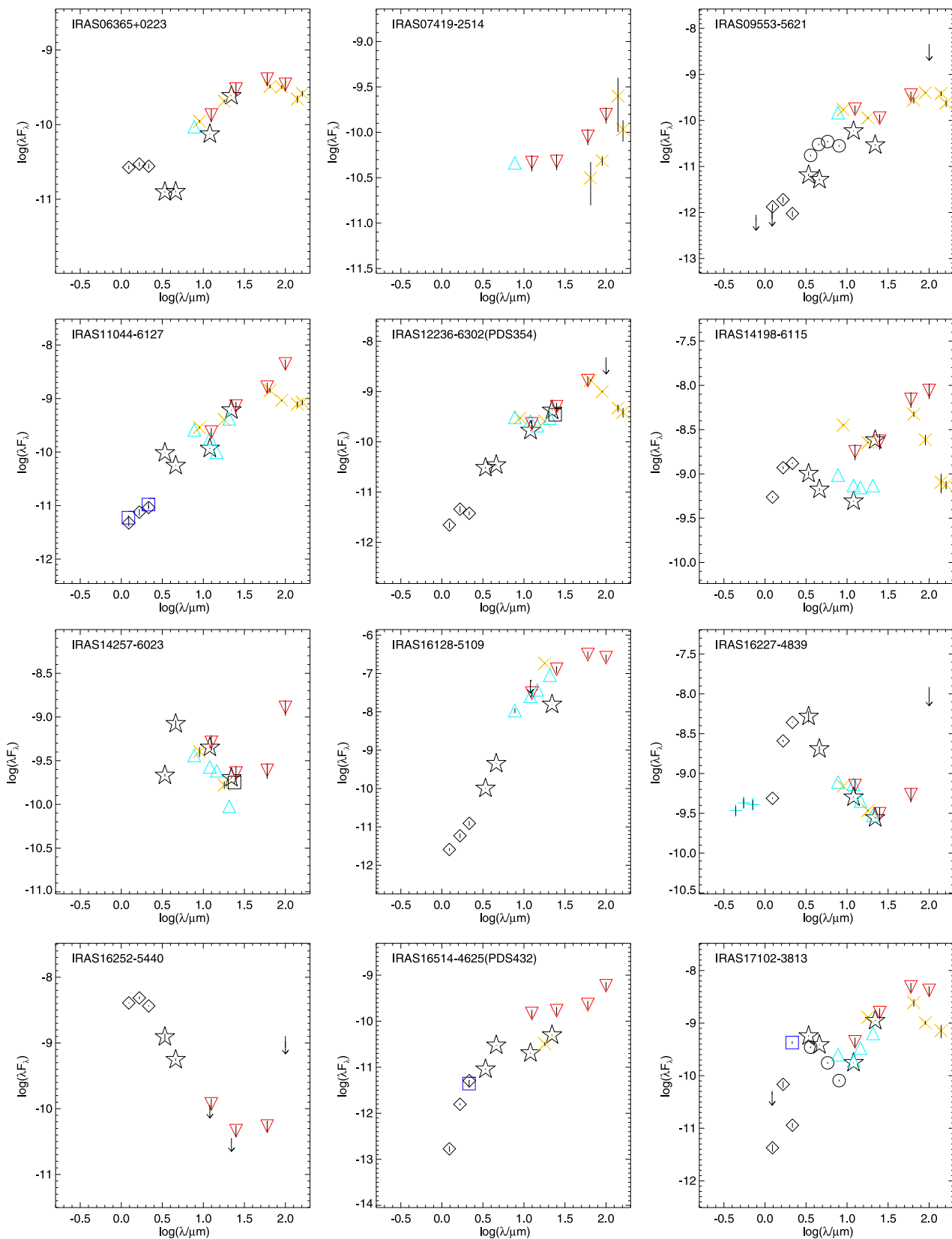
Figure 8. SEDs for things that are likely subject to source confusion, part 1. Notation for all SEDs in this paper is as follows. The axes are log λF_λ in cgs units (erg s^{-1} cm^{-2}) and log λ in microns. Symbols: cyan + are literature *UBRI$_c$*; black + are SDSS *ugriz*; black diamonds are 2MASS *JHK$_s$*; blue squares are Denis *IJK*; black circles are from *Spitzer*/IRAC; black stars are *WISE*; yellow × are *AKARI*; cyan triangles are *MSX*; black squares are *Spitzer*/MIPS (24 μm); red downward pointing triangles are *IRAS* PSC and FSC. Any arrows are limits at the corresponding wavelength. Error bars are indicated as vertical black bars at the center of each point. See text and Table 4 for discussion of individual objects.
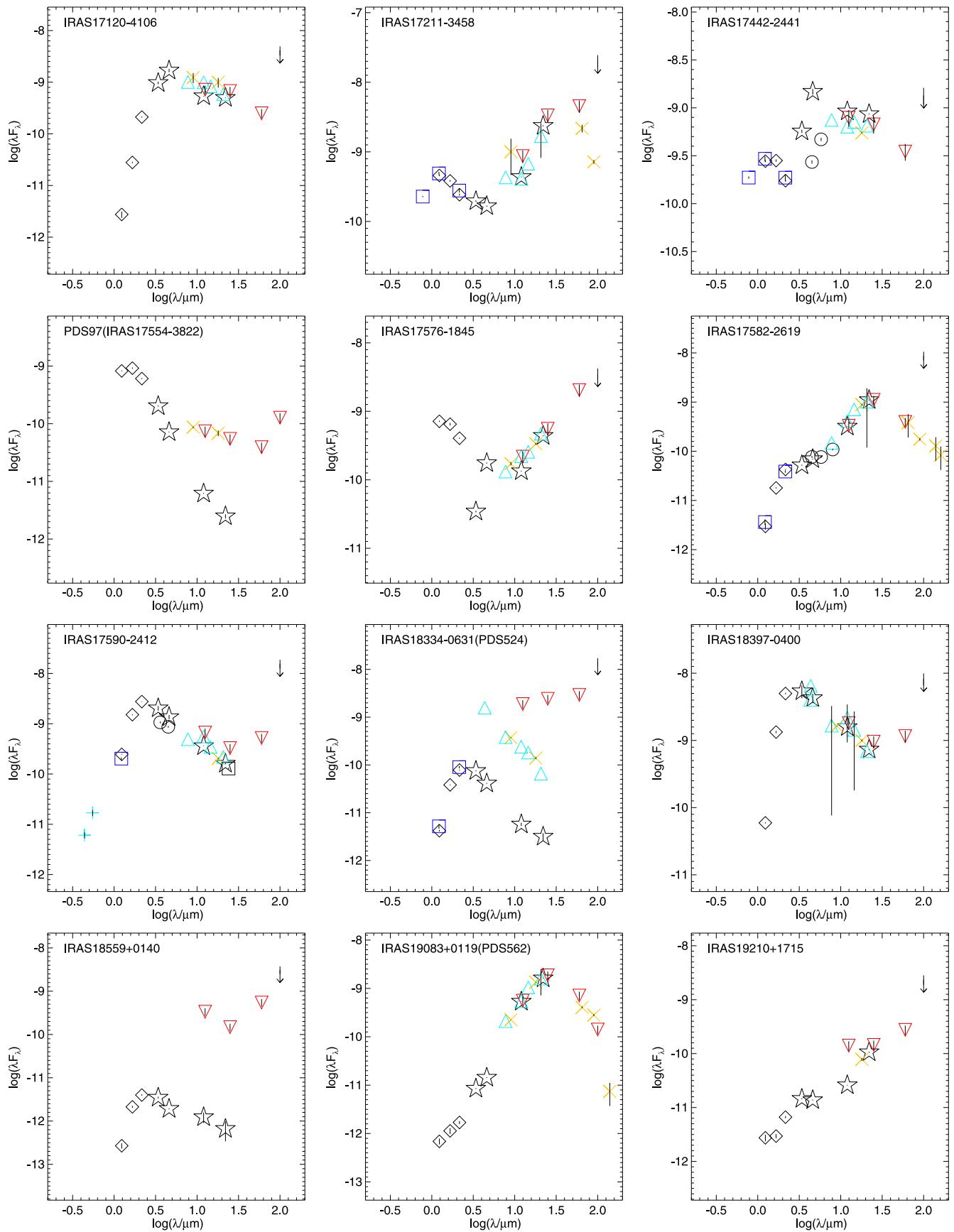
Figure 9. SEDs for things that are likely subject to source confusion, part 2; notation is as described in Figure 8. See text and Table 4 for discussion of individual objects.
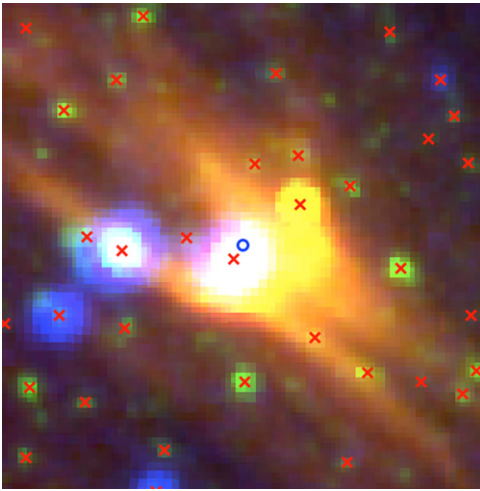
Figure 10. Three-color image of IRAS17211–3458, about an arcminute on a side, north-up. Blue plane is DSS 2 red plates, green plane is IRAC-2 (4.5 μm), and red plane is IRAC-4 (8 μm). Blue circle is target position, and red $\times$ are sources from the 2MASS (point source) catalog. The target position is $\sim$2″ from the source taken as the 2MASS match. There is complex long-wavelength emission here. Photometric measurements >10 μm combine flux densities from more than one source, plus nebulosity, and so we have left this source in the set of sources likely subject to source confusion.

have placed this object in this section with the other large excesses; we might have included it in the set of objects with more subtle excesses (following the method laid out in Section 5.4 below, $\chi_{K,[22]} = 6.8$), but close inspection of the SED shows that points >10 μm are probably above the photosphere. Moreover, the *AKARI* points, if detecting flux density truly associated with this source, identify a substantial IR excess at the bands >50 μm. This source appears in Castilho et al. (2000) and Pereyra et al. (2006) as a Li-rich giant, but it may be too cool to be a K giant. Its reported $T_{\rm eff}$ in the literature (Castilho et al. 2000) is $\sim$3400–3600 K. It is also identified in McDonald et al. (2012) as having an IR excess (their $E_{\rm IR} = 1.932$) and having $T_{\rm eff} = 3400$.

IRAS12327–6523(PDS 355). The IR excess for this source appears by 3.4 μm, and increases from there. *WISE, MSX, AKARI,* and *IRAS* are all in good agreement with each other (despite large errors on the *MSX* points). This is part of the dlR97 sample. Torres et al. (2000) list it as a confirmed giant, but also mention that there is some reddening here that likely comes from the Coalsack, and the star may be only 200 pc away, so the IR may be contaminated. Reddy & Lambert (2005) confirm the evolved nature of the star. de la Reza et al. (2015) categorizes this source as an early AGB star.

PDS 365(IRAS13313–5838). This star's IR excess likely starts between 2 and 3 μm; there is more energy density near 20 μm (from dust) than near 1 μm (from the photosphere). There is good agreement among *WISE, MSX, AKARI,* and *IRAS.* This star is part of the dlR97 sample and was identified in Kumar et al. (2015) as having an IR excess. While it is a confirmed Li-rich K giant (e.g., Drake et al. 2002; Kumar et al. 2011, among others), SIMBAD lists it as a "Post-AGB Star (proto-PN)."

PDS 68(IRAS13539–4153). The IR excess here starts abruptly between 5 and 8 μm; 3.4 and 4.6 μm are on the photosphere if K_s is as well. *WISE, AKARI,* and *IRAS* are in good agreement. If the longest wavelength *AKARI* bands are detecting flux attributable solely to this source, it suggests that the SED is rising again at the longest bands. This star was

identified in Kumar et al. (2015) as having an IR excess. While it is listed as a confirmed Li-rich K giant in several studies (e.g., Kumar & Reddy 2009; Kumar et al. 2011, among others), it also appears in Valenti et al. (2003) as a T Tauri candidate, though no useable spectra are reported of this object in that paper. SIMBAD has adopted the "T Tauri" categorization. The ^{12}C/^{13}C ratio is only a limit (>20; Reddy & Lambert 2005), and cannot conclusively determine whether early RGB first dredge-up mixing (which lowers ^{12}C/^{13}C from the main sequence value) has occurred.

IRAS16086–5255(PDS 410). This star's IR excess likely starts between 2 and 3 μm; there is more energy density near 20 μm (from dust) than near 1 μm (from the photosphere). There is good agreement among *WISE, MSX, AKARI,* and *IRAS.* This star is part of the dlR97 sample, and is listed in Torres et al. (2000) as a confirmed giant. However, SIMBAD categorizes it as "post-AGB, proto-PN," and Szczerba et al. (2007) retain it as a candidate AGB. No $T_{\rm eff}$ is available.

IRAS17578–1700. This star has a substantial IR excess that may start at K_s; it may also be too cool for K_s to be on the R-J side of the SED. There is good agreement between *MSX, AKARI, WISE,* and *IRAS,* though there are no viable *WISE* points at the shortest two bands. This object is part of the dlR97 sample. Chen et al. (2007), and references therein including Lloyd Evans (1991) identify it as a J-type carbon star based on optical spectra and IR excesses, and that categorization is inherited by SIMBAD. This star is likely too cool to be a K giant, and moreover is likely to be a carbon star.

IRAS17596–3952(PDS 485). This object is part of the dlR97 sample, and its position had to be slightly adjusted from the nominal *IRAS* position to pick up the counterparts, but the field is relatively clean and is not suggestive of source confusion. This star's IR excess likely starts between 2 and 3 μm; there is a larger excess by $\sim$10 μm, and *WISE, AKARI,* and *IRAS* are in good agreement where the points exist. This star was identified in Kumar et al. (2015) as having an IR excess. It is a confirmed Li-rich K giant (e.g., Reddy & Lambert 2005; Kumar et al. 2011).

V385 Sct. This is a very bright star, and the K_s mag may not be on the R-J side of the SED; it may be too cool to be a K giant. There are no *WISE* data for the shortest two bands, and *MSX* fills the gap between 2 and 10 μm. There is scatter among the *MSX, WISE, AKARI,* and *IRAS* data, likely because it is so bright. It does seem to have an obvious IR excess, however. It appears in Castilho et al. (2000) and Pereyra et al. (2006) as a Li-rich K giant. However, it appears as GCSS 557 in Stephenson (1976) and is identified as star of type S in there and subsequent literature (such as Stephenson 1984, where it is CSS 1043). Stars of type S have ZrO bands as well as TiO bands, and other abundance anomalies; they are thermally pulsing AGBs that experience substantial dredge-up. It seems unlikely to be a first-ascent Li rich K giant. The $T_{\rm eff}$ value for it from the literature (Castilho et al. 2000) is $\sim$3300 K, so it is also too cool to be a first-ascent K giant.

PDS 100. There may be a small excess at 3.4 and 4.6 μm, but there is a clear excess by $\sim$10 μm, as seen by *WISE, AKARI,* and *IRAS.* This star is part of the dlR97 set, and is also known as V859 Aql. SIMBAD indicates it as a T Tauri, but the literature is clear that it is instead a Li-rich K giant (Reddy et al. 2002, among others). This star was identified in Kumar et al. (2015) as having an IR excess.

HD 219025. This star is also known as BI Ind, and its IR excess starts between 2 and 3 μm. There is a viable *WISE*

Table 5
Sources with IR Excesses[a]

Name	[3.4]–[22]	$\chi_{[3.4],[22]}$	Sample	Data Codes[b]	Drop?[c]	Lit?[d]	Start[e]
IRAS00483–7347	4.71	(large)	Castilho et al. (1998)	W M A I S	D?	···	<2
NGC 362 V2	1.13	9.7	Smith et al. (1999)	W S	···	···	5
HD 19745	2.32	(large)	dlR97, Kumar et al. (2011)	W A I	···	IRx	10
IRAS03520–3857	8.80	(large)	dlR97	W A I	···	···	2?
IRASF04376–3238	3.83	(large)	Torres et al. (2000)	W A I	···	···	3?
IRAS07227–1320(PDS 132)	6.64	(large)	dlR97	W M A I	···	···	5?
IRAS07456–4722(PDS 135)	5.40	(large)	dlR97	W A I	···	···	3?
HD 65750	···	···	dlR97, Castilho et al. (2000)	(W) A I	···	IRx	2?
IRAS07577–2806(PDS 260)	8.75	(large)	dlR97	W M A I	···	···	3?
HD 233517	5.53	(large)	dlR97, Kumar et al. (2011)	W A I	···	IRx	10
IRASF08359–1644	6.00	(large)	Torres et al. (2000)	W A I	···	···	3?
G0928+73.2600	0.63	6.4	C12	W	···	···	22
HD 96195	···	···	Castilho et al. (2000)	(W) M A I	D?	IRx	10
Tyc0276-00327-1	0.36	3.4	C12	W A	···	···	22
IRAS12327–6523(PDS 355)	3.56	(large)	dlR97	W M A I	···	···	2
HD 111830	0.63	3.7	dlR97	W A I S	···	···	22
PDS 365(IRAS13313–5838)	7.37	(large)	dlR97, Kumar et al. (2011)	W M A I	···	IRx	2?
PDS 68(IRAS13539–4153)	6.04	(large)	dlR97, Kumar et al. (2011)	W A I	···	IRx	10
IRAS16086–5255(PDS 410)	9.75	(large)	dlR97	W M A I	···	···	3?
HD 146834	1.07	2.6	dlR97	W A S	···	IRx	20?
IRAS17578–1700	···	···	dlR97	(W) M A I	D	···	<2
IRAS17596–3952(PDS 485)	5.15	(large)	dlR97, Kumar et al. (2011)	W A I	···	IRx	3?
V385 Sct	···	···	Castilho et al. (2000)	(W) M A I	D	···	3?
IRAS19012–0747	1.39	7.2	dlR97	W M A I	···	···	10?
IRAS19038–0026	1.45	4.9	Castilho et al. (2000)	W A I	D?	···	10?
PDS 100	5.86	(large)	dlR97, Kumar et al. (2011)	W A I	···	IRx	4?
Tyc9112-00430-1	0.86	3.1	Ruchti et al. (2011)	W	···	···	22
HD 219025	3.74	9.6	dlR97, Kumar et al. (2011)	W A I	···	IRx	3

Notes.

[a] Note that up to two more stars with IR excess could be identified from the relatively sparse SEDs in Section 4.2; these are For 90067 and SDSS J0632+2604, with SDSS J0632+2604 being more compelling.

[b] W = *WISE* data in SED, with "(W)" meaning some bands are missing; M = *MSX* data in SED; A = *AKARI* data in SED; I = *IRAS* data in SED; S = *Spitzer* data in SED.

[c] This column is populated if there is a reasonable likelihood that the star is not a first ascent K giant, e.g., of the sort appropriate for this study. "D" means we are fairly confident it should be dropped, and "D?" means there is some doubt as to whether it should be dropped; see text.

[d] This column is populated if recent literature has already identified this source as having an IR excess.

[e] This column contains the approximate wavelength, in microns, of the start of the IR excess.

detection at 3.4 μm, but not at 4.6 μm; there is good agreement past ∼10 μm among *WISE*, *AKARI*, and *IRAS*. It has a substantial IR excess. This star is part of the dlR97 set, and is identified in many places in the literature as a Li-rich K giant (e.g., Kumar et al. 2011). SIMBAD has this as an RS CVn, but it is unlikely to be such an object. This star was also identified in Kumar et al. (2015) as having an IR excess. Jasniewicz et al. (1999) and Whitelock et al. (1991) have previously found a NIR excess for this star. They verify using *Hipparcos* parallax that this is a RG and not a young star. It is also a rapid rotator.

5.4. Overview: Sources with Small Excesses

Identifying smaller excesses around the remaining stars requires more analysis than simple SED inspection. We can quantitively compare the brightness at 2–3 μm (which should be dominated by the stellar photosphere in these cases where there is not much circumstellar dust to create an IR excess) with that at relatively long wavelengths, where dust emission may be present. In considering significant IR excesses, the IR excess is larger than any uncertainties in calibration. However, for small excesses, well-defined errors are important, uncertainties in calibration should be taken into account, and it becomes more important to use data that are uniformly obtained, calibrated, and processed so as to minimize systematics. Additionally, data obtained not over decades but obtained close in time minimize influence from intrinsic stellar variation.

WISE data meet these criteria, as the data are uniformly obtained (at nearly the same time), reduced, and calibrated. Therefore, [3.4]–[22] is essentially an ideal metric with which to identify IR excesses.

There have been several approaches in the literature used to determine with confidence whether or not a star has an IR excess. For example, Mizusawa et al. (2012) tested several methods of finding IR excesses in F stars. To identify sources with small IR excesses, we adopt here the following approach (as in Mizusawa et al. 2012, or Trilling et al. 2008). We calculate χ:

$$\chi_{[3.4],[22]} = \frac{\left(([3.4]-[22])_{observed} - ([3.4]-[22])_{predicted} \right)}{\sigma_{([3.4]-[22])}} \quad (1)$$

and take as a significant excess those stars for which $\chi > 3$. For K giants, [3.4]–[22]$_{predicted}$ is 0, but for cooler objects (such as M giants), the predicted value is not 0 (see, e.g., Gautier et al. 2007). Mizusawa et al. (2012) were able to combine χ
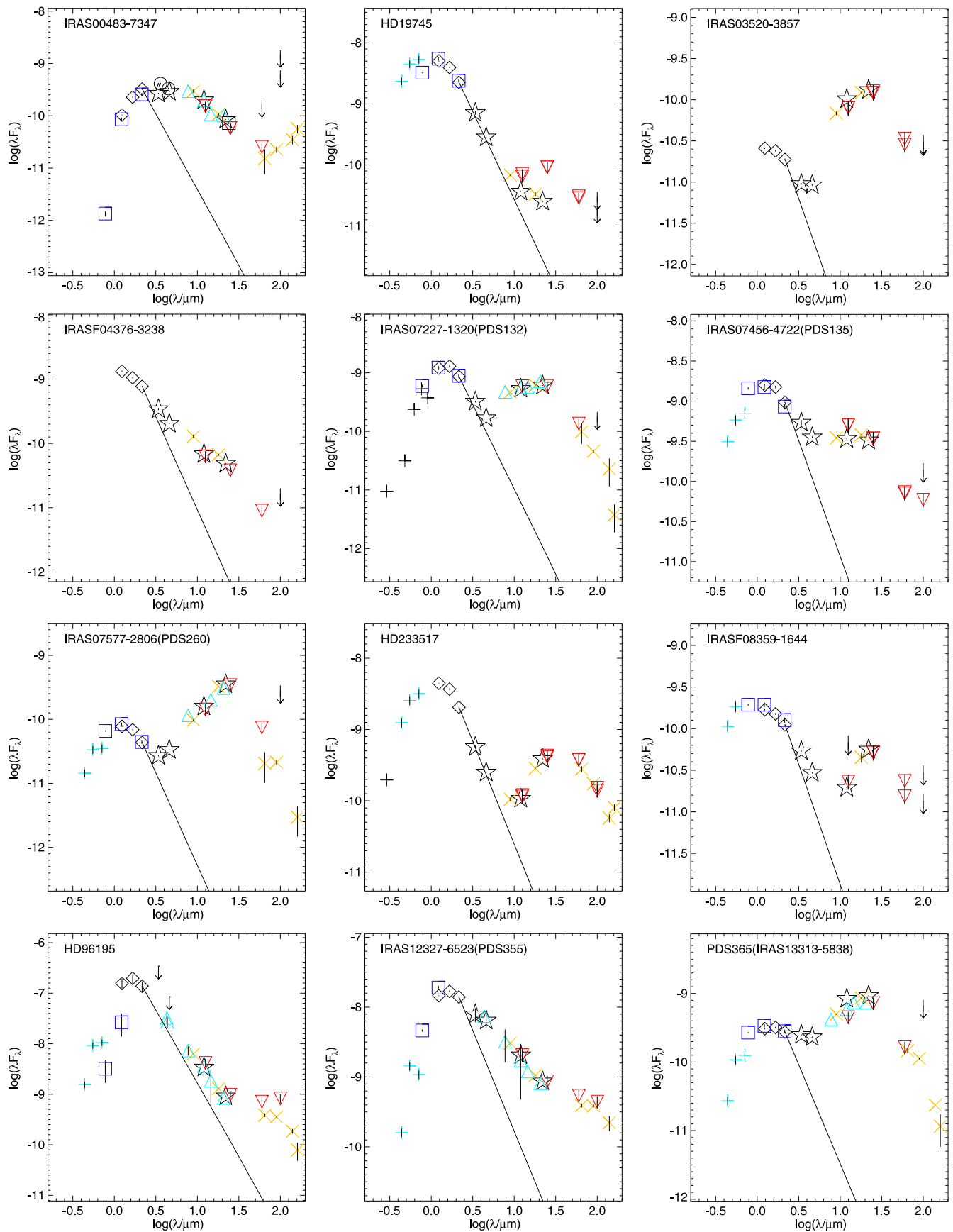
Figure 11. SEDs for sources with large IR excesses, part 1; notation is as described in Figure 8, with an additional line with a Rayleigh–Jeans slope extended from K_s (e.g., if K_s is on the photosphere, the photosphere longward of K_s should fall on this line). All of these objects have a significant excess above this line. See text and table for discussion of individual objects.
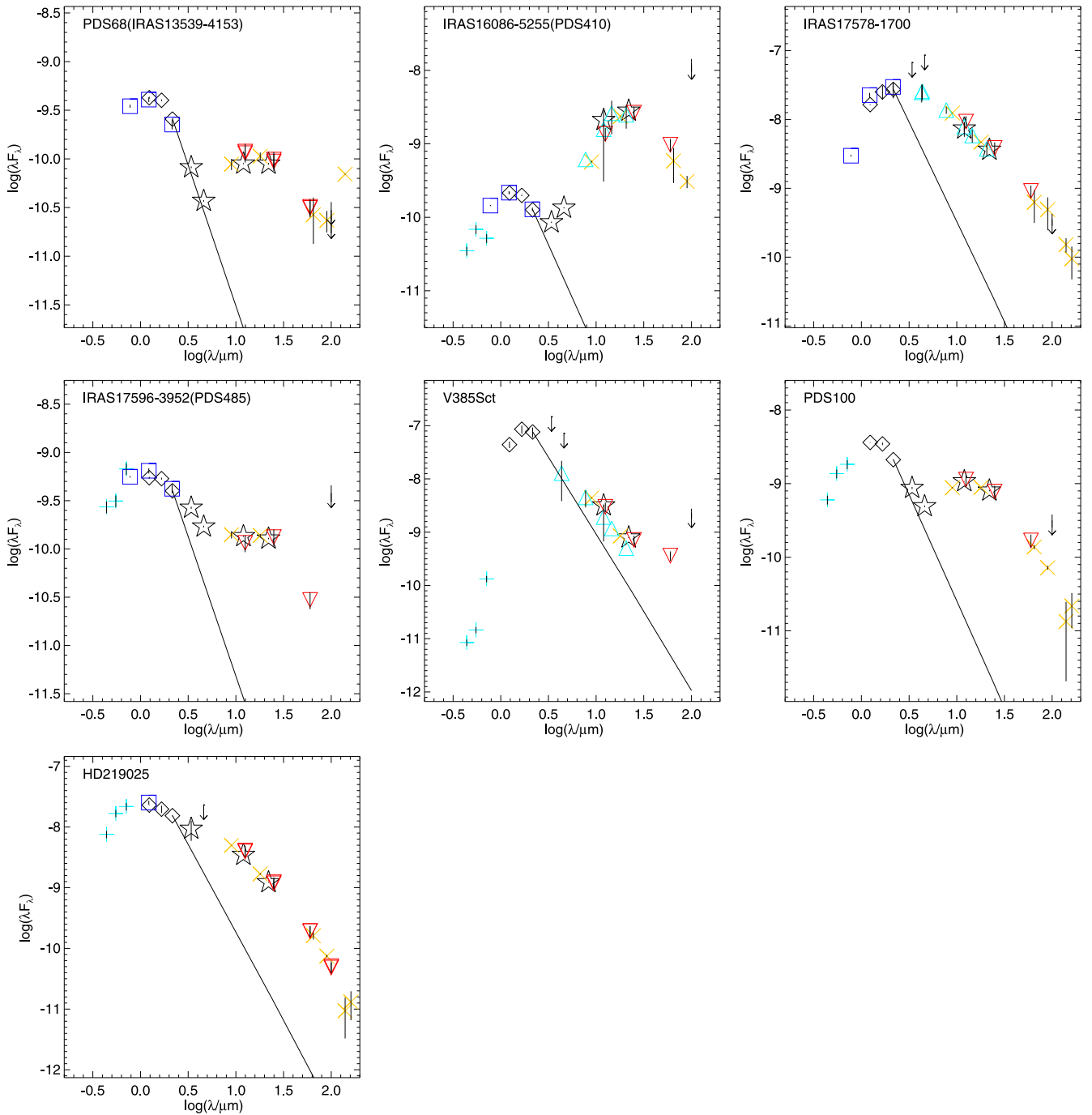
Figure 12. SEDs for sources with large IR excesses, part 2; notation is as in Figure 11. See text and table for discussion of individual objects.

calculations for two independent measures of IR excess for most of the targets in their sample, using K_s–[24] and [3.4]–[22]. We do not have such uniform independent measures of IR excess, so for the most part, we use $\chi_{[3.4],[22]}$. In order for the χ calculation to be successful, however, one needs good estimates of the star's brightness at the relevant bands, as well as good estimates of the error on that measurement. Many of our targets are very bright, and saturated in K_s and [3.4], which limits our ability to correctly estimate brightnesses (and errors) and therefore χ. However, we can use the existing measurements and reported errors to identify objects that are likely to have a small IR excess.

Table 5 includes [3.4]–[22] and $\chi_{[3.4],[22]}$ for the sources with IR excesses. (Note that the χ values as calculated for the objects with large and obvious IR excesses above in Section 5.2 are often >100, despite there being, in some cases, an IR excess even at 3.4 μm.)

There are nine stars we identify as having small but significant excesses, and their SEDs appear in Figure 13. Two of the stars with small IR excesses are from the C12 sample, three are from the dlR97 sample, and the remaining four come from the literature sample of Li-rich giants. One may be too cool to be a K giant. Two have been recently identified in the literature as having an IR excess. Comments on each of these excess objects follow in the next section.
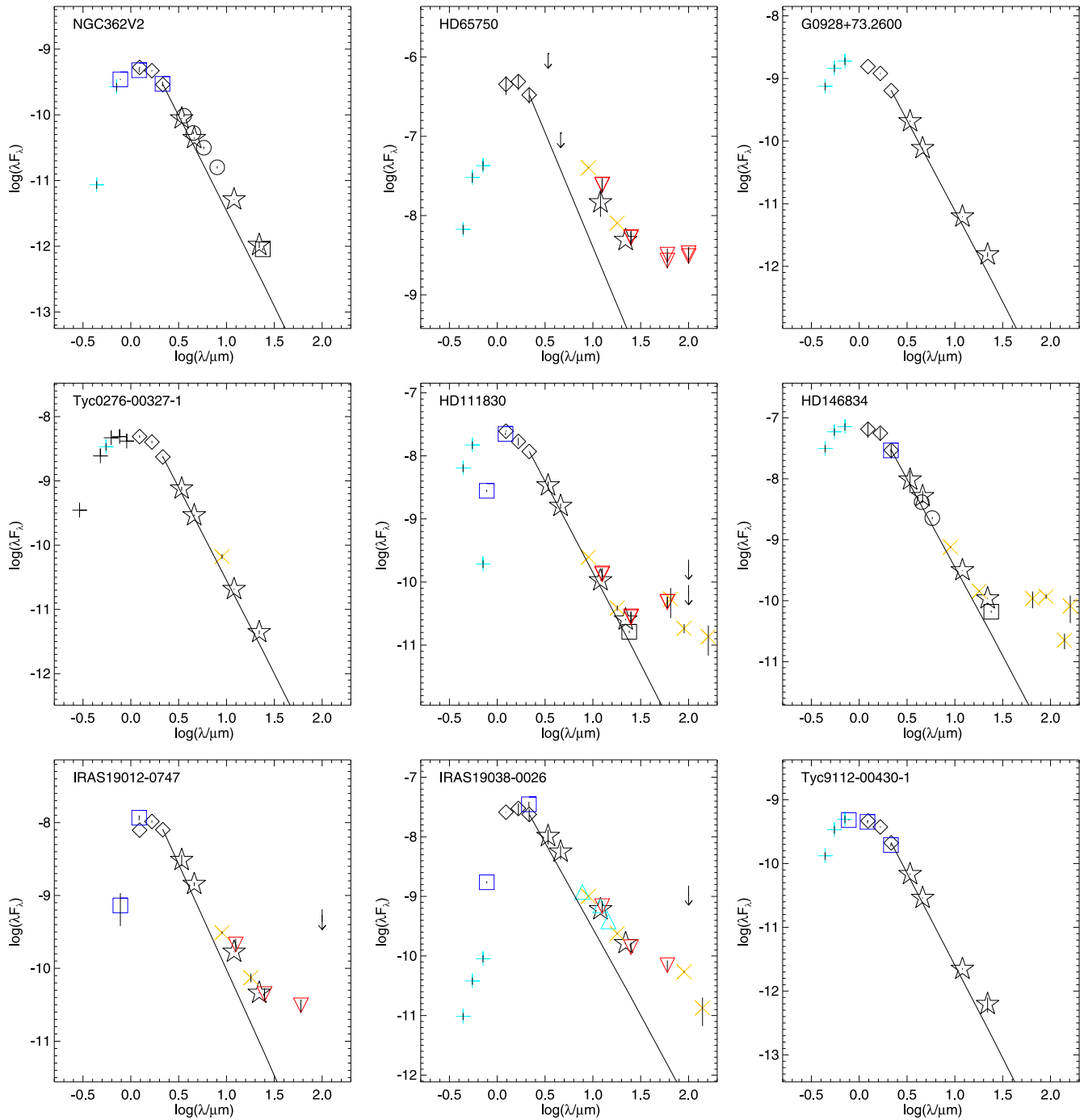
Figure 13. SEDs for sources with smaller IR excesses; notation is as in Figure 11. See text and table for discussion of individual objects.

5.5. Notes on Sources with Small Excesses

NGC 362 V2. There are *Spitzer* data for this source, and *Spitzer* agrees well with *WISE*. There is a small IR excess here. By inspection of the SED, the excess probably starts relatively early in the SED, $\sim$5 μm, for a small excess. (The specific values are [3.4]–[22] = 1.13 mag, $\chi_{[3.4],[22]} = 9.7$.) The star is identified as a Li-rich K giant in Smith et al. (1999).

HD 65750. This star is very bright, and as such is missing 3.4 and 4.6 μm data (and the K_s data come from NOMAD). There are, however, *WISE*, *AKARI*, and *IRAS*, all of which are in good agreement with each other. This source can be seen in the SED to have an excess; it has no [3.4], but $\chi_{K,[22]} = 11$. It is highly

nebulous at POSS, though not at longer bands, so the measured IR flux is not likely contaminated by extended emission. This source comes from the dlR97 sample; it appears in Castilho et al. (2000) as a Li-rich giant. SIMBAD says this is V341 Car, a pulsating variable star of type M0III. It has a T_{eff} of 3600, so it is most likely a borderline case for being a first ascent K giant. McDonald et al. (2012) identified it as having an IR excess in their study of IR excesses around *Hipparcos* stars, calling it out (HIP 38834) in their Table 3 of luminous giant stars with detected circumstellar emission (their $E_{IR} = 5.88$).

G0928+73.2600. This star does not have a very well-populated SED, or an immediately obvious IR excess based on the SED, but the χ calculation supports there being a small but

significant IR excess here ([3.4]–[22] = 0.63 mag, $\chi_{[3.4],[22]}$ = 6.4). This star is identified as a particularly interesting source in C12 and Carlberg et al. (2010) because it has particularly high Li (A(Li)$_{\mathrm{NLTE}}$ = 3.30 dex), relatively rapid rotation (8.4 km s^{-1}), and high ^{12}C/^{13}C (28). We have more discussion of this source in Section 6.4 below.

Tyc0276-00327-1. This source does not have an immediately obvious IR excess from the SED (which is also not terribly well populated), but the χ calculation supports there being a very small but significant IR excess here ([3.4]–[22] = 0.36 mag, $\chi_{[3.4],[22]}$ = 3.4). In the images, it appears within the extended halo of emission associated with an extended source (possibly a galaxy) that is bright at [12] and [22]. It is possible that this may affect the IR excess, though the AllWISE catalog does profile fitting photometry that should take into account this higher background. Additional data to secure the association of the IR excess with this object would be helpful. This object is from the C12 sample, but is unremarkable in that study, showing low Li, slow rotation, and average ^{12}C/^{13}C.

HD 111830. On first glance at the SED, this object seems to have good agreement with photospheric measurements from K_s to 25 μm, with *WISE*, *AKARI*, *IRAS*, and even *Spitzer*/MIPS falling on the R-J line to 25 μm. However, *IRAS* and *AKARI*, if detecting flux density truly associated with this source, identify a substantial IR excess at bands longer than 50 μm. There turns out to be a small but significant excess at 22 μm ([3.4]–[22] = 0.63 mag, $\chi_{[3.4],[22]}$ = 3.7). K_s–[24] = 0.4 mag, consistent with a small excess. This star is part of the dlR97 sample; it appears in Jasniewicz et al. (1999) as Li-rich but is listed in their table with an upper limit on the Li abundance.

HD 146834. This source is also HR 6076. In POSS, there is nebulosity (and SIMBAD categorizes it as "star in nebula"). It is very bright in 2MASS and *WISE*, with no strong nebular emission, though there is some faint extended emission in the background at 12 and 22 μm. It has *WISE*, *Spitzer* (IRAC and MIPS), and *AKARI* data, all of which are in fairly good agreement. However, near 20 μm, it is confusing. *AKARI* measures 860 ($\pm$15) mJy at 18 μm, *WISE* measures 797 ($\pm$12) mJy at 22 μm, and MIPS measures significantly less, 528 mJy, at 24 μm. The original error at 24 μm reported in the SEIP is $\pm$16 mJy, and is likely underestimated, so we have added a 4% error floor, as described above; the net error is 21 mJy, still not enough to bring the measures into alignment within 1σ. The K_s mag is bright, and its error is also likely underestimated. Following the measurements and errors as reported, however, [3.4]–[22] = 1.07, $\chi_{[3.4],[22]}$ = 2.6, and K_s–[24] = 1.19, $\chi_{K,[24]}$ = 3.2. The errors on [3.4] and K_s are both large, which lowers the χ values. It is difficult to decide if the excess here is real and significant. We have opted to call the excess significant because there are three measures of the brightness near 20 μm, and it does seem to be significantly brighter near 20 μm than the photospheric expectations based on the brightness near 2–3 μm. It also has some long-wavelength *AKARI* detections; if *AKARI* is measuring flux associated solely with this star, then it has a significant long-wavelength excess. It appears in McDonald et al. (2012) as having a small IR excess in their study of IR excesses around *Hipparcos* stars (their E_{IR} = 1.532). It is from the dlR97 sample.

IRAS19012–0747. There are two sources here in close proximity in POSS, but the target position matches one of the two optically bright sources. Both sources can be seen in *J* through [12], though the target source is clearly dominating, and

overwhelms any flux from the apparent companion by [22] (and presumably in *IRAS*). While source confusion is possible, it's reasonably likely that a spectrum was obtained of the source of most of the IR flux. This source has *WISE*, *AKARI*, and *MSX* data, all of which are in good agreement with each other. *IRAS* and *AKARI*, if detecting flux density truly associated with this source, identify a substantial IR excess at bands longer than 25 μm. At ∼20 μm, it has a weaker excess—[3.4]–[22] = 1.39, $\chi_{[3.4],[22]}$ = 7.2. This star is part of the dlR97 sample (though its name was incorrectly IRAS19012–0742 in the published table). It appears in Pereyra et al. (2006) as a Li-rich K giant.

IRAS19038–0026. K_s for this object may not be on the R-J side of the SED; it may be too cool to be a K giant. There does not seem to be significant IR excess at 3.4 or 4.6 μm, but the *MSX*, *AKARI*, *WISE*, and *IRAS* points suggest an excess may be present starting at ∼10 μm. By >20 μm, assuming that the *IRAS* and *AKARI* points are detecting flux density truly associated with this source, there is a substantial IR excess. At ∼20 μm, it has a more subtle excess—3.4–[22] = 1.45, $\chi_{[3.4],[22]}$ = 4.9. This object appears in Castilho et al. (2000) and Pereyra et al. (2006) as a Li rich giant, but it may be too cool to be a K giant. The T_{eff} that appears in the literature for it is ∼3600 K.

Tyc9112-00430-1. This source does not have an immediately obvious IR excess from the SED, but the χ calculation supports there being a small but significant IR excess here: [3.4]–[22] = 0.86, $\chi_{[3.4],[22]}$ = 3.1. It is identified as a Li-rich K giant in Ruchti et al. (2011).

6. DISCUSSION: CHARACTERISTICS OF THE ENTIRE IR EXCESS SAMPLE

We started with 316 sources. Out of those, 10 have too sparsely populated SEDs for us to sensibly place any strong restrictions on whether or not there is an excess. There are 36 sources that have relatively sparse SEDs, and are often missing at least the [22] band. For these, we can put some constraints on whether or not there is an IR excess, and 2 out of those 36 sources could plausibly have an IR excess. There are 24 sources that we suspect are subject to source confusion, and we drop them from the sample. There are 218 sources with well-populated SEDs and no evidence for IR excesses out to ∼20 μm. There are 28 sources that have well-populated SEDs that do, in fact, have evidence for an IR excess. Out of those 28, 5 are probably giants but may not be K giants. We conclude that IR excesses are rare among our sample of K giants, at best ∼10%. Given the biases in our sample (described in detail below), this fraction is probably less in Li-rich RGs and substantially less in Li-poor RGs.

We now examine our ensemble population in several different ways.

6.1. Comparison of IR Excesses to Literature

Not all of our IR excess sources are newly identified as having an IR excess; after all, dlR97 and others in the literature identified these sources based on their IR properties. However, one important goal of our paper was to reassess the IR excesses in these sources given the higher spatial resolution data now available. Other recent papers have identified IR excesses in some of our targets using similar or the same data; McDonald et al. (2012) and Kumar et al. (2015) both identify sources with IR excesses. Kumar et al. (2015) has similar goals to our paper, and many targets overlap. We recover all 7 of their IR excess K giants.

McDonald et al. (2012) did an analysis of more than 107,000 *Hipparcos* stars, incorporating data from *IRAS*, SDSS, DENIS, 2MASS, *MSX*, *AKARI*, and *WISE*, in order to identify stars with an IR excess. Out of our targets, 118 are included in the catalog presented in McDonald et al. (2012). Only some of the IR excess objects are explicitly discussed in McDonald et al. (2012), so only one of our objects (HD 65750) is mentioned there as having an IR excess; we agree that it has an IR excess. Following the prescription laid out in their paper (in their Figure 7 and associated discussion), however, 5 more objects (out of the 118 we have in common) can be identified as having at least potentially significant IR excesses: HD 6665, HD 96195, Tyc3917-01107-1, HD 203136, and HD 219025. Two of those (HD 96195, HD 219025) are ones we have already identified above as having IR excesses. The remaining three (HD 6665, Tyc3917-01107-1, and HD 203136) do not appear to us to have excesses (Figure 14); we investigated why the McDonald et al. calculations might have identified them as excess objects. HD 6665 has the *IRAS* 12 μm point slightly above the photosphere, but all other detections are on the photosphere ([3.4]–[22] = 0.09); the value of E_{IR} calculated by McDonald et al. is 2.16, likely a result of the *IRAS* point being slightly high. Tyc3917-01107-1 is in a nearly identical situation, though in this case, the *IRAS* 12 μm point is closer to the photosphere; the McDonald et al. E_{IR} is 1.73, and [3.4]–[22] = 0.07, so again, not likely to have a real excess. HD 203136 has some irregularities in its SED, where there is a lot of scatter among the the *MSX*, *AKARI*, and *IRAS* points near 8–12 μm; they are inconsistent with each other and the rest of the SED, and all of them are too high compared to the *WISE* [12] and [22] points. The McDonald et al. E_{IR} comes out to be 4.89 most likely because the *MSX*, *AKARI*, and *IRAS* photometric points are high. We take *WISE* to be the most reliable, because it has the highest spatial resolution; [3.4]–[22] = –0.21 $\pm$ 0.14, so there is no detectable IR excess in this object.

Thus, we conclude that we have recovered all of the recent literature-identified IR excess sources. We have identified 18 more objects out of our aggregate data that have IR excesses, though not all of them may be first ascent K giants.

Many of the sources in our sample had been identified as IR excess sources from *IRAS* measurements. All 21 of the sources with the largest *IRAS* IR excesses ([12]–[25] > 0.5 mag) from detections—not limits—in the PSC are recovered as IR excess sources here. Nearly all, 11 of 14, of the sources with detections and [12]–[25] > 0.5 in the FSC are recovered.

There are just three sources (HD 76066, HD 112859, HD 203251) for which the FSC detections at [12] and [25] result in [12]–[25] > 0.5, but the measured *WISE* flux densities are substantially lower than the *IRAS* FSC flux densities, such that these stars do not have detectable IR excesses. The [3.4]–[22] for these objects are 0.05, 0.08, 0.08 mag, respectively, so these sources do not have measurable IR excesses to 22 μm. This is probably a direct result of the higher spatial resolution of *WISE* better measuring the flux density of the target.

However, many of the sources with smaller measured *IRAS* excesses are not recovered as IR excess sources. In the SEDs for these cases, one can often see the *IRAS* PSC suggesting an IR excess, the *IRAS* FSC suggesting less of an excess, and *WISE* (and sometimes *AKARI*) suggesting a smaller or no excess. (Similarly, and more dramatically, the upper limits are often pushed lower and lower in the SEDs.) In these cases, what is most likely going on is that the increased spatial resolution and the fainter sensitivity reached resolves out
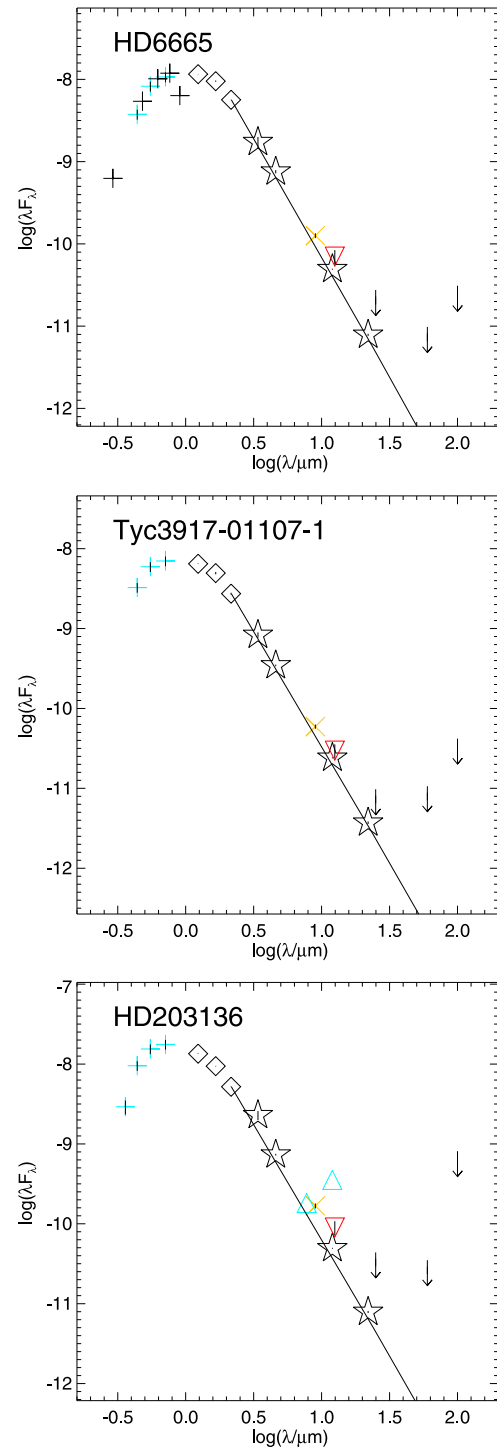
Figure 14. SEDs for three sources identified in McDonald et al. (2012) as potentially having IR excesses, but for which we do not identify an IR excess. Notation is as in Figure 11. See text for discussion of individual objects.

extended emission and/or source multiplicity, lowering the overall measured flux density. However, there are also some noticable calibration offsets between *IRAS* and 2MASS+*WISE*; see Section 6.5 below.

6.2. SED Interpretation

IR excess around stars is commonly interpreted as due to circumstellar dust in a shell or disk or ring. In Table 5, we

Figure 15. [3.4] vs. [3.4]–[22] for the entire sample where [3.4] and [22] are both detected (upper left), the dlR97 sample alone (upper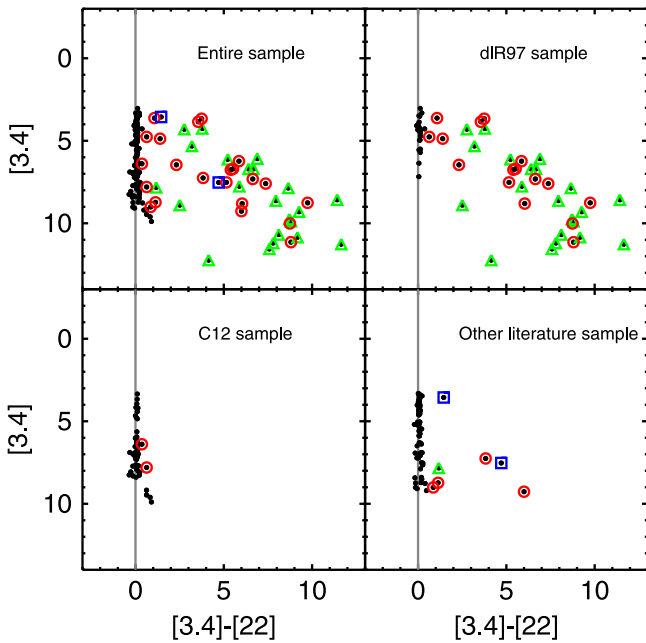 right), the C12 sample alone (lower left), and the remaining literature sample (lower right). All of the sources subject to source confusion (Section 4.3) have additional green triangles overplotted. The sources we identify as having an IR excess (Section 5) are circled in red; the sources we called out as having an IR excess but potentially not K giants (Section 5) are overplotted in blue squares (some of these are not detected at [3.4] and thus do not appear). The vertical line at [3.4]–[22] = 0 indicates the value expected for photospheres. All of the sources significantly redward of [3.4]–[22] ∼ 0 are either identified as IR excess sources or are likely to be subject to source confusion.

Figure 16. K_s vs. K_s–[22] for the entire sample where K_s and [22] are both detected (upper left), the dlR97 sample alone (upper right), the C12 sample alone (lower left), and the remaining literature sample (lower right). Notation is as in Figure 15. There are more sources in this plot than in the prior plot, but the same conclusions apply—all of the sources significantly redward of K_s–[22] ∼ 0 are either identified as IR excess sources or are subject to source confusion. The scatter in the K_s–[22] = 0 locus is larger in this plot, reflecting larger K_s uncertainties.

include an approximate wavelength at which the excess appears. Sources where the IR excess is already present between 2 and 5 μm likely have very large disks or envelopes of dust that reach nearly all the way in to the star. Sources where the IR excess does not start until 10 or 20 μm likely have shells or rings of dust, where there is a gap between the star and the dust. Obtaining total dust masses would require detailed modeling of the star+dust SED (plus assumptions about the composition of the dust) and is beyond the scope of this paper. On the whole, larger excesses likely correspond to larger quantities of dust. For the seven sources modeled by Kumar et al. (2015), under the array of assumptions they made, they find dust temperatures between 75 and 260 K, but they do not estimate total dust mass.

The circumstellar dust around these stars could plausibly be dust ejected by the K giant, but it could also be residual debris disk dust in the system heated afresh by the first ascent onto the RGB (e.g., Jura 1999). However, debris disks are typically relatively low-mass, producing small IR excesses; (re-) illumination of an old debris disk is not a particularly reasonable explanation for the very large IR excesses.

6.3. Color–Magnitude Diagrams

Another view of the IR excesses for the entire sample can be obtained by plotting [3.4] versus [3.4]–[22], as illustrated in Figure 15. Photospheres (that is, stars without any circumstellar dust) should have [3.4]–[22] ∼ 0. All of the sources significantly redward of [3.4]–[22] ∼ 0 are either identified as IR excess sources or are identified as subject to source confusion
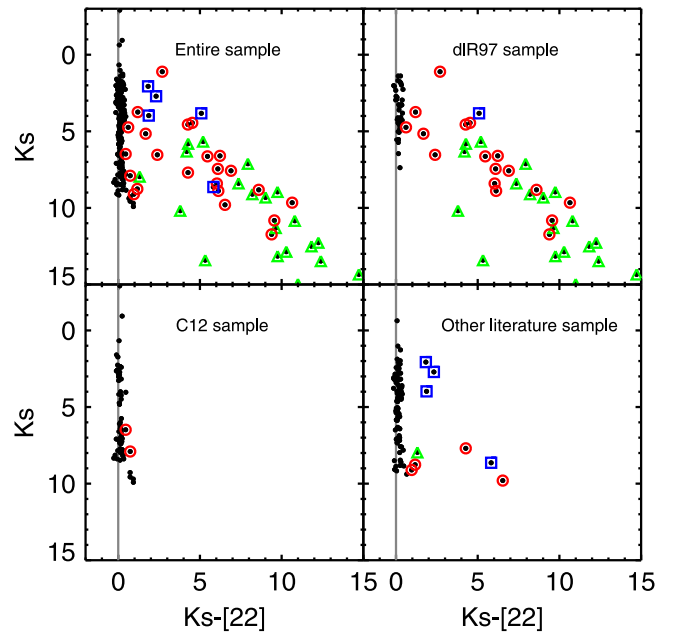
(Section 4.3 above). Even though [3.4]–[22] is a nearly ideal metric with which to assess IR excesses, many of our objects are saturated at [3.4]. Therefore, it is worthwhile to examine the K_s–[22] plot as well; see Figure 16. More sources are included in this plot, and there are still very large excesses here, even among the objects thought to be K giants. There is more scatter in the K_s–[22] = 0 photospheric locus, reflecting some of the larger uncertainties in the measurements of the (bright) stars in K_s.

Many of the reddest sources (redward of [3.4]–[22] ∼ 5 or K_s–[22] ∼ 5) in either of these figures are the dropped sources; their location in this diagram is not surprising given some of the SEDs shown in Figuers 8 and 9. Still, many of the large IR excess K giants we identified above are very red in this diagram. For context, young stars in Taurus (which are known to have substantial dusty disks and envelopes) have a typical [3.4]–[22] ∼ 4, though some extend to [3.4]–[22] ∼ 10 (Rebull et al. 2011). The range of IR excesses for the objects we believe to be K giants is comparable to the range of IR excesses found in young stars. Some of the IR excesses seen in these K giants are very large indeed, with many well past 4 out to 10. However, these large IR excesses are not distributed uniformly among the subsamples. The dlR97 sample includes the large excesses; the excesses in the literature Li-rich sample are much more moderate. The C12 sample has very few excesses, and those are quite small.

6.4. C12 Sample

Recall that the dlR97 sample is biased toward IR-bright sources, and the literature sample is strongly biased toward high A(Li) stars. The C12 sample of RGs is unbiased with respect to A(Li) and IR excess, though it does have a larger proportion of fast rotators than a random RG field population.

Additionally, it has A(Li), $v \sin i$, and $^{12}C/^{13}C$ measured for every star in the sample, in contrast to the rest of the sources, for which only some of these parameters are available. We had hoped that we would detect IR excesses in enough of these sources to look for correlations. However, only two of the C12 sources (G0928+73.2600 and Tyc0276-00327-1) have any excesses, and they are both small, <0.6 mag. Out of the whole 86-star C12 sample, the fraction of stars with an IR excess is 2%. Considering just those with well-populated SEDs to 22 μm, 2/79 ($3^{+4}_{-0.9}$%) of the stars have an excess by [22] (using the binomial statistics from the appendix in Burgasser et al. 2003 to obtain uncertainties).

The three best candidates for planet accretion listed in C12 are G0928+73.2600, Tyc0647-00254-1, and Tyc3340-01195-1. If the IR excess production process is directly related to planet accretion, one would expect all three of these to have an IR excess, but only one of these has a measurable IR excess. The SEDs for Tyc0647-00254-1 and Tyc3340-01195-1 do not suggest excesses at 22 μm. Admittedly, for Tyc0647-00254-1, the sole non-*WISE* point beyond 3 μm is an *AKARI* 9 μm point that is slightly above the photosphere, though the *WISE* 12 and 22 μm points are not consistent with *AKARI* and do not suggest an IR excess. (In comparison, Tyc0276-00327-1 has a very similar SED, but in that case, the 22 μm point is enough above the photosphere that a small IR excess is suggested.) Tyc3340-01195-1 has no points other than *WISE* beyond 3 μm, and neither does G0928+73.2600.

The two stars with a significant IR excess are split in terms of properties. Tyc0276-00327-1 seems to be a relatively unremarkable star in the C12 data; it has a subsolar Li abundance (A(Li)$_{NLTE}$ = −0.24 dex), is a slow rotator (4.2 km s^{-1}), and has an average $^{12}C/^{13}C$ (17). However, G0928+73.2600 is a particularly interesting star (C12; Carlberg et al. 2010) because it has particularly high Li (A(Li)$_{NLTE}$ = 3.30 dex), relatively rapid rotation (8.4 km s^{-1}), and high $^{12}C/^{13}C$ (28).

G0928+73.2600 was also included in the ensemble of Li-rich stars in Kumar et al. (2011). Its location on a Hertzsprung-Russell (H–R) diagram is similar to many other Li-rich RGs in that sample. Kumar et al. (2011) noted that many Li-rich RGs have properties consistent with red clump stars, and suggested the possibility that an episode of Li regeneration may occur during the He flash for some RGs. G0928 is noteworthy among that sample of RGs for having the largest $^{12}C/^{13}C$. (The importance of $^{12}C/^{13}C$ in interperting Li-rich stars is described in more detail in Section 7 below.) Carlberg et al. (2010) and C12 argued in favor of external replenishment as a source of the high Li given given its relatively high $^{12}C/^{13}C$.

6.5. The dlR97 Sample and the Original IRAS Color–Color Diagram

The dlR97 sample is strongly biased toward sources that are bright in the IR, and so it is not surprising that there are many more bright IR sources, and large IR excesses, found in the dlR97 sample than in either the C12 or the "other literature" samples. In de la Reza et al. (1996), dlR97, and Siess & Livio (1999), there is a plot of *IRAS* colors for their targets, which they use to describe a proposed evolutionary sequence of objects in the diagram. This plot is described as a color–color diagram, where the following is their definition of color:

$$[\lambda_1 - \lambda_2] = \log(\lambda_2 F_1) - \log(\lambda_1 F_2) \qquad (2)$$

where λ is wavelength and F is flux density. In more recent papers, driven at least in part by *Spitzer* and *WISE* work, the convention for color is instead truly a difference of magnitudes:

$$M_1 - M_2 = 2.5 \times \log\left(\frac{F_2}{F_1}\right). \qquad (3)$$

And in the IR, where the band names are often the wavelength of the bandpass, this difference in magnitudes would be written, e.g., $[\lambda_1] - [\lambda_2]$. In any case, the *shape* (if not the specific *values*) of the distribution of points in the dlR97 color–color plot is recovered by using [12]–[25] and [25]–[60] defined as in Equation (3).

In Figure 17, we have made the plot analogous to that from dlR97 and collaborators, namely [25]–[60] against [12]–[25], just for the original dlR97 sample. The first panel uses the values from the *IRAS* PSC, as in dlR97. The shape of the overall distribution is similar to what they have obtained, in that there is a locus near [12]–[25] $\sim$ 0 extending up to a range of [25]–[60] values, and a broad "bubble" of points extending to the right. However, we find that the upper envelope of the distribution (near [12]–[25] = 1–4, and [25]–[60] $\sim$ 3–4) is defined entirely by objects we suspect should be dropped from the sample because they are subject to source confusion. Removing these points from the plot signficantly reduces the range of colors found for K giants. We have also indicated which of these sources are the ones for which we have identified an IR excess. Most of the PSC points that are still thought to be K giants with [12]–[25] > 0.5 are also ones we identify as having an IR excess, but there are several that we do not recover. These sources are identified in at least one of [12], [25], or [60] with data quality flag = 1, e.g., a limit, not a detection. dlR97 started from the Pico dos Dias Survey (PDS; Gregorio-Hetem et al. 1992), which reports having started from the *IRAS* PSC, only the high-quality detections. However, several of the points in our version of this diagram (which, again, is just the dlR97 sample) do not have high quality detections at all 3 of the relevant *IRAS* bands.

The second panel of Figure 17 uses the *IRAS* FSC instead of the PSC, again, just for the dlR97 sample. (Recall from Section 3.2 above that 36 of the dlR97 objects are also detected in the FSC in any band, so not all of the objects from the first panel appear in the second panel.) All of the objects we suspect should be dropped do not have FSC measurements, so they do not appear in the second panel. Again, most of the sources with detections (not limits) in [12], [25], and [60], and large excesses with [12]–[25] > 0.5, are also ones we identify as having an IR excess, but there is one that we do not recover. (It is HD 76066, discussed above as having significantly lower *WISE* flux densities than *IRAS*, and not really having an excess.) Interestingly, in moving between the PSC and FSC plots, the envelope delineating the red excursion of the distribution of points shrinks dramatically in size, and there are fewer points within the "bubble"—more points are on the [12]–[25] $\sim$ 0 locus where no IR excess is measured. Whereas $\sim$45% of the K giants in the first panel have [12]–[25] > 0.5 mag, by the second panel, just $\sim$30% have [12]–[25] > 0.5 mag. However, there are fewer objects overall in the second panel.

We can carry this further—both *IRAS* and *WISE* had a 12 μm channel, and *IRAS* had a 25 μm channel, close to the *WISE* 22 μm channel. Though the filter bandpasses are far from identical, they ought to give similar estimates of the
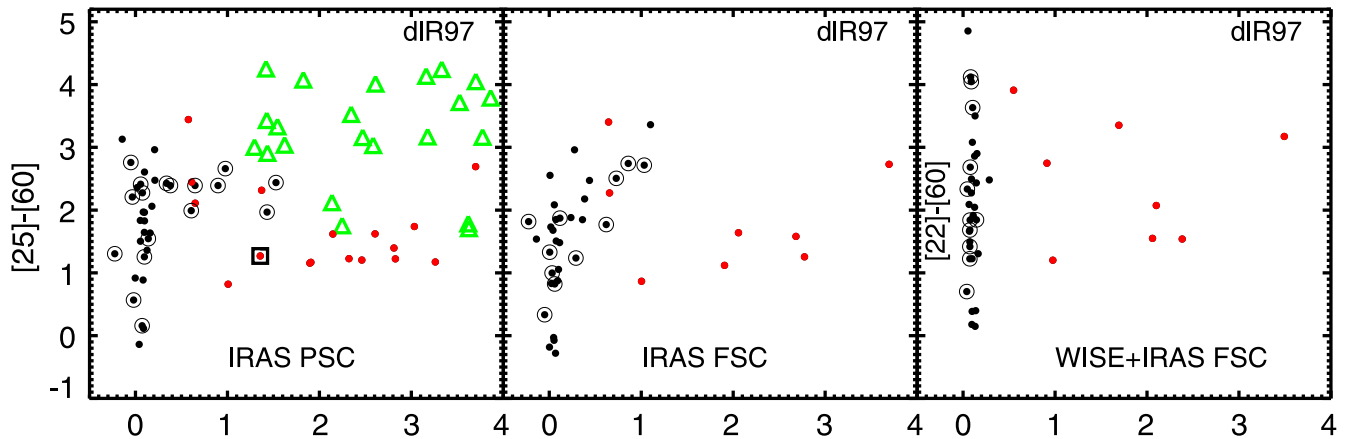
Figure 17. Color–color plot of the dlR97 sample in the style of those found in de la Reza et al. (1996), dlR97, and Siess & Livio (1999), where the *IRAS* [25]–[60] color is plotted against the *IRAS* [12]–[25] color (see text for clarification of units). The left panel uses *IRAS* PSC, the middle panel uses *IRAS* FSC, and the right panel combines *WISE* [12] and [22] with *IRAS* FSC [60]. Green triangles (first panel only) are objects we identify as likely subject to source confusion. Red dots are objects we identify as having an IR excess. The square (first panel only) indicates the only object appearing in this plot which we identify as having an IR excess, but that we suspect may not be a K giant. Additional circles around sources are those for which the *IRAS* PSC (or FSC) data quality flag in at least one of the relevant bands is 1, indicating a limit. Objects may not be the same between the first and second panels; all the objects in the third panel also appear in the second panel. The most important features in these plots are: (1) the bulk of the distribution delineating the reddest IR excesses is composed of objects likely subject to confusion; (2) the envelope of the distribution shrinks when going from the PSC to the FSC, and shrinks further when *WISE* is used, suggesting that the apparent IR excesses measured in *IRAS* vanish when higher spatial resolution observations are used. (3) All of the largest excess K giants (those with detections and [12]–[25] > 0.5 mag) are recovered as IR excess sources, except for HD 76066, discussed in Section 6.1.

broadband IR excess near their respective wavelengths. In the third panel of Figure 17, we have used the *WISE* [12] in place of the *IRAS* [12], and *WISE* [22] in place of the *IRAS* [25]; for 60 μm, we retain the *IRAS* FSC values. All of the objects from the middle panel with *WISE* detections at [12] and [22] appear in the third panel. The distribution continues to shrink toward the [12]–[22] = 0 locus, with now only ~20% of the sources having [12]–[22] > 0.5 mag. As higher spatial resolution and more sensitive observations are available, the apparent IR excesses shrink.

However, in using *WISE* in place of the *IRAS* bands, we are implicitly assuming that the two missions are calibrated in the same fashion, or at least consistently with each other. It is possible that the change in distributions (the shrinking of the "bubble") of points between the panels of Figure 17 can be accounted for, at least in part, by different calibrations of the instruments. To investigate this, we compared the *IRAS* PSC to the FSC first, as a check, to make sure that they were internally calibrated consistently with respect to each other. Then, we compared the *IRAS* FSC to the *WISE* values. In all cases, we used our entire sample, but only those with data quality flags 3 or 2. The comparison of the 12 and 25 μm channels (calculating (PSC-FSC)/PSC with the values in magnitudes) shows that they are indeed well-matched to each other, with no significant average offset between them. For [12], the center of the best-fit Gaussian to the distribution is 0 mag, with a width of 0.04 mag. For [25], the center is 0.02 mag, and the width is 0.04 mag. However, in comparing the *WISE* and *IRAS* FSC 12 μm channels, there is a clear offset of ~30% between *WISE* and *IRAS*, in the direction of the FSC being brighter. (At [12], calculating (FSC-*WISE*)/FSC in mag, the center of the Gaussian is 0.26 mag and the width is 0.05 mag.) For 25 μm, we expected larger differences between *WISE* and *IRAS* because of the different bandpasses. There is an offset between *IRAS* FSC and *WISE* of ~15%. (The center of the Gaussian is 0.14 mag, and the width is 0.06 mag.) It is again in the direction of the FSC being brighter. Once one is made aware of this offset, one can see it systematically in the SEDs of the

ensemble where both *IRAS* and *WISE* are available. This effect is in the same direction one would expect if the higher spatial resolution of *WISE* was resolving out background contributions to the *IRAS* flux, which may still be a part of what is going on. (We note that we only did this comparison for the objects in our sample, not the entire *IRAS* or *WISE* catalogs or over a controlled range of backgrounds. Such a comparison is beyond the scope of our study.) Nonetheless, the net effect in the last panel of Figure 17 is to move the envelope of points left and up. First, on the *x*-axis in this panel, [12] and [22] now both come from *WISE*, and are internally well-calibrated, so stars without excesses are closely clumped near 0 in [12]–[22]. They are more tightly clumped than they were for *IRAS*, which collapses part of the distribution. Stars with excesses have slightly smaller [12]–[22] (from *WISE*) on average than [12]–[25] (from *IRAS*), because the systematic calibration offset for [12] is slightly larger than for [25] ([22]). Second, on the *y*-axis, [60] is still from *IRAS*, presumably well-calibrated internally to the other *IRAS* bands. Since both [12] and [25] are slightly systematically brighter compared to *WISE*, if we assume [60] is also slightly brighter as a result of calibration systematics, this will push the distribution of points slightly up in the diagram—which can be seen in the figure.

So, we conclude that some (but not all) of the reduction in the range of points in Figure 17 can be accounted for in the different calibrations of *IRAS* and *WISE*. The average calibration effect for the ensemble is on the order of a few tenths of a magnitude. However, the movement of individual objects between plots is primarily a reflection of more accurate measurements of the IR flux from the stars.

Kumar et al. (2015) also made plots like our Figure 17, though in the same units as dlR97 (using Equation (2)). Their plots have similar distributions of points as ours do.

7. ABUNDANCES AND ROTATION RATES

One of our original goals of this paper was to seek a correlation between lithium abundance (and rotation rate and

the ^{12}C/^{13}C ratio) and IR excess in K giants, but with only ∼10% of our sample likely to have IR excesses, our ability to test correlations with IR excess is somewhat limited. However, we can still infer some things about the relationship among these parameters. In order to better understand these relationships, however, we need to make sure that our already biased sample is as clean and internally consistent as possible.

We now discuss how we limit the sample to identify Li-rich stars, and likely first ascent K giants, and look at the relationship between IR excess, Li abundance, rotation rate, and ^{12}C/^{13}C.

7.1. Definition of Li-rich

A substantial number of objects were added to our sample on the basis of a paper in the literature asserting that the K giant was Li-rich. However, everyone does not use the same definition of Li-rich. For example, dlR97 did not report Li abundances, but identified certain stars as Li-rich based on equivalent widths. C12 included Li abundances, and determined them under both LTE and NLTE assumptions. Other literature sources sometimes report only equivalent widths, or only LTE abundances. If we were to rely solely on literature reporting, 183/316 sources are Li-rich.

However, we wished to be a bit more restrictive, or at least internally consistent. For those sources for which we have NLTE Li abundances, we took those with $A(\mathrm{Li})_{\mathrm{NLTE}} \geqslant 1.5$ dex as Li-rich. If there was no NLTE abundance available, we took those with $A(\mathrm{Li})_{\mathrm{LTE}} \geqslant 1.5$ dex as Li-rich. If there was no abundance in the literature (e.g., just equivalent widths), we did not identify it as Li-rich. If we thought (based on the analysis above) that it was not a K giant, we did not identify it as Li-rich (that includes the 24 dropped sources, the carbon star, and the S-type star). A total of 62 sources are missing $A(\mathrm{Li})$, including the dropped sources. Using this approach, 139 stars in our sample are Li-rich. Unfortunately, 10 of these sources are the ones with very sparse SEDs, and 29 more have relatively sparse SEDs (though both of the sources identified as having an IR excess from these SEDs are Li-rich). Just 9 of the remaining 100 sources have well-populated SEDs and an IR excess. There are 115 that are Li-poor, 7 of which have sparse SEDs, and 6 of which have an IR excess.

7.2. Restrictions on Log g and T_{eff}

This study is aimed at understanding the Li-IR connection for K giants (first ascent RGB stars and red clump stars); however, we have already noted above that some of our sample are suspected to be more evolved AGB stars or other non K-giant contaminants. We can try to limit the contamination by requiring that there be an estimate of log g and T_{eff}, and that these values fall within a certain range.

We identify stars with log $g > 3.5$ as not likely giants. This selection should weed out subgiant and dwarf stars for which high Li may not be unusual. Out of the entire set of 316(–24 confused sources), 46 have no log g estimate available to our knowledge. Of the remaining sources, 16 have log $g > 3.5$ (with 2 more having exactly 3.5 being left in the sample).

We can put both upper and lower constraints on T_{eff}. Temperatures <3700 K are likely to be AGB stars, not first ascent K giants, because the AGB reaches cooler temperatures. On the upper end, temperatures >5200 K are likely to be dwarf stars or subgiants that have not yet completed first dredge-up

(the deepening of the convection zone that reduces the surface Li abundances during the post-MS phase). Out of the entire set of 316(–24 confused sources), 20 have no T_{eff} estimate at all. Of the ones with T_{eff}, 6 are cooler than 3700 K, several of which we identified above as "likely too cool" for our sample. There are 3 stars with $T_{\mathrm{eff}} = 5200$ K (left in our sample), and there are 19 hotter than 5200 K.

The net loss of objects out of our sample by requiring that there be an $A(\mathrm{Li})$ and that T_{eff} and log g are in the correct range is 97 objects (some objects counted in more than one omission category above), leaving 219 in the sample. That sample includes the 10 very sparse SEDs, and 33 of the relatively sparse SEDs. Of the 219, 119 (54% ± 6%)[13] are Li-rich as per our definition above (with 10 + 26 of those being the very sparse/ relatively sparse SEDs). Just 13/219 (6% ± 2%) of this sample have an IR excess. Bringing Li into it, 11/119 (9 ±3%) of the Li-rich stars have an IR excess, and 2/100 ($2^{+3}_{-0.6}$%) of the Li-poor stars have an IR excess (with 7 sparse SEDs included).

The sparse SEDs included in the above calculation likely miss more subtle IR excesses, so we can repeat the analysis on the subset of 176 stars with well-populated SEDS. There are 83 stars in this sub-sample that are Li-rich, 93 that are Li-poor, and 11 that have an IR excess. Of the Li-rich stars, 9/83 (11^{+4}_{-3}%) have an IR excess; of the Li-poor stars, 2/93 (2^{+3}_{-1}) have an IR excess. Although we are well into the regime of small-number statistics, IR excesses appear to be at least 2–3 times as common among Li-rich stars compared to Li-poor stars. Kumar et al. (2015) came to a similar conclusion, that IR excesses are rare in the general K giant population. They found that only ∼1% of RGs (their sample is dominated by Li-poor stars) have an IR excess. Of the 40 Li-rich stars in their sample, they find 7 (18^{+8}_{-4}%) with an IR excess.

7.3. Relationships Among $A(\mathrm{Li})$, $v \sin i$, ^{12}C/^{13}C, and IR Excess

For the rest of this section, we will only use the cleanest possible sample of 176 RGs with T_{eff} and log g consistent with K giant stars, and with well-populated SEDs, from the prior section.

Figure 18 shows $A(\mathrm{Li})_{\mathrm{NLTE}}$ versus [3.4]–[22] for the 176 stars in the cleanest possible sample. This plot suggests that if a star has a large IR excess, it probably has a large $A(\mathrm{Li})$, but having a large $A(\mathrm{Li})$ does not mean that it necessarily has a large IR excess. Smaller excesses can be found at all abundance levels. Very similar results are obtained if LTE rather than NLTE lithium abundances are used, or if K_s–[22] is used instead of [3.4]–[22]. Within the sample of Li-rich objects with IR excesses, there does not seem to be a trend that, say, the largest Li abundances are always found with the largest IR excesses.

Figure 19 shows $A(\mathrm{Li})_{\mathrm{NLTE}}$ versus $v \sin i$. Fast-rotating stars also often (but not exclusively) have large $A(\mathrm{Li})$, which has been previously noted (e.g., Drake et al. 2002). What is further revealed by this plot is that many of the fast rotating, Li-rich stars are also those with IR excesses. Half of the Li-rich stars that also show fast rotation have an IR excess, whereas only one Li-rich star among the more populated slow rotators has an IR excess. Additionally, only one RG with an IR excess shows neither high rotation nor enriched Li. Thus, having both high Li and fast rotation is a stronger predictor for an IR excess than high Li

---

[13] The errors presented here are assumed to be the larger of either Poisson errors or the binomial approximation found in the appendix of Burgasser et al. (2003).
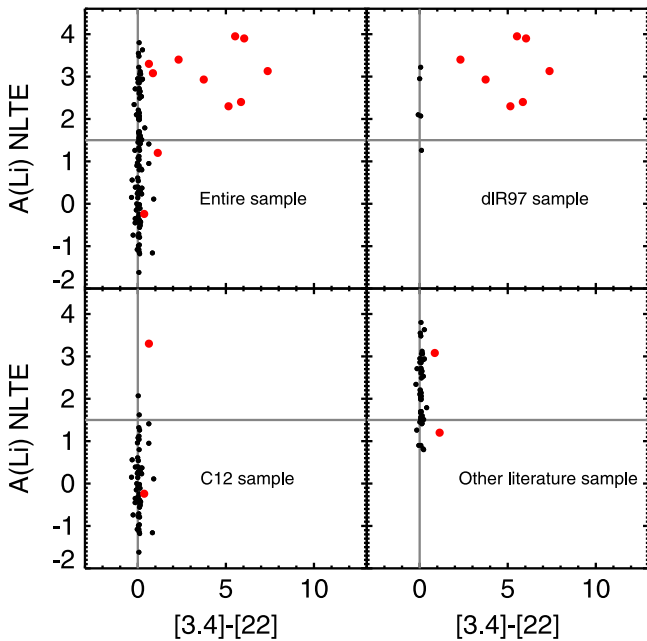
Figure 18. $A(\text{Li})_{\text{NLTE}}$ vs. [3.4]–[22] for the 176 stars in the cleanest possible sample. The vertical line at [3.4]–[22] = 0 indicates the photospheric locus, and the red points are the IR excess stars. The horizontal line at $A(\text{Li}) = 1.5$ dex indicates our adopted division between Li-rich and not Li-rich. The entire (available) sample is plotted in the upper left, and the component samples (dIR97, C12, and the other literature) are shown in separate panels. A very similar plot is obtained if $A(\text{Li})_{\text{LTE}}$ is used instead of $A(\text{Li})_{\text{NLTE}}$, or K_s–[22] rather than [3.4]–[22]. If a star has a large IR excess, it probably has a large $A(\text{Li})$, but having a large $A(\text{Li})$ does not necessarily indicate it has a large IR excess.

Figure 19. $A(\text{Li})_{\text{NLTE}}$ vs. $v \sin i$ in km s^{-1} for the cleanest possible sample. The vertical line at 8 km s^{-1} divides the fast from the slow rotators. The red points are the IR excess stars. The horizontal line at $A(\text{Li}) = 1.5$ dex is the division between Li-rich and not Li-rich. The entire (available) sample is plotted in the upper left, and the component samples (dIR97, C12, and the other literature) are shown in separate panels. A very similar plot is obtained if $A(\text{Li})_{\text{LTE}}$ is used instead of $A(\text{Li})_{\text{NLTE}}$. Fast-rotating stars also often (but not exclusively) have large $A(\text{Li})$, and often also have an IR excess.

alone. This suggests that relatively enhanced angular momentum is necessary for the ejection of circumstellar shells in Li-enriched stars. We note that there are several IR excess sources unable to be plotted in this diagram because no $v \sin i$ is available, and that a fundamental uncertainty in the use of projected rotational velocities is that inclination effects can mask rapid rotation.

As seen in Figure 20, no correlations can be found between IR excess and the carbon isotope ratio, $^{12}\text{C}/^{13}\text{C}$. Very low $^{12}\text{C}/^{13}\text{C}$ is thought to indicate substantial extra mixing. IR excess sources (extreme and moderate) are found with both low and high $^{12}\text{C}/^{13}\text{C}$, where we have taken 15 as the division between low and high values. The largest IR excesses do not have unusual carbon ratios. However, we note that relatively few of our stars have a measure of $^{12}\text{C}/^{13}\text{C}$, so this may introduce some additional biases.

In Figure 21, we plot the $A(\text{Li})$ versus $^{12}\text{C}/^{13}\text{C}$, a plot that should give some insight into the Li enrichment mechanism. In the presence of extra mixing, the surface values of both $^{12}\text{C}/^{13}\text{C}$ and $A(\text{Li})$ will be reduced if the mixing proceeds slowly (e.g., Denissenkov & VandenBerg 2003). However, when the mixing proceeds rapidly, newly synthesized Li can be brought into the convection zone, where it is long-lived, such that the surface Li is enhanced while $^{12}\text{C}/^{13}\text{C}$ decreases (e.g., Denissenkov & Herwig 2004). Once the source of the Li (^{3}He) is considerably depleted, a net destruction of Li begins and $A(\text{Li})$ will again be reduced. The physical mechanism behind this very fast mixing is still under investigation. Denissenkov & Herwig (2004) argued that rotation-induced mixing was required, and since RGs are slow rotators, an outside source of angular momentum such as binary interactions or planet engulfment was required. However, Palacios et al. (2006) argued that the shear turbulence caused by
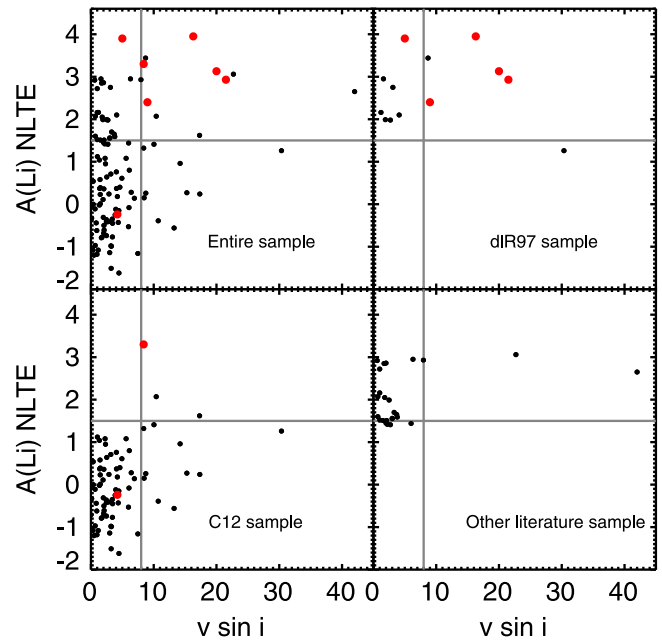
differential rotation was not sufficiently fast to increase Li at the surface. Magnetic buoyancy is another possible model (e.g., Guandalini et al. 2009).

Planet engulfment that does *not* trigger fast mixing could be identified with higher than expected Li, but with a relatively high $^{12}\text{C}/^{13}\text{C}$. In Figure 21, the C12 sample shows the most homogeneously measured $^{12}\text{C}/^{13}\text{C}$ and the only sample unbiased toward Li. The stars generally show the expected linear trend of lower $^{12}\text{C}/^{13}\text{C}$ and lower $A(\text{Li})$ for stars that experience different degrees of mixing. Other panels of the plot show the addition of the large sample of all the literature Li-rich stars, which span a large range of $^{12}\text{C}/^{13}\text{C}$. Red circles again indicate IR excess. Stars with the clearest sign of substantial internal mixing (very low $^{12}\text{C}/^{13}\text{C}$ and high Li) show no evidence of an IR excess. However, this is not entirely unexpected. As pointed out by Denissenkov & Herwig (2004), the timescale over which a shell is ejected and dissipates (e.g., the timescale for the IR excess to appear/disappear) is of order 10^4–10^5 years, compared to the timescale of Li regeneration, which is of order 10^5–10^6 years. Very low values of $^{12}\text{C}/^{13}\text{C}$ are only reached at the latest stages of Li regneration, well after the IR excess has disappeared. Figure 21 does, however, exhibit a tantalizing correlation between the Li and $^{12}\text{C}/^{13}\text{C}$ of many of the IR excess stars in this plot. We offer no explanation for this trend but suggest that it may be informative on the conditions of the star when the shell is ejected. Adding additional objects to this plot (via determinations of $^{12}\text{C}/^{13}\text{C}$) will likely further illuminate any relationship.

Given the relative shortness of the IR phase compared to the Li synthesis phase, one would expect little change in $A(\text{Li})$ for any particular star as it traverses the IR color–color diagram (Figure 17). This expectation is confirmed by the fact that we
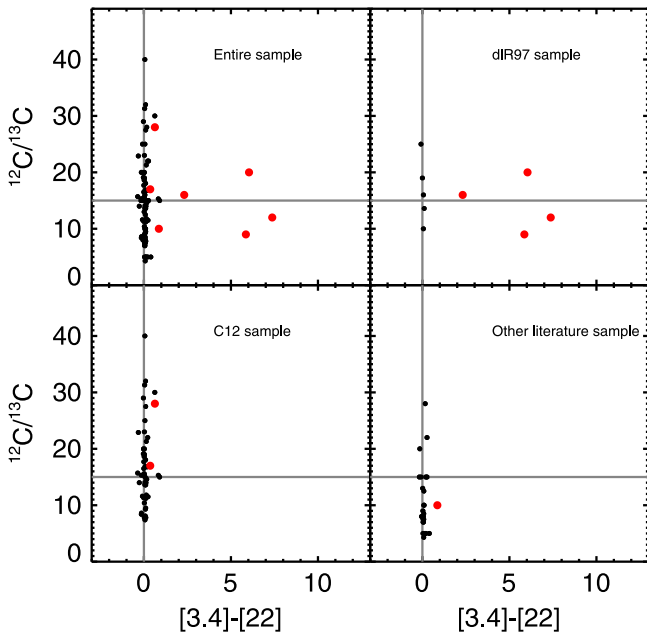
Figure 20. $^{12}C/^{13}C$ vs. [3.4]–[22] for the cleanest possible sample. The vertical line at [3.4]–[22] = 0 indicates the photospheric locus, and the red points are the IR excess stars. The horizontal line at $^{12}C/^{13}C = 15$ is the division between a high and low ratio. The entire (available) sample is plotted in the upper left, and the component samples (dIR97, C12, and the other literature) are shown in separate panels. A very similar plot is obtained if $A(Li)_{LTE}$ is used instead of $A(Li)_{NLTE}$. There is no discernible correlation of IR excess with $^{12}C/^{13}C$.

Figure 21. $A(Li)$ vs. $^{12}C/^{13}C$ for the cleanest possible sample. The vertical line at $^{12}C/^{13}C = 15$ is the division between a high and low ratio; the horizontal line at $A(Li) = 1.5$ is the division between Li-rich and Li-poor. The red points highlight the IR excess stars; smaller circles are the smaller excesses, and larger circles are larger excesses ([3.4]–[22] > 1). The entire (available) sample is plotted in the upper left, and the component samples (dIR97, C12, and the other literature) are shown in separate panels.

do not see a correlation between level of Li-richness and the strength of the IR-excess (Figure 18). Furthermore, since IR excess is seen around a wide range of $A(Li)$, we can speculate that the Li regneration reaches different maximum $A(Li)$ values in each star.

7.4. Biases and Future Work

An additional concern in interpreting Figuers 18–20 is that our sample has many substantial biases within it. One very significant bias is that many of the sources were discovered based on their *IRAS* colors, e.g., they are biased toward IR-bright sources. The subsamples are separated out in Figures 18–20 specifically because of this bias—a substantial fraction of the dIR97 sample and a smaller fraction of the literature sample is based on *IRAS* colors. In Figure 18, it can be seen that all of the large IR excesses are from the dIR97 sample. (Some of the large excesses seen in, e.g., the literature sample in Figure 15 do not appear in this plot because they do not have log g or T_{eff} in the correct range, etc.) Those largest excesses draw the eye and dominate the relationships found in the plots. The relationships are not as obvious in just the C12 sample, which is the least biased with respect to IR properties.

To first order, we hoped we could try to constrain the influence of this bias by omitting K giants known primarily by their *IRAS* names. Only five of the sources making it into our "cleanest possible" sample have *IRAS* names, but four of them are among the largest IR excesses ([3.4]–[22] > 2).

We also have biases in the sample due to the incomplete information for stars in the sample. A number of the IR excess sources have no T_{eff} and/or log g and were removed from our detailed analysis of IR excess among K giants. Furthermore, half of the Li-rich sample has no measure of $^{12}C/^{13}C$ and/or $v \sin i$. This makes comparisons between, e.g., Figures 19 and

20, difficult because the IR excess stars appearing in each plot are not all the same stars. Follow-up high resolution optical spectra to measure these missing stellar parameters would be extremely valuable.

It is also worth considering if the objects with the largest excesses are not really old dusty giants ascending the giant branch, but young dusty giants, still contracting along their Hayashi track. This could explain both the very large excesses as well as the high lithium abundances, since young stars are known to often have high $A(Li)$. Young, actively accreting stars with substantial disks would have strong and variable Hα profiles, and have significant variability at essentially all wavelengths, both of which are different than expectations for old giant stars. Detailed isotopic ratios (such as $^{12}C/^{13}C$) that trace mixing and chemical evolution would also be of help. Additional detailed spectroscopic data and modeling is required to distinguish old dusty stars from young dusty stars.

8. CONCLUSIONS

In the past, dIR97 and others have suggested a connection between enhanced lithium and IR excesses in K giants. However, others (e.g., Fekel & Watson 1998; Jasniewicz et al. 1999; Lebzelter et al. 2012; Kumar et al. 2015) have questioned the association between Li and IR abundances. We have assembled a set of 316 targets thought to be K giants, two-thirds of which are thought to be Li-rich, in order to test the association between IR excesses and lithium abundances. The targets come from the dIR97 study (biased toward IR-bright sources), the C12 study (assembled with limited biases to test correlations of various stellar parameters), and a wide variety of literature identifying Li-rich K giants. For these targets, we assembled a multiwavelength catalog spanning optical through

100 μm data, using SDSS, NOMAD, 2MASS, DENIS, *WISE*, *IRAS*, *AKARI*, *MSX*, and *Spitzer* data.

We inspected each source in as many different images as possible. In 24 cases, all identified first as IR-bright sources with *IRAS*, we believe that source confusion is playing a role, in that either (a) the source that is bright in the optical (and most likely the source of which a spectrum was obtained to assess lithium) is not responsible for the IR flux, or (b) there is more than one source responsible for the IR flux as measured in *IRAS*.

We looked for IR excesses by ~ 20 μm using two different approaches: (a) simple SED construction and assessment, and (b) an approach drawn from studies of young stars used to identify small but significant IR excesses. We identify 19 stars with large IR excesses, and 9 more stars that have small but significant IR excesses. However, 5 of these 28 may not be first ascent K giants. (There are 2 more K giants that may have IR excesses by ~ 10 μm, identified from relatively sparse SEDs.) Ten of the 28 clear IR excess K giants were already recently identified in the literature as having IR excesses, but this is the first recent confirmation of IR excess for 18 of these targets. Some of these giants have IR excesses that start at or before 5 μm, but others have excesses that start near 20 μm.

IR excesses by 20 μm, though rare, are about twice as common among Li-rich K giants (11^{+4}_{-3}%) as in Li-poor K giants (2^{+3}_{-1}%). Despite identifying very few IR excesses (by number or fraction of sample), we find that if a RG has a large IR excess, it probably has a large A(Li) and is a fast rotator, but having a large A(Li) (or being a fast rotator) does not mean that it necessarily has a large IR excess. Smaller excesses can be found at all abundance levels. This is consistent with the idea that the IR excess lifetime of a single ejected shell is very short-lived compared to the timescale of Li enrichment. It could also suggest that not all Li-rich stars eject shells, and some other parameter (such as fast rotation, or even rotation history) dictates whether shell ejection occurs. Stars with the clearest sign of substantial internal mixing (very low ^{12}C/^{13}C and high Li) show no evidence of an IR excess. This could be also explained by a shorter timescale for the IR excess than the Li regeneration, since the lowest ^{12}C/^{13}C are realized near the end of the Li-enrichment stage. An external Li regeneration mechanism identified in the literature is planet injestion. However, we identify only one of the three best candidates for planet accretion listed in C12 as having a measurable IR excess, and it is a small excess. The largest IR excesses are all found in the dlR97 sample, which is strongly biased toward IR-bright objects. There remains a possibility that at least some of these largest excess objects may not be old dusty stars, but instead young dusty stars.

APPENDIX
NOTES ON INDIVIDUAL SOURCES

Table 6 contains human-readable notes on the entire set of sources; position, photometric, and abundance data are in the machine-readable table in Table 1. Detailed notes on the sources we suspect are subject to source confusion appear in Table 4. Much more detailed notes on the sources we believe have IR excesses are in Section 5.

Table 6
Special Notes on Targets

Name	dlR97	C12	Other Lit	Status	Notes	A(Li), log g, T_{eff}?
HD 787	dlR97	...	...	(no excess)	...	...
Tyc3663-01966-1	...	...	Adamów et al. (2014)	(no excess)	...	Not Li rich.
HD 4893	...	...	Castilho et al. (2000)	(no excess)	May be too cool to be a K giant.	Not Li rich.
IRAS00483−7347	...	...	Castilho et al. (1998)	IR excess (but maybe not K giant)	May be too cool to be a K giant.	No A(Li). No T_{eff}. No log g.
Scl 1004838	...	...	Kirby et al. (2012)	sparse SED but probably no IR excess	...	...
Scl 1004861	...	...	Kirby et al. (2012)	sparse SED but probably no IR excess	...	...
NGC 362 V2	...	...	Smith et al. (1999)	IR excess (small)	...	Not Li rich.
HD 6665	...	...	Kumar et al. (2011)	(no excess)	Identified in McDonald et al. (2012) as having an IR excess, but IR excess is not real.	...
HD 7087	...	...	Liu et al. (2014)	(no excess)	...	...
HD 8676	...	...	Kumar et al. (2011)	(no excess)	...	...
HD 9746	dlR97	...	...	(no excess)	...	...
HD 10437	...	...	Kumar et al. (2011)	(no excess)	...	...
HD 12203	...	...	Kumar et al. (2011)	(no excess)	...	...
CPD-55395	dlR97	...	...	(no excess)	...	Not Li rich. No T_{eff}. No log g.
HD 13189	...	C12	...	(no excess)	...	Not Li rich.
HD 15866	...	...	Liu et al. (2014), Luck & Heiter (2007)	(no excess)	...	T_{eff} too warm to be RG. log g too large to be RG.
For 55609	...	...	Kirby et al. (2012)	sparse SED but probably no IR excess	...	...
For 60521	...	...	Kirby et al. (2012)	sparse SED but probably no IR excess	...	...
Tyc3300-00133-1	...	...	Adamów et al. (2014)	(no excess)	...	...
For 90067	...	...	Kirby et al. (2012)	sparse SED but possible IR excess	...	...
For 100650	...	...	Kirby et al. (2012)	sparse SED but probably no IR excess	...	...
Tyc3304-00090-1	...	...	Adamów et al. (2014)	(no excess)	...	...
Tyc1780-00654-1	...	C12	...	(no excess)	...	Not Li rich.
HD 17144	...	...	Drake et al. (2002)	(no excess)	...	Not Li rich. No log g.
SDSS J0245+7102	...	...	Martell & Shetrone (2013)	(no excess)	...	...
Tyc0647-00254-1	...	C12	...	(no excess)	...	...
SDSS J0301+7159	...	...	Martell & Shetrone (2013)	(no excess)	...	...
G0300+00.29	...	C12	...	sparse SED but probably no IR excess	...	Not Li rich.
Tyc3318-01333-1	...	...	Adamów et al. (2014)	(no excess)	...	...
SDSS J0304+3823	...	...	Martell & Shetrone (2013)	sparse SED but probably no IR excess	...	...
Tyc5868-00337-1	...	C12	...	(no excess)	...	Not Li rich.
HD 19745	dlR97	...	...	IR excess	Also identified in Kumar et al. (2015) as an IR excess star.	...
Tyc3314-01371-1	...	...	Adamów et al. (2014)	(no excess)	...	Not Li rich.
HD 21078	...	...	Fekel & Watson (1998)	(no excess)	...	Not Li rich. No log g.
G0319+56.5830	...	C12	...	(no excess)	...	Not Li rich.
HD 21018	...	...	Kumar et al. (2011)	(no excess)	...	...
G0319+56.6888	...	C12	...	(no excess)	...	Not Li rich.

Table 6
(Continued)

Name	dlR97	C12	Other Lit	Status	Notes	A(Li), log g, $T_{\rm eff}$?
Tyc5881-01156-1	...	C12	...	(no excess)	...	Not Li rich.
IRAS03520–3857	dlR97	...	...	IR excess	Given position is offset $\sim$11″ from object taken as match (which is large in the context of the rest of this data set), but relatively isolated source and relatively clean field (e.g., unlikely to be confused).	No A(Li). No $T_{\rm eff}$. No log g.
HD 26162	...	C12	...	(no excess)	...	Not Li rich.
Tyc3340-01195-1	...	C12	...	(no excess)	...	Not Li rich.
HD 27497	...	...	Jasniewicz et al. (1999)	(no excess)	...	Not Li rich.
RAVEJ043154.1–063210	...	...	Ruchti et al. (2011)	sparse SED but probably no IR excess	...	$T_{\rm eff}$ too warm to be RG.
IRASF04376-3238	...	...	Torres et al. (2000)	IR excess	Also CD-32 1919.	No A(Li). No $T_{\rm eff}$. No log g.
HD 30238	dlR97	...	...	(no excess)	...	Not Li rich.
HD 30197	...	...	Liu et al. (2014), Luck & Heiter (2007)	(no excess)	...	...
Tyc0684-00553-1	...	...	Adamów et al. (2014)	(no excess)	...	...
HD 30834	dlR97	...	...	(no excess)	...	...
Tyc5904-00513-1	...	C12	...	(no excess)	...	Not Li rich.
G0453+00.90	...	C12	...	sparse SED but probably no IR excess	...	Not Li rich.
HD 31993	dlR97	C12	...	(no excess)	Only target in common between dlR97 and C12	Not Li rich.
HD 34198	...	C12	...	(no excess)	Also UU Lep	Not Li rich.
HD 33798	...	...	Drake et al. (2002)	(no excess)	...	log g too large to be RG.
HD 33363	...	C12	...	(no excess)	...	Not Li rich.
HD 35984	...	...	Liu et al. (2014), Luck & Heiter (2007)	(no excess)	...	$T_{\rm eff}$ too warm to be RG. log g too large to be RG.
SDSS J0535+0514	...	...	Martell & Shetrone (2013)	sparse SED but probably no IR excess	...	...
HD 37719	...	...	Kumar et al. (2011)	(no excess)	...	...
Be 21 T50	...	...	Hill & Pasquini (1999)	sparse SED but probably no IR excess	Hill & Pasquini call this T33 but it is not; based on photometry from Tosi et al. (1998), it is T50.	...
HD 39853	dlR97	...	...	(no excess)	...	...
HD 40359	...	...	Fekel & Watson (1998)	(no excess)	...	Not Li rich. No log g.
HD 40168	...	...	Kumar et al. (2011)	(no excess)	...	...
HD 40827	...	...	Kumar et al. (2011)	(no excess)	...	...
HD 43827	...	...	Jasniewicz et al. (1999)	(no excess)	...	Not Li rich. No log g.
Tyc1890-01314-1	...	C12	...	(no excess)	...	Not Li rich.
HD 44889	...	...	Castilho et al. (2000)	(no excess)	...	Not Li rich.
SDSS J0632+2604	...	...	Martell & Shetrone (2013)	sparse SED but probably IR excess	...	...
Tr5 3416	...	...	Monaco et al. (2014)	sparse SED but probably no IR excess	...	...
HD 47536	...	C12	...	(no excess)	*WISE* measurements from AllWISE reject catalog	Not Li rich.
IRAS06365+0223	dlR97	...	...	drop due to source confusion	2MASS measurements from Extended Source Catalog; *WISE* has two similar sources at this location in catalog, but not in image, so taking slightly closer. Extended source is origin of most of IR emission.	No A(Li). No $T_{\rm eff}$. No log g.
G0639+56.6179	...	C12	...	(no excess)	...	Not Li rich.

Table 6
(Continued)

Name	dlR97	C12	Other Lit	Status	Notes	A(Li), log g, $T_{\rm eff}$?
SDSS J0652+4052	⋯	⋯	Martell & Shetrone (2013)	(no excess)	⋯	⋯
Tyc3402-00280-1	⋯	C12	⋯	(no excess)	⋯	Not Li rich.
SDSS J0654+4200	⋯	⋯	Martell & Shetrone (2013)	sparse SED but prob-ably no IR excess	⋯	⋯
HD 51367	⋯	⋯	Kumar et al. (2011)	(no excess)	⋯	⋯
G0653+16.552	⋯	C12	⋯	sparse SED but prob-ably no IR excess	⋯	Not Li rich.
G0654+16.235	⋯	C12	⋯	sparse SED but prob-ably no IR excess	⋯	Not Li rich.
HIP 35253	⋯	C12	⋯	(no excess)	⋯	Not Li rich.
SDSS J0720+3036	⋯	⋯	Martell & Shetrone (2013)	sparse SED but prob-ably no IR excess	⋯	$T_{\rm eff}$ too warm to be RG.
HD 57669	⋯	⋯	Jasniewicz et al. (1999)	(no excess)	⋯	No log g.
IRAS07227−1320(PDS 132)	dlR97	⋯	⋯	IR excess	Also GSC 05408–03215.	No A(Li). No $T_{\rm eff}$. No log g.
HD 59686	⋯	C12	⋯	(no excess)	⋯	Not Li rich.
HIP 36896	⋯	C12	⋯	(no excess)	⋯	Not Li rich.
NGC 2423 3	⋯	⋯	J. K. Carlberg et al. (2015, in preparation)	(no excess)	⋯	⋯
IRAS07419–2514	⋯	⋯	Torres et al. (2000)	drop due to source confusion	Target position is photocenter of small group of objects. Torres et al. (2000) notes *IRAS* flux may come from CO cloud WB 1046.	No A(Li). No $T_{\rm eff}$. No log g.
HD 62509(Pollux)	⋯	C12	⋯	(no excess)	⋯	Not Li rich.
IRAS07456–4722(PDS 135)	dlR97	⋯	⋯	IR excess	⋯	No A(Li). No $T_{\rm eff}$. No log g.
Tyc5981-00414-1	⋯	C12	⋯	(no excess)	⋯	Not Li rich.
HD 63798	⋯	⋯	Kumar et al. (2011)	(no excess)	⋯	⋯
HD 65750	dlR97	⋯	⋯	IR excess (small)	POSS images have strong nebulosity. Also V341 Car—a pulsating variable star. Identified in McDonald et al. (2012) as having an IR excess.	Not Li rich. $T_{\rm eff}$ too cool to be RG.
HD 65228	⋯	⋯	Liu et al. (2014)	(no excess)	⋯	$T_{\rm eff}$ too warm to be RG.
Tyc1938-00311-1	⋯	C12	⋯	(no excess)	⋯	Not Li rich.
IRAS07577–2806(PDS 260)	dlR97	⋯	⋯	IR excess	⋯	No A(Li). No $T_{\rm eff}$. No log g.
G0804+39.4755	⋯	C12	⋯	(no excess)	⋯	Not Li rich.
SDSS J0808_0815	⋯	⋯	Martell & Shetrone (2013)	sparse SED but prob-ably no IR excess	⋯	⋯
Tyc0195-02087-1	⋯	C12	⋯	(no excess)	⋯	Not Li rich.
HD 70522	⋯	⋯	Liu et al. (2014), Luck & Hei-ter (2007)	(no excess)	⋯	$T_{\rm eff}$ too warm to be RG. log g too large to be RG.
HD 233517	dlR97	⋯	⋯	IR excess	Also identified in Kumar et al. (2015) as an IR excess star, among many other references.	⋯
Tyc0205-01287-1	⋯	C12	⋯	(no excess)	⋯	Not Li rich.
G0827−16.3424	⋯	C12	⋯	(no excess)	⋯	Not Li rich. log g too large to be RG.
SDSS J0831+5402	⋯	⋯	Martell & Shetrone (2013)	sparse SED but prob-ably no IR excess	⋯	⋯
IRASF08359–1644	⋯	⋯	Torres et al. (2000)	IR excess	⋯	No A(Li). No $T_{\rm eff}$. No log g.

Table 6
(Continued)

Name	dlR97	C12	Other Lit	Status	Notes	A(Li), log g, $T_{\rm eff}$?
HD 73108	...	C12	...	(no excess)	...	Not Li rich.
G0840+56.9122	...	C12	...	(no excess)	...	Not Li rich.
G0840+56.5839	...	C12	...	(no excess)	...	Not Li rich.
HD 76066	dlR97	...	...	(no excess)	*IRAS* FSC [12]–[25] > 0.5 but *WISE* says no excess.	No A(Li). No $T_{\rm eff}$. No log g.
HD 77361	...	...	Kumar et al. (2011)	(no excess)	...	...
HD 78668	...	...	Liu et al. (2014)	(no excess)	...	...
G0909–05.211	...	C12	...	(no excess)	...	Not Li rich.
Tyc3809-01017-1	...	C12	...	(no excess)	...	Not Li rich.
G0912–05.11	...	C12	...	(no excess)	...	Not Li rich.
G0928+73.2600	...	C12	...	IR excess (small)	...	...
HD 82227	dlR97	...	...	(no excess)	...	No A(Li). No log g.
HD 82421	dlR97	...	...	(no excess)	...	No A(Li). No log g.
HD 82734	...	...	Liu et al. (2014)	(no excess)	...	...
SDSS J0936+2935	...	...	Martell & Shetrone (2013)	sparse SED but probably no IR excess	...	...
G0935-05.152	...	C12	...	sparse SED but probably no IR excess	...	Not Li rich.
G0946+00.48	...	C12	...	sparse SED but probably no IR excess	...	Not Li rich.
HD 85444	...	...	Liu et al. (2014)	(no excess)	...	...
IRAS09553–5621	dlR97	...	...	drop due to source confusion	Target position is in between two sources	No A(Li). No $T_{\rm eff}$. No log g.
LeoI 71032	...	...	Kirby et al. (2012)	sparse SED but probably no IR excess	...	...
LeoI 60727	...	...	Kirby et al. (2012)	sparse SED but probably no IR excess	...	...
LeoI 32266	...	...	Kirby et al. (2012)	sparse SED but probably no IR excess	...	...
LeoI 21617	...	...	Kirby et al. (2012)	sparse SED but probably no IR excess	...	...
C1012254-203007	...	...	Ruchti et al. (2011)	sparse SED but probably no IR excess	...	...
HD 88476	...	...	Kumar et al. (2011)	(no excess)	...	...
Tyc3441-00140-1	...	C12	...	(no excess)	...	Not Li rich.
BD+202457	...	...	J. K. Carlberg et al. (2015, in preparation)	(no excess)	...	Not Li rich.
Tyc5496-00376-1 = BD-12d3141	...	...	Ruchti et al. (2011)	(no excess)	...	...
HD 90082	...	...	Castilho et al. (2000)	(no excess)	*WISE* measurements from AllWISE reject catalog	Not Li rich. $T_{\rm eff}$ too cool to be RG.
Tyc3005-00827-1	...	C12	...	(no excess)	...	Not Li rich.
HD 90633	...	...	Kumar et al. (2011)	(no excess)	...	...
HD 92253	dlR97	...	...	(no excess)	...	No A(Li). No log g.
G1053+00.15	...	C12	...	(no excess)	...	Not Li rich.
Tyc2521-01716-1	...	C12	...	(no excess)	...	Not Li rich.
HD 95799	dlR97	...	...	(no excess)	...	...

Table 6
(Continued)

Name	dlR97	C12	Other Lit	Status	Notes	A(Li), log g, T_{eff}?
HD 96195	...	...	Castilho et al. (2000)	IR excess (but maybe not K giant)	May be too cool to be a K giant. Identified in McDonald et al. (2012) as having an IR excess.	Not Li rich. T_{eff} too cool to be RG.
SDSS J1105+2850	...	...	Martell & Shetrone (2013)	sparse SED but probably no IR excess	...	T_{eff} too warm to be RG. log g too large to be RG.
IRAS11044–6127	dlR97	...	...	drop due to source confusion	Optical counterpart hard to locate, steep SED.	No A(Li). No T_{eff}. No log g.
HD 96996	dlR97	...	...	(no excess)	...	No A(Li). No T_{eff}. No log g.
HD 97472	dlR97	...	...	(no excess)	...	No A(Li). No log g.
LeoII C-7-174	...	...	Kirby et al. (2012)	sparse SED but probably no IR excess	...	...
LeoII C-3-146	...	...	Kirby et al. (2012)	sparse SED but probably no IR excess	...	...
G1124–05.61	...	C12	...	(no excess)	...	Not Li rich.
Tyc3013-01489-1	...	C12	...	(no excess)	...	Not Li rich.
G1127–11.60	...	C12	...	sparse SED but probably no IR excess	...	Not Li rich.
G1130+39.9414	...	C12	...	(no excess)	G1130+37.9414 in C12 is a misprint for G1130+39.9414. It is also Tyc3013-01163-1.	Not Li rich.
HD 102845	...	...	Liu et al. (2014)	(no excess)	...	...
Tyc5523-00830-1	...	C12	...	(no excess)	...	Not Li rich.
Tyc0276-00327-1	...	C12	...	IR excess (small)	Also HD 103915. In halo of bright galaxy(?) that appears by 12, 22 μm. Likely high background, but probably ok.	Not Li rich.
G1200+67.3882	...	C12	...	(no excess)	...	Not Li rich.
Tyc6094-01204-1	...	C12	...	(no excess)	...	Not Li rich.
HD 104985	...	C12	...	(no excess)	...	Not Li rich.
Tyc2527-01442-1	...	C12	...	(no excess)	...	Not Li rich.
G1213+33.15558	...	C12	...	(no excess)	...	Not Li rich.
HD 107484	...	...	Kumar et al. (2011)	(no excess)	...	...
NGC 4349 127	...	...	J. K. Carlberg et al. (2015, in preparation)	(no excess)	...	Not Li rich.
HD 108225	...	C12	...	(no excess)	...	Not Li rich.
IRAS12236–6302(PDS 354)	dlR97	...	...	drop due to source confusion	Cluster of possible sources. Steep SED. Torres et al. (2000) mention that optical spectrum of source taken as counterpart has strong Hα emission and could be an H II region.	No A(Li). No T_{eff}. No log g.
HD 108471	dlR97	...	...	(no excess)	...	...
IRAS12327–6523(PDS 355)	dlR97	...	...	IR excess	...	No A(Li).
HD 109742	...	C12	...	(no excess)	...	Not Li rich.
M68-A96=Cl* NGC 4590 HAR 1257	...	...	Ruchti et al. (2011)	sparse SED but probably no IR excess	The coordinates in the paper are incorrect; used finding chart, Figure 2, in Alcaino (1977) to ID by eye.	...
G1240+56.8464	...	C12	...	(no excess)	...	Not Li rich.
HD 112127	dlR97	...	...	(no excess)	...	...
HD 111830	dlR97	...	...	IR excess (small)	...	No A(Li). No log g.
HD 112859	...	C12	...	(no excess)	*IRAS* FSC [12]–[25] > 0.5 but *WISE* says no excess.	...
SDSS J1310_0012	...	...	Martell & Shetrone (2013)	sparse SED but probably no IR excess	...	...
HD 115478	...	C12	...	(no excess)	*WISE* measurements from AllWISE reject catalog	Not Li rich.
HD 115659	...	...	Liu et al. (2014)	(no excess)	...	...

Table 6
(Continued)

Name	dlR97	C12	Other Lit	Status	Notes	A(Li), log g, $T_{\rm eff}$?
HD 116010	⋯	C12	⋯	(no excess)	⋯	Not Li rich.
HD 116292	⋯	⋯	Liu et al. (2014), Kumar et al. (2011)	(no excess)	⋯	⋯
CVnI 195_195	⋯	⋯	Kirby et al. (2012)	sparse SED but probably no IR excess	⋯	⋯
CVnI 196_129	⋯	⋯	Kirby et al. (2012)	sparse SED but probably no IR excess	⋯	⋯
G1331+00.13	⋯	C12	⋯	(no excess)	⋯	Not Li rich.
PDS 365(IRAS13313−5838)	dlR97	⋯	⋯	IR excess	⋯	⋯
HD 118319	⋯	⋯	Kumar et al. (2011)	(no excess)	⋯	⋯
HD 118344	dlR97	⋯	⋯	(no excess)	⋯	No A(Li). No log g.
HD 118839	⋯	C12	⋯	(no excess)	⋯	Not Li rich.
M3-IV101=Cl* NGC 5272 SK 557	⋯	⋯	Kraft et al. (1999), Pilachowski et al. (2003), Ruchti et al. (2011)	sparse SED but probably no IR excess	⋯	⋯
HD 119853	dlR97	⋯	⋯	(no excess)	⋯	No A(Li). No log g.
HD 120048	⋯	⋯	Liu et al. (2014)	(no excess)	⋯	⋯
HD 120602	dlR97	⋯	⋯	(no excess)	⋯	⋯
HD 121710(9Boo)	dlR97	⋯	⋯	(no excess)	⋯	Not Li rich. No log g.
PDS 68(IRAS13539−4153)	dlR97	⋯	⋯	IR excess	Also GSC 07798−00578.	⋯
Tyc3027-01042-1	⋯	C12	⋯	(no excess)	⋯	Not Li rich.
HD 122430	⋯	C12	⋯	(no excess)	⋯	Not Li rich.
Tyc0319-00231-1	⋯	C12	⋯	(no excess)	⋯	Not Li rich.
HD 124897(Arcturus)	⋯	C12	⋯	(no excess)	high enough proper motions that automatic merging not possible; matches done via SIMBAD and by hand	Not Li rich.
HD 125618	dlR97	⋯	⋯	(no excess)	⋯	No A(Li). No $T_{\rm eff}$. No log g.
Tyc1469-01108-1	⋯	C12	⋯	(no excess)	⋯	Not Li rich.
IRAS14198−6115	dlR97	⋯	⋯	drop due to source confusion	Cluster of possible sources.	No A(Li). No $T_{\rm eff}$. No log g.
G1421+28.4625	⋯	C12	⋯	(no excess)	⋯	Not Li rich.
RAVEJ142546.2-154629	⋯	⋯	Ruchti et al. (2011)	(no excess)	⋯	⋯
HD 126868	⋯	⋯	Jasniewicz et al. (1999)	(no excess)	⋯	$T_{\rm eff}$ too warm to be RG. No log g.
IRAS14257−6023	dlR97	⋯	⋯	drop due to source confusion	Cluster of possible sources.	No A(Li). No $T_{\rm eff}$. No log g.
SDSS J1432+0814	⋯	⋯	Martell & Shetrone (2013)	sparse SED but probably no IR excess	⋯	⋯
HD 127740	⋯	⋯	Liu et al. (2014), Luck & Heiter (2007)	(no excess)	⋯	$T_{\rm eff}$ too warm to be RG. log g too large to be RG.
Tyc0913-01248-1	⋯	C12	⋯	(no excess)	⋯	Not Li rich.
Tyc0914-00571-1	⋯	C12	⋯	(no excess)	⋯	Not Li rich.
HD 128309	dlR97	⋯	⋯	(no excess)	⋯	No A(Li). No $T_{\rm eff}$. No log g.
HD 129955	dlR97	⋯	⋯	(no excess)	⋯	No A(Li). No $T_{\rm eff}$. No log g.
HD 131530	dlR97	⋯	⋯	(no excess)	⋯	No A(Li). No log g.
HD 133086	⋯	⋯	Kumar et al. (2011)	(no excess)	⋯	⋯
Tyc0347-00762-1	⋯	C12	⋯	(no excess)	⋯	Not Li rich.

Table 6
(Continued)

Name	dlR97	C12	Other Lit	Status	Notes	A(Li), log g, $T_{\rm eff}$?
M5 V42	⋯	⋯	Carney et al. (1998)	(no excess)	⋯	⋯
SDSS J1522+0655	⋯	⋯	Martell & Shetrone (2013)	sparse SED but probably no IR excess	⋯	⋯
HD 137759	⋯	C12	⋯	(no excess)	⋯	Not Li rich.
HD 138525	⋯	⋯	Liu et al. (2014), Luck & Heiter (2007)	(no excess)	⋯	$T_{\rm eff}$ too warm to be RG. log g too large to be RG.
HD 138688	⋯	⋯	Jasniewicz et al. (1999)	(no excess)	⋯	Not Li rich.
G1551+22.9456	⋯	C12	⋯	(no excess)	⋯	Not Li rich.
SDSS J1607+0447	⋯	⋯	Martell & Shetrone (2013)	sparse SED but probably no IR excess	⋯	⋯
HD 145206	⋯	⋯	Jasniewicz et al. (1999)	(no excess)	⋯	Not Li rich.
HD 145457	⋯	⋯	Kumar et al. (2011)	(no excess)	⋯	⋯
IRAS16086–5255(PDS 410)	dlR97	⋯	⋯	IR excess	⋯	No A(Li). No $T_{\rm eff}$. No log g.
IRAS16128–5109	dlR97	⋯	⋯	drop due to source confusion	Appears in SIMBAD as an H II region; the morphology of the image suggests a dense clump of sources from which emanate long streamers of extended emission.	No A(Li). No $T_{\rm eff}$. No log g.
HD 146850	dlR97	⋯	⋯	(no excess)	⋯	⋯
HD 146834	dlR97	⋯	⋯	IR excess (small)	Also HR 6076. Also identified in McDonald et al. (2012) as having an IR excess.	No A(Li). No log g.
HD 148293	dlR97	⋯	⋯	(no excess)	⋯	⋯
Tyc2043-00747-1	⋯	C12	⋯	(no excess)	⋯	Not Li rich.
IRAS16227–4839	dlR97	⋯	⋯	drop due to source confusion	Match forced to be IR-bright source (not found automatically given this position).	No A(Li). No $T_{\rm eff}$. No log g.
HD 148317	⋯	⋯	Liu et al. (2014), Luck & Heiter (2007)	(no excess)	⋯	$T_{\rm eff}$ too warm to be RG. log g too large to be RG.
IRAS16252–5440	dlR97	⋯	⋯	drop due to source confusion	Also PDS 146. Cluster of IR-bright sources.	No A(Li). No $T_{\rm eff}$. No log g.
HD 150902	⋯	⋯	Kumar et al. (2011)	(no excess)	⋯	⋯
HIP 81437	⋯	C12	⋯	(no excess)	⋯	Not Li rich.
G1640+56.6327	⋯	C12	⋯	(no excess)	⋯	Not Li rich.
IRAS16514–4625(PDS 432)	dlR97	⋯	⋯	drop due to source confusion	Torres et al. (2000) list it as a confirmed giant but the source that was measured may not be responsible for the IR flux. Cluster of soruces, steep SED.	No A(Li). No $T_{\rm eff}$. No log g.
HD 153135	dlR97	⋯	⋯	(no excess)	⋯	No A(Li). No log g.
HD 152786	⋯	⋯	Jasniewicz et al. (1999)	(no excess)	⋯	Not Li rich.
HD 153687	⋯	⋯	Jasniewicz et al. (1999)	(no excess)	⋯	Not Li rich.
HD 155646	⋯	⋯	Liu et al. (2014), Luck & Heiter (2007)	(no excess)	⋯	$T_{\rm eff}$ too warm to be RG. log g too large to be RG.
IRAS17102–3813	dlR97	⋯	⋯	drop due to source confusion	Cluster of sources.	No A(Li). No $T_{\rm eff}$. No log g.
IRAS17120–4106	dlR97	⋯	⋯	drop due to source confusion	Two possible sources.	No A(Li). No $T_{\rm eff}$. No log g.
HD 156115	dlR97	⋯	⋯	(no excess)	⋯	No A(Li). $T_{\rm eff}$ too cool to be RG. No log g.

Table 6
(Continued)

Name	dlR97	C12	Other Lit	Status	Notes	A(Li), log g, T_{eff}?
HD 156061	dlR97	...	...	(no excess)	...	No A(Li). No log g.
IRAS17211–3458	dlR97	...	...	drop due to source confusion	Two possible sources.	No A(Li). No T_{eff}. No log g.
HD 157457	...	...	Jasniewicz et al. (1999)	(no excess)	...	...
HD 157919	...	...	Liu et al. (2014), Luck & Heiter (2007)	(no excess)	...	T_{eff} too warm to be RG. log g too large to be RG.
IRAS17442–2441	dlR97	...	...	drop due to source confusion	Cluster of possible sources.	No A(Li). No T_{eff}. No log g.
PDS 97(IRAS17554–3822)	...	...	de la Reza et al. (1996)	drop due to source confusion	Target position in between two sources of comparable brightness.	No A(Li). No T_{eff}. No log g.
IRAS17576–1845	dlR97	...	...	drop due to source confusion	The multi-wavelength images suggest extinction in this field. Coadella et al. (1995) list it as a candidate to be related to high-mass star forming regions with an ultracompact H II region, though it remained undetected in their survey.	No A(Li). No T_{eff}. No log g.
IRAS17578–1700	dlR97	...	...	IR excess (but maybe not K giant)	Also C* 2514, CGCS 3922—likely carbon star.	No A(Li). No T_{eff}. No log g.
HD 162298	dlR97	...	...	(no excess)	...	No A(Li). No log g.
G1800+61.12976	...	C12	...	(no excess)	...	Not Li rich.
IRAS17582–2619	dlR97	...	...	drop due to source confusion	Brightest source in IR has no optical counterpart. SIMBAD lists this as an OH/IR star. Yoon et al. (2014) and references therein identify it as a post-AGB star (OH4.02-1.68).	No A(Li). No T_{eff}. No log g.
IRAS17590–2412	dlR97	...	...	drop due to source confusion	Position shifted slightly to pick up *WISE* source. Diffuse emission can also be seen in the field in various bands. Messineo et al. (2004) identify a SiO emitter in this region but suggest that it may not be associated with the source from which an optical spectrum had been obtained by dlR97. They note that this *IRAS* source is the only mid-infrared source within their 86 GHz beam.	No A(Li). No T_{eff}. No log g.
IRAS17596–3952(PDS 485)	dlR97	...	...	IR excess	Position shifted slightly to pick up *WISE* source. Also identified in Kumar et al. (2015) as IR excess star.	...
Tyc0435-03332-1	...	...	Adamów et al. (2014)	(no excess)	...	...
HD 164712	dlR97	...	...	(no excess)	...	No A(Li). No T_{eff}. No log g.
HD 167304	...	...	Kumar et al. (2011)	(no excess)	...	...
HD 170527	...	...	Kumar et al. (2011)	(no excess)	...	...
HD 169689	...	...	Jasniewicz et al. (1999)	(no excess)	...	Not Li rich.
V385 Sct	...	...	Castilho et al. (2000)	IR excess (but maybe not K giant)	Too cool to be a K giant. S-type star.	Not Li rich. T_{eff} too cool to be RG.
IRAS18334–0631(PDS 524)	dlR97	...	...	drop due to source confusion	No optical source at the target position, and cluster of IR sources.	No A(Li). No T_{eff}. No log g.
Tyc3105-00152-1	...	...	Adamów et al. (2014)	(no excess)	...	...
Tyc3917-01107-1	...	...	Adamów et al. (2014)	(no excess)	Identified in McDonald et al. (2012) as having an IR excess, but IR excess is not real.	...
IRAS18397–0400	dlR97	...	...	drop due to source confusion	Brightest source in the IR has no optical counterpart.	No A(Li). No T_{eff}. No log g.
Tyc3930-00681-1	...	...	Adamów et al. (2014)	(no excess)	...	Not Li rich.
HD 175492	...	...	Jasniewicz et al. (1999)	(no excess)	...	Not Li rich. T_{eff} too warm to be RG.

Table 6
(Continued)

Name	dlR97	C12	Other Lit	Status	Notes	A(Li), log g, T_{eff}?
IRAS18559+0140	dlR97	⋯	⋯	drop due to source confusion	No optical source at the target position, and cluster of IR sources.	No A(Li). No T_{eff}. No log g.
HD 176588	dlR97	⋯	⋯	(no excess)	⋯	⋯
SDSS J1901+3808	⋯	⋯	Martell & Shetrone (2013)	sparse SED but probably no IR excess	⋯	⋯
HD 176884	⋯	⋯	Jasniewicz et al. (1999)	(no excess)	⋯	Not Li rich.
IRAS19012–0747	dlR97	⋯	⋯	IR excess (small)	Name as appearing in dlR97 had a typo; this is the correct name.	No A(Li).
HD 177830	⋯	C12	⋯	(no excess)	⋯	Not Li rich.
IRAS19038–0026	⋯	⋯	Castilho et al. (2000)	IR excess (small but maybe not K giant)	May be too cool to be a K giant.	Not Li rich. T_{eff} too cool to be RG.
HD 177366	dlR97	⋯	⋯	(no excess)	⋯	No A(Li). No log g.
HD 178168	⋯	⋯	Castilho et al. (2000)	(no excess)	⋯	Not Li rich.
SDSS J1909+3837	⋯	⋯	Martell & Shetrone (2013)	sparse SED but probably no IR excess	⋯	⋯
IRAS19083+0119(PDS 562)	dlR97	⋯	⋯	drop due to source confusion	Brightest source in the IR has no optical counterpart. Steep SED.	No A(Li). No T_{eff}. No log g.
KIC 5000307	⋯	⋯	Silva Aguirre et al. (2014)	(no excess)	⋯	⋯
HD 181154	dlR97	⋯	⋯	(no excess)	⋯	No A(Li). No log g.
IRAS19210+1715	dlR97	⋯	⋯	drop due to source confusion	Brightest source in the IR has no optical counterpart. Steep SED.	No A(Li). No T_{eff}. No log g.
HD 182900	⋯	⋯	Liu et al. (2014), Luck & Heiter (2007)	(no excess)	⋯	T_{eff} too warm to be RG. log g too large to be RG.
HD 182901	⋯	⋯	Liu et al. (2014), Luck & Heiter (2007)	(no excess)	⋯	T_{eff} too warm to be RG. log g too large to be RG.
HD 183492	⋯	⋯	Kumar et al. (2011)	(no excess)	⋯	⋯
HD 183202	dlR97	⋯	⋯	(no excess)	⋯	No A(Li). No T_{eff}. No log g.
PDS 100	dlR97	⋯	⋯	IR excess	Also V859 Aql and *IRAS*19285+0517. Also identified in Kumar et al. (2015) as IR excess star.	⋯
G1936+61.14369	⋯	C12	⋯	(no excess)	⋯	Not Li rich.
HD 185194	⋯	⋯	Liu et al. (2014)	(no excess)	⋯	⋯
KIC 4937011	⋯	⋯	Anthony-Twarog et al. (2013)	sparse SED but probably no IR excess	⋯	⋯
HD 187114	dlR97	⋯	⋯	(no excess)	⋯	No A(Li). No log g.
RAVEJ195244.9–600813	⋯	⋯	Ruchti et al. (2011)	(no excess)	⋯	⋯
Tyc1058-02865-1	⋯	⋯	Adamów et al. (2014)	(no excess)	⋯	Not Li rich.
HD 188376	⋯	⋯	Liu et al. (2014), Luck & Heiter (2007)	(no excess)	⋯	T_{eff} too warm to be RG. log g too large to be RG.
HD 188993	⋯	⋯	Liu et al. (2014), Luck & Heiter (2007)	(no excess)	⋯	T_{eff} too warm to be RG. log g too large to be RG.
HD 190299	dlR97	⋯	⋯	(no excess)	⋯	No A(Li). No T_{eff}. No log g.
HD 191277	⋯	C12	⋯	(no excess)	⋯	Not Li rich.
SDSS J2019+6012	⋯	⋯	Martell & Shetrone (2013)	sparse SED but probably no IR excess	⋯	⋯

Table 6
(Continued)

Name	dlR97	C12	Other Lit	Status	Notes	A(Li), log g, $T_{\rm eff}$?
HD 194317(39Cyg)	dlR97	⋯	⋯	(no excess)	⋯	Not Li rich. No log g.
HD 194937	⋯	⋯	Liu et al. (2014), Luck & Heiter (2007), Kumar et al. (2011)	(no excess)	⋯	⋯
Tyc9112-00430-1	⋯	⋯	Ruchti et al. (2011)	IR excess (small)	⋯	⋯
Tyc2185-00133-1	⋯	C12	⋯	(no excess)	⋯	Not Li rich.
HD 202261	⋯	⋯	Liu et al. (2014)	(no excess)	⋯	⋯
HD 203136	⋯	⋯	Kumar et al. (2011)	(no excess)	Identified in McDonald et al. (2012) as having an IR excess, but IR excess is not real.	⋯
HD 203251	dlR97	⋯	⋯	(no excess)	*IRAS* FSC [12]–[25] > 0.5 but *WISE* says no excess.	Not Li rich. No $T_{\rm eff}$. No log g.
HD 204540	dlR97	⋯	⋯	(no excess)	⋯	No A(Li). No log g.
HD 205349	⋯	⋯	Kumar et al. (2011)	(no excess)	⋯	⋯
HD 206445	⋯	C12	⋯	(no excess)	⋯	Not Li rich.
Tyc6953-00510-1	⋯	⋯	Ruchti et al. (2011)	(no excess)	⋯	⋯
G2200+56.3466	⋯	C12	⋯	(no excess)	⋯	Not Li rich.
SDSS J2200+4559	⋯	⋯	Martell & Shetrone (2013)	sparse SED but probably no IR excess	⋯	⋯
SDSS J2206+4531	⋯	⋯	Martell & Shetrone (2013)	sparse SED but probably no IR excess	⋯	⋯
HD 212271	⋯	⋯	Liu et al. (2014)	(no excess)	⋯	⋯
HD 212430	⋯	⋯	Liu et al. (2014)	(no excess)	⋯	⋯
HD 213619	⋯	⋯	Liu et al. (2014), Luck & Heiter (2007)	(no excess)	⋯	$T_{\rm eff}$ too warm to be RG. log g too large to be RG.
HD 213930	⋯	⋯	Liu et al. (2014)	(no excess)	⋯	⋯
HD 214995	⋯	⋯	Liu et al. (2014), Luck & Heiter (2007), Kumar et al. (2011)	(no excess)	⋯	⋯
HD 217352	⋯	⋯	Kumar et al. (2011)	(no excess)	⋯	⋯
HD 218527	dlR97	⋯	⋯	(no excess)	⋯	No A(Li). No $T_{\rm eff}$. No log g.
Tyc8448-00121-1	⋯	⋯	Ruchti et al. (2011)	(no excess)	⋯	⋯
HD 219025	dlR97	⋯	⋯	IR excess	Also BI Ind. Also identified in Kumar et al. (2015) as an IR excess star.	⋯
HD 219449	⋯	C12	⋯	(no excess)	⋯	Not Li rich.
HD 221776	dlR97	⋯	⋯	(no excess)	⋯	No A(Li). No log g.
HD 221862	⋯	C12	⋯	(no excess)	⋯	Not Li rich.
SDSS J2353+5728	⋯	⋯	Martell & Shetrone (2013)	(no excess)	⋯	⋯
SDSS J2356+5633	⋯	⋯	Martell & Shetrone (2013)	(no excess)	⋯	⋯

REFERENCES

Adamów, M., Niedzielski, A., Villaver, E., Wolszczan, A., & Nowak, G. 2014, A&A, 569, 55

Ahn, C., Alexandroff, R., Allende Prieto, C., et al. 2014, ApJS, 211, 17

Alcaino, G. 1977, A&AS, 29, 9

Anthony-Twarog, B., Deliyaniis, C., Rich, E., & Twarog, B. 2013, ApJ, 767, 19

Beichman, C., Neugebauer, G., Habing, H., Clegg, P., & Chester, T. 1988, Infrared Astronomical Satellite (*IRAS*) Catalogs and Atlases (Washington, DC: GPO) (http://irsa.ipac.caltech.edu/IRASdocs/exp.sup/)

Burgasser, A. J., Kirkpatrick, J. D., Reid, I. N., et al. 2003, ApJ, 586, 512

Carlberg, J., Cunha, K., Smith, V., & Majewski, S. 2012, ApJ, 757, 109

Carlberg, J., Smith, V., Cunha, K., Majewski, S., & Rood, R. 2010, ApJ, 723, 103

Carney, B., Fry, A., & Gonzalez, G. 1998, AJ, 116, 2984

Castilho, B., Gregorio-Hetem, J., Spite, F., Barbuy, B., & Spite, M. 2000, A&A, 364, 674

Castilho, B., Gregorio-Hetem, J., Spite, F., Spite, M., & Barbuy, B. 1998, A&AS, 127, 139

Chen, P.-S., Yang, X.-H., & Zhang, P. 2007, AJ, 134, 214

Coadella, C., Palumbo, G., Pareschi, G., et al. 1995, MNRAS, 276, 57

Cutri, R., Wright, E., Conrow, T., et al. 2014, Explanatory Supplement to the AllWISE Data Release Products, http://wise2.ipac.caltech.edu/docs/release/allwise/expsup/

de la Reza, R., Drake, N., & da Silva, L. 1996, ApJL, 456, L115

de la Reza, R., Drake, N., da Silva, L., Torres, C., & Martin, E. 1997, ApJ, 482, 77

de la Reza, R., Drake, N., Oliveira, I., & Rengaswamy, S. 2015, ApJ, 808, 86

Denissenkov, P. A., & Herwig, F. 2004, ApJ, 612, 1081

Denissenkov, P. A., & VandenBerg, D. A. 2003, ApJ, 593, 509

Drake, N., de la Reza, R., da Silva, L., & Lambert, D. 2002, AJ, 123, 2703

Egan, M., Price, S., Kraemer, K., et al. 2013, yCat, 5114, 0

Fekel, F., & Watson, L. 1998, AJ, 116, 2466

García-Lario, P., Manchado, A., Pych, W., & Pottasch, S. 1997, A&AS, 126, 479

Gautier, T., Rieke, G., Stansberry, J., et al. 2007, ApJ, 667, 527

Gillett, F. 1986, in Light on Dark Matter, ed. F. P. Israel (Dordrecht: Reidel), 61

Gregorio-Hetem, J., Lépine, J., Quast, G., Torres, C., & de la Reza, R. 1992, AJ, 103, 549

Guandalini, R., Palmerini, S., Busso, M., & Uttenthaler, S. 2009, PASA, 26, 168

Hill, V., & Pasquini, L. 1999, A&A, 348, 21

Jasniewicz, G., Parthasarathy, M., de Laverny, P., & Thévenin, F. 1999, A&A, 342, 831

Jura, M. 1999, ApJ, 515, 706

Kirby, E., Fu, X., Guhathakurta, P., & Deng, L. 2012, ApJ, 752, 16

Kraft, R., Peterson, R., Guhathakurta, P., et al. 1999, ApJ, 518, 53

Kumar, Y., & Reddy, B. 2009, ApJ, 703, 46

Kumar, Y., Reddy, B., & Lambert, D. 2011, ApJ, 730, 12

Kumar, Y., Reddy, B., Muthumariappan, C., & Zhao, G. 2015, A&A, 577, A10

Lebzelter, T., Uttenthaler, S., Busson, M., Schultheis, M., & Aringer, B. 2012, A&A, 538, 36

Liu, Y., Tan, K., Wang, L., et al. 2014, ApJ, 785, 94

Lloyd Evans, T. 1991, MNRAS, 249, 409

Luck, R. E., & Heiter, U. 2007, AJ, 133, 2464

Magnani, L., Caillault, J.-P., Buchalter, A., & Beichman, C. A. 1995, ApJS, 96, 159

Martell, S., & Shetrone, M. 2013, MNRAS, 430, 611

McDonald, I., Zijlstra, A., & Boyer, M. 2012, MNRAS, 427, 343

Messineo, M., Habing, H., Menten, K., Omont, A., & Sjouweman, L. 2004, A&A, 418, 103

Mizusawa, T., Rebull, L., Stauffer, J., et al. 2012, AJ, 144, 135

Monaco, L., Boffin, H., Bonifacio, P., et al. 2014, A&A, 546, 6

Moshir, M., Kopan, G., Conrow, T., et al. 1992, Explanatory Supplement to the IRAS Faint Source Survey, version 2, JPL D-10015 8/92 (Pasadena, CA: JPL) (http://irsa.ipac.caltech.edu/IRASdocs/surveys/D-10015.pdf)

Murakami, H., Baba, H., Barthel, P., et al. 2007, PASJ, 59, 369

Neugebauer, G., Habing, H., van Duinen, et al. 1984, ApJ, 278, 1

Palacios, A., Charbonnel, C., Talon, S., & Siess, L. 2006, A&A, 453, 261

Paresce, F., & Burrows, C. 1987, ApJ, 319, 23

Pereyra, A., Castilho, B., & Magalhães, A. 2006, A&A, 449, 211

Pilachowski, C., Sneden, C., Freeland, E., & Casperson, J. 2003, AJ, 125, 794

Ramos-Larios, G., Guerrero, M., Suárez, O., Miranda, L., & Gómez, J. 2012, A&A, 545, 20

Rebull, L., Koenig, X., Padgett, D., et al. 2011, ApJS, 196, 4

Reddy, B., & Lambert, D. 2005, AJ, 129, 2831

Reddy, B., Lambert, D., Hrivnak, B., & Bakker, E. 2002, AJ, 123, 1993

Ruchti, G., Fulbright, J., Wyse, R., et al. 2011, ApJ, 743, 107

Saunders, W., Sutherland, W., Maddox, S., et al. 2000, MNRAS, 317, 55

Siess, L., & Livio, M. 1999, MNRAS, 308, 1133

Silva Aguirre, V., Ruchti, G., Hekker, S., et al. 2014, ApJ, 748, 16

Skrutskie, M., Cutri, R. M., Stiening, R., et al. 2006, AJ, 131, 1163

Smith, V., Shetrone, M., & Keane, M. 1999, ApJ, 516, 73

Stephenson, C. 1976, PW&SO, 2, 21

Stephenson, C. 1984, PW&SO, 3, 1

Suárez, O., García-Lario, P., Manchado, A., et al. 2006, A&A, 458, 173

Szczerba, R., Siódmiak, N., Stasinska, G., & Borkowski, J. 2007, A&A, 469, 799

Torres, C., Quast, G., de la Reza, R., & da Silva, L. 2000, IAUS, 198, 320

Torres, C., Quast, G., de la Reza, R., Gregorio-Hetem, J., & Lépine, J. 1995, AJ, 109, 2146

Tosi, M., Pulone, L., Marconi, G., & Bragaglia, A. 1998, MNRAS, 299, 834

Trilling, D., Bryden, G., Beichman, C., et al. 2008, ApJ, 674, 1086

Valenti, J., Fallon, A., & Johns-Krull, C. 2003, ApJS, 147, 305

Wang, L., & Rowan-Robinson, M. 2009, MNRAS, 398, 109

Werner, M., Roellig, T., Low, F., et al. 2004, ApJS, 154, 1

Whitelock, P., Menzies, J., Catchpole, R., et al. 1991, MNRAS, 250, 638

Wright, E., Eisenhardt, P. R. M., Mainzer, A. K., et al. 2010, AJ, 140, 1868

Yoon, D.-H., Chos, S.-H., Kim, J., Yun, Y., & Park, Y.-S. 2014, ApJS, 211, 15

Zacharias, N., Monet, D. G., Levine, S. E., et al. 2005, yCat, 1297, 0